CALIFORNIA INSTITUTE OF TECHNOLOGY

EARTHQUAKE ENGINEERING RESEARCH LABORATORY

SYSTEM IDENTIFICATION OF HYSTERETIC STRUCTURES

By

Arturo O. Cifuentes

EERL 84-04

A Report on Research Conducted Under a Grant
from the National Science Foundation

Pasadena, California
1984

This investigation was sponsored by Grant No. CEE81-19962 from the National Science Foundation, Division of Problem-Focused Research Applications, under the supervision of W. D. Iwan. Any opinions, findings, and conclusions or recommendations expressed in this publication are those of the author and do not necessarily reflect the views of the National Science Foundation.

SYSTEM IDENTIFICATION OF HYSTERETIC STRUCTURES

Thesis by

Arturo O. Cifuentes

In Partial Fulfillment of the Requirements
for the Degree of
Doctor of Philosophy

California Institute of Technology
Pasadena, California

1985

(Submitted September 14, 1984)

To my friend, Charlin, for the many

things we have shared and dreamed.

ACKNOWLEDGMENTS

I would like to thank the California Institute of Technology for the excellent education that I received and for the financial aid that made it possible. Being a member of the Caltech community these four years has been a great experience.

I am deeply indebted to my advisor, Dr. Wilfred Iwan, for his guidance while pursuing my Ph.D. He encouraged me very enthusiastically during the course of this research and he always made himself available when needed. His bright insight and many useful suggestions were a decisive factor in the completion of this thesis.

Coffee breaks, corridor conversation and other related activities with my peers at Thomas Laboratory are greatly acknowledged since they made my stay here much more enjoyable.

Thanks are extended to Garrett Jeong for his assistance in computer matters and to Gloria Jackson for doing a fine job typing the manuscript.

I am particularly grateful to my family in Chile for the great deal of support and encouragement they gave me during the course of my studies. Especially to my parents Arturo and Lucia who have followed every single detail of my career with steady devotion.

Finally, I wish to express my eternal gratitude to my friend and wife, Ventura Charlin, with whom I shared the ups and downs of going through graduate school. Without her love and companionship this

adventure would have been a nightmare. I owe her many things, among others the joy of living.

ABSTRACT

This thesis is concerned with the earthquake response of hysteretic structures subjected to strong ground acceleration. Several earthquake records corresponding to different instrumented buildings are analyzed. Based on these observations, a new model for the dynamic behavior of reinforced concrete buildings is proposed. In addition, a suitable system identification algorithm to be used with this new model is introduced. This system identification algorithm is based upon matching the restoring force behavior of the structure rather than the time history of the response. As a consequence, the new algorithm exhibits significant advantages from a computational point of view. Some numerical examples using actual earthquake data are discussed.

TABLE OF CONTENTS

TABLE OF CONTENTS (CONTINUED)

TABLE OF CONTENTS (CONTINUED)

TABLE OF CONTENTS (CONTINUED)

CHAPTER I

INTRODUCTION

This thesis is concerned with the hysteretic response of reinforced concrete buildings subjected to strong ground acceleration.

Earthquake records provide the most reliable source of information concerning the dynamic behavior of structures. They are particularly important since no test can shake a building with the strength an earthquake does. Prior to 1971, very few earthquake records of buildings affected by a strong ground motion had been obtained. However, after the 1971 San Fernando earthquake, data from several severely shaken structures became available. These records, plus the records obtained during the 1979 Imperial Valley earthquake, have made it possible to investigate the response of structures subjected to strong dynamic excitation in greater detail.

Previous research by Iemura and Jennings [1], Beck [2] and McVerry [3] has indicated that the response of many of these buildings has been markedly nonlinear. Iemura and Jennings [1] studied the performance of Millikan Library during the San Fernando event. They concluded that it was not possible to reproduce the behavior of the building by means of a linear or bilinear stationary model.

Beck [2] analyzed the response of the JPL-180 building during the San Fernando earthquake. By studying the earthquake records within small time intervals (5 seconds) he observed that there was a consistent variation of the parameters of the equivalent linear model. That is,

the fundamental period of the structure increased as the shaking progressed.

McVerry [3] provided a more extensive source of information regarding the performance of buildings during the San Fernando earthquake. He attempted to fit a linear model to the data obtained from some damaged structures: the Bank of California, Holiday Inn Orion and Holiday Inn Marengo buildings. He concluded that the response of these structures had exceeded the elastic range by far and it was not possible to describe the response behavior using time-invariant linear models. Rojahn and Mork [4] and Pauschke et al. [5] studied the records of the Imperial County Services Building that was extensively damaged during the 1979 earthquake. As expected, the response of this structure was also in the nonlinear range.

Several models have been proposed to describe the hysteretic behavior of structures excited beyond the elastic range [6],[7],[8]...[21]. These models range from relatively simple but not very realistic models to some very sophisticated representations in which the interpretation of the loading and unloading rules is somewhat obscure. At one extreme is the elastoplastic model which depends only on two parameters, but unfortunately has given very poor approximations when tested against experimental data [7]. At the other extreme is Takeda's model which, according to some experimental results using reinforced concrete specimens and simulated earthquake motions, has produced satisfactory results [11]. The problem with Takeda's model is

that it consists of sixteen different rules depending on the loading regime.

So far, none of the models proposed has gained wide acceptance among the analysts and no model has proven entirely satisfactory using actual earthquake data. As a consequence, there is still no definitive answer to the question of what type of model is adequate to represent the hysteretic behavior of reinforced concrete structures subjected to strong excitation. The main goal of this thesis is to present an answer to this question. A second goal is to introduce a suitable system identification algorithm to be used in conjunction with the model herein introduced.

In order to answer the major question posed by this thesis, it will be necessary to accurately characterize or "identify" the response behavior of a structure subjected to strong ground shaking. In general, the structural identification problem has been solved by minimizing an error which is defined in terms of the time history of the structure's response. This approach, although feasible, has a numerical disadvantage. It requires the solution of a differential equation each time the error is evaluated. An alternative approach is to define an error based on the restoring force behavior of the structure. This method, presented in detail in this thesis, introduces important advantages from a computational point of view.

The body of this thesis has been organized into six chapters. The first chapter is the Introduction. Chapter II examines the nature of structural behavior of several buildings during real earthquakes. The

most important features of the dynamic response of these structures are discussed. In addition, a general methodology for analyzing the earthquake data is introduced.

Chapter III discusses several models for the dynamic behavior of buildings. First, the linear model and some nonlinear models are examined in the light of the conclusions drawn in the previous chapter. Next, a new model for the dynamic behavior of reinforced concrete structures is introduced.

Chapter IV presents the new system identification algorithm based upon matching the restoring force behavior of the structure and model. This new algorithm is compared to the traditional approach for this type of problem.

In Chapter V some numerical examples are discussed. The proposed model is tested using actual earthquake data corresponding to the Bank of California, Holiday Inn and Imperial County Services buildings. The approximations given by the new model are compared to those obtained using a linear model.

General conclusions and recommendations for further study are presented in Chapter VI.

REFERENCES

[1] Iemura, H. and Jennings, P.C., "Hysteretic Response of a Nine-Story Reinforced Concrete Building," International Journal of Earthquake Engineering and Structural Dynamics, Vol. 3, 183-201, 1974.

[2] Beck, J.L., "Determining Models of Structures from Earthquake Records," Earthquake Engineering Research Laboratory Report No. EERL 78-01, California Institute of Technology," Pasadena, California, June 1978.

[3] McVerry, G.H., "Frequency Domain Identification of Structural Models from Earthquake Records," Earthquake Engineering Research Laboratory Report No. EERL 79-02, California Institute of Technology, Pasadena, California, October 1979.

[4] Rojahn, C. and Mork, P.N., "An Analysis of Strong-Motion Data from a Severely Damaged Structure -- The Imperial County Services Building, El Centro, California," recorded by the California Division of Mines and Geology Strong-Motion Network, The Imperial Valley, California, Earthquake of October 15, 1979, Geology Survey Professional Paper 1254, U.S. Dept. of the Interior, 357-375. U.S. Government Printing Office, Washington D.C., 1982.

[5] Pauschke, J.M., Oliveira, C.S., Shah, H.C. and Zsutty, T.C., "A Preliminary Investigation of the Dynamic Response of the Imperial County Services Building During the October 15, 1979 Imperial Valley Earthquake," The John A. Blume Earthquake Engineering

Center, Department of Civil Engineering, Stanford University, Report No. 49, January 1981.

[6] Otani, S., "Nonlinear Dynamic Analysis of 2-D Reinforced Concrete Building Structures," Third Canadian Conference on Earthquake Engineering, Canadian Committee on Earthquake Engineering, Vol. 2, 1979, 1009-1037.

[7] Saiidi, M., "Influence of Hysteresis Models on Calculated Seismic Response of R/C Frames," Proceedings of the 7th World Conference on Earthquake Engineering, Vol. 5, Rome, Italy, 1973, 423-430.

[8] Clough, R.W. and Johnston, S.B., "Effect of Stiffness Degradation on Earthquake Ductility Requirements," Proceedings, Japan Earthquake Engineering Symposium, Tokyo, Japan, October 1966, 227-232.

[9] Iwan, W.D., "A Distributed-Element Model for Hysteresis and Its Steady-State Dynamic Response," Journal of Applied Mechanics, Vol. 33, No. 4, Trans. ASME, Vol. 88, Series E, Dec. 1966, 893-900.

[10] Iwan, W.D., "On a Class of Models for the Yielding Behavior of Continuous and Composite Systems," Journal of Applied Mechanics, Vol. 34, No. 3, September 1967, 612-617.

[11] Takeda, T., Sozen, M.A. and Nielsen, N.N., "Reinforced Concrete Response to Simulated Earthquake," ASCE, Journal of the Structural Division, Vol. 96, December 1970, 2557-2573.

[12] Toussi, S. and Yao, J., "Identification of Hysteretic Behavior for Existing Structures," Report CE-STR-80-19, School of Civil Engineering, Purdue University, December 1980.

[13] Toussi, S. and Yao, J., "Hysteretic Identification of Multi-Story Buildings," Report CE-STR-81-15, School of Civil Engineering, Purdue University, May 1981.

[14] Masri, S.F. and Caughey, T.K., "A Nonparametric Identification Technique for Nonlinear Dynamic Problems," Journal of Applied Mechanics, Vol. 46, June 1979, 433-447.

[15] Wen, Y.K., "Method for Random Vibration of Hysteretic Systems," ASCE, Journal of the Engineering Mechanics Division, Vol. 102, April 1976, 249-263.

[16] Saiidi, M. and Sozen, M., "A Naive Model for Nonlinear Response of Reinforced Concrete Buildings," Proceedings of the 7th World Conference on Earthquake Engineering, Istanbul, Turkey, 1980, Vol. 7, 8-14.

[17] Muguruma, M., Tominaga, M. and Watanabe, F., "Response Analysis of Reinforced Concrete Structures Under Seismic Forces," Proceedings of the Fifth World Conference on Earthquake Engineering, Rome, Italy, 1974, Vol. 1, 1389-1392.

[18] Aoyama, H., "Simple Nonlinear Models for the Seismic Response of Reinforced Concrete Buildings," Proceedings of the Review Meeting U.S.-Japan Cooperative Research Program in Earthquake Engineering, Tokyo, Japan, 1976, 291-309.

[19] Atalay, B. and Penzien, J., "Inelastic Cyclic Behavior of Reinforced Concrete Flexural Members," Proceedings of the Sixth World Conference on Earthquake Engineering, New Delhi, India, 1977, Vol. III, 3062-3068.

[20] Gates, N.C., "The Earthquake Response of Deteriorating Systems," Earthquake Engineering Research Laboratory Report No. EERL-77-03, California Institute of Technology, Pasadena, California, March 1977.

[21] Kreger, M. and Sozen, M., "A Study of the Causes of Column Failures in the Imperial County Services Building During the 15 October 1979, Imperial Valley Earthquake," Report UILU-ENG-83-2013, Civil Engineering Studies, Structural Research Series No. 509, University of Illinois at Urbana-Champaign, Urbana, Illinois, August 1983.

CHAPTER II

DETERMINING THE NATURE OF STRUCTURAL BEHAVIOR FROM EARTHQUAKE RECORDS

2.1 INTRODUCTION

The objective of this chapter is to present insight, concerning the dynamic behavior of actual buildings subjected to strong ground motions. For this purpose, several earthquake records will be analyzed and some conclusions regarding the nature of the restoring force behavior will be drawn.

It will be assumed that data are available on the earthquake response of a building which has been instrumented with at least two accelerographs; typically, one at the roof level, and the other at the basement or first floor level. The accelerographs provide records corresponding to the absolute horizontal acceleration, $\ddot{y}(t)$ and $\ddot{z}(t)$, as shown in Figure 2.1.

After processing, the accelerograph records will consist of a sequence of points containing discrete values of acceleration. A common practice is to consider 50 points per second. By means of numerical integration, it is possible (at least in principle), to obtain the absolute velocities and displacements $\dot{y}(t)$, $\dot{z}(t)$, $y(t)$ and $z(t)$, as well as the relative acceleration, velocity and displacement $\ddot{x}(t)$, $\dot{x}(t)$ and

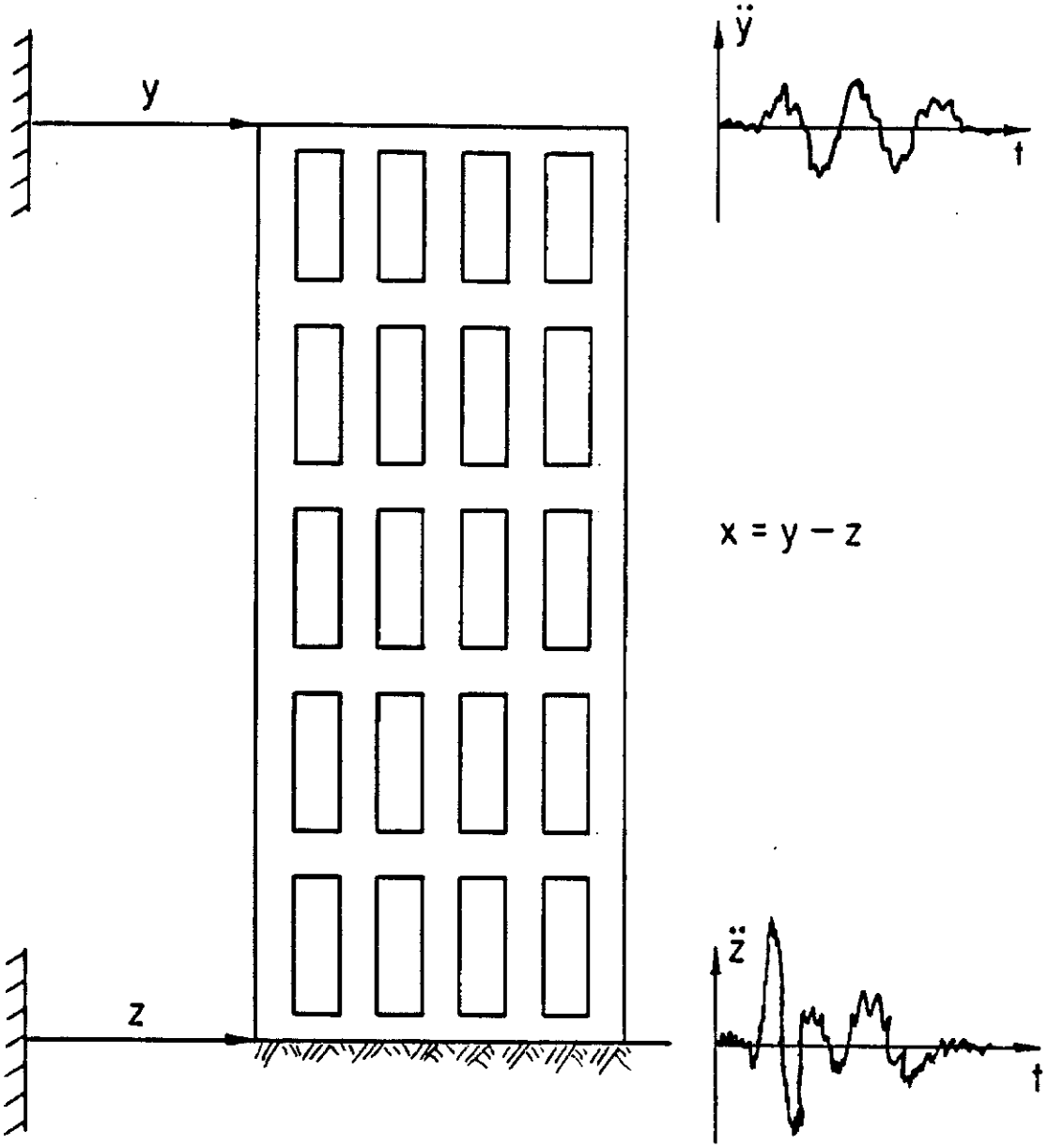

Figure 2.1 Typical building instrumented with two accelerographs, one at the roof level and one at the basement level.

$\ddot{z}(t)$. Two results, those corresponding to $\ddot{z}(t)$ and $x(t)$, will play a crucial role in the present study.

2.2 RESTORING FORCE AND STRUCTURAL BEHAVIOR

This section is concerned with the role of the restoring force as a vehicle to study the nature of the dynamic behavior of a structural system.

2.2.1 The Single-Degree-of-Freedom Oscillator

It will be assumed that the relationship between the relative displacement of the roof of the building under study (x), and the ground acceleration ($\ddot{z}$), can be represented as a single-degree-of-freedom (SDOF) oscillator. The equation of motion will then be:

$$M\ddot{x} + F(x,\dot{x}) = -M\ddot{z} \tag{2.1}$$

in which $F(x,\dot{x})$ represents the restoring force due to relative velocity, $\dot{x}$; and relative displacement, x; M is an equivalent mass. This assumption is based on the fact that normally the first mode dominates the time history of the earthquake response of a building.

It is important to notice that the nature of the response of the system will be reflected in the restoring force $F(x,\dot{x})$. Therefore, the structural behavior of the system can be investigated through this function. Consider for example the case in which the restoring force can be expressed as a function of the form

$$F(x,\dot{x}) = C\dot{x} + g(x) \tag{2.2}$$

where C is the viscous damping coefficient, and g(x) represents the contribution due to the stiffness of the system or "spring force". Depending on the characteristics of g(x), two types of behavior that will be of particular interest in this study can be distinguished, i.e., linear behavior and hysteretic behavior. In the case of linear behavior the function g(x) is expressed as

$$g(x) = Kx \tag{2.3}$$

where K is the linear stiffness of the system. Notice that in this case the contribution to the total restoring force at a particular given time, depends only on the value of x at that time, as illustrated in Figure 2.2(a). On the contrary, in the case of hysteretic systems the contribution to the total restoring force -- arising from g(x) -- is essentially history dependent, i.e., the value of the function g(x) at a given time depends not only on the value of x at that time, but also on the previous values of x.

For the purpose of this study it is important to discuss the hysteretic systems that exhibit stiffness reduction. These systems can be divided in two categories: nondeteriorating systems and deteriorating systems. The features of each one can be appreciated better by means of the restoring force diagrams shown in Figure 2.2(b) and 2.2(c). Figure 2.2(b) shows a typical function g(x) for a hysteretic non-deteriorating system. It is noted that even though there is a reduction

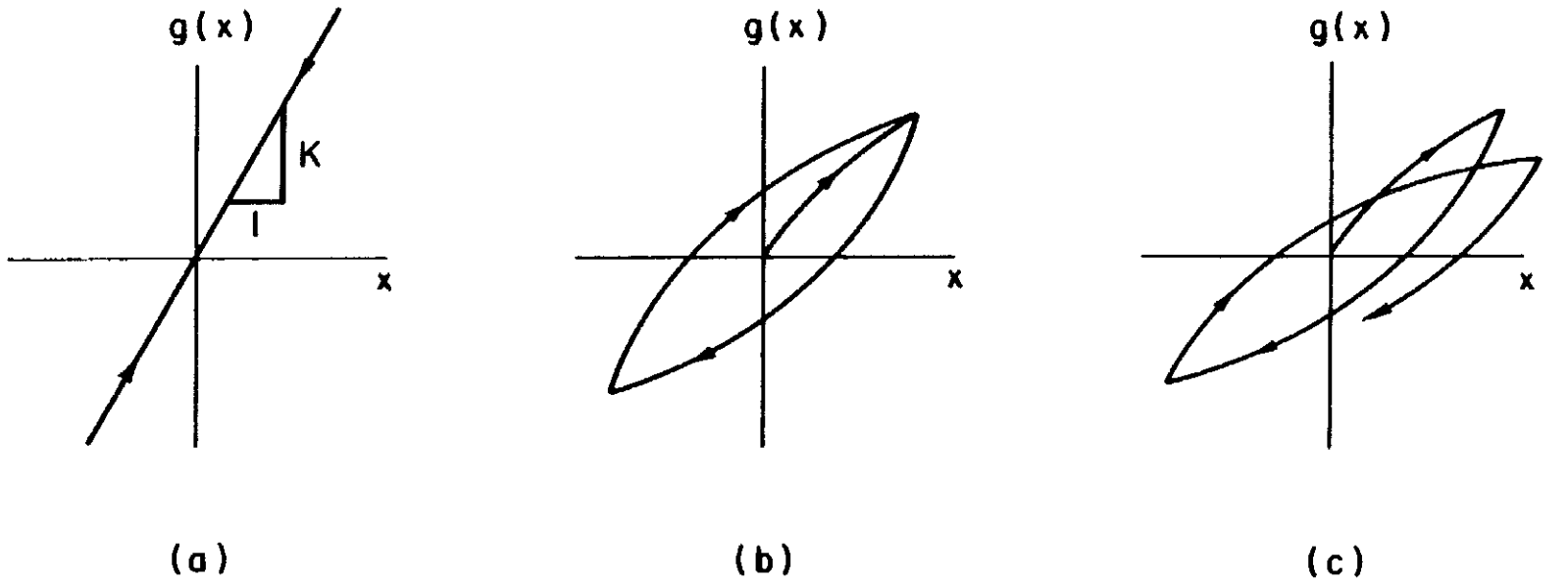

Figure 2.2 Function g(x) for three different cases, (a) linear system (b) hysteretic non-deteriorating system and (c) hysteretic deteriorating system.

of stiffness when x increases, this is not permanent. In fact, provided one chooses the appropriate loading-unloading pattern it is possible to reproduce again the relationship observed between x and g(x) in a previous cycle. Figure 2.2(c) depicts the restoring force g(x) in the case of a hysteretic deteriorating system. In this case a progressive loss of stiffness with cyclic loading is observed and it is not possible to reproduce the relationship observed between x and g(x) in a previous cycle, no matter what loading-unloading pattern is chosen. That is, the system exhibits permanent reduction of stiffness with cyclic loading. This phenomenon is known as stiffness degradation or more simply, deterioration. The loops that describe the relationship between the restoring force and relative displacement in a loading-unloading cycle for the case of hysteretic systems, are called hysteresis loops.

2.2.2 The Linear Single-Degree-of-Freedom Oscillator

In this section, some characteristics of the linear SDOF oscillator will be discussed in more depth. This background is important in understanding the difference between linear behavior, and that exhibited by buildings in which linear models have failed to match the earthquake response.

The equation of motion of a linear SDOF oscillator is (2.1), in which

$$F(x,\dot{x}) = Kx + C\dot{x} \qquad (2.4)$$

where K is the linear stiffness and C is the viscous damping coefficient. Then (2.1) can be written as,

$$\ddot{x} + 2\zeta\omega_0\dot{x} + \omega_0^2 x = -\ddot{z} \tag{2.5}$$

where,

$$\omega_0^2 = \frac{K}{M} \tag{2.6}$$

and

$$\zeta = \frac{C}{2\sqrt{KM}} \tag{2.7}$$

ω_0 is the natural frequency of the system and ζ is the fraction of critical damping.

Consider the response to a harmonic forcing function of the form

$$\ddot{z}(t) = -a_0 \sin \omega t \tag{2.8}$$

The steady-state solution in this case is given by

$$x(t) = A \sin \theta \tag{2.9}$$

where,

$$A = \frac{-a_0}{\left[(\omega_0^2-\omega^2)^2 + (2\zeta\omega\omega_0)^2\right]^{1/2}} \tag{2.10}$$

and

$$\theta = \omega t - tg^{-1}\left(\frac{2\zeta\omega\omega_0}{\omega_0^2-\omega^2}\right) \tag{2.11}$$

Noting that

$$\dot{x}(t) = A\omega \cos\theta \tag{2.12}$$

and combining (2.9) and (2.12) the following relationship can be established between x and $\dot{x}$,

$$x^2 + \frac{\dot{x}^2}{\omega^2} = A^2 \tag{2.13}$$

Using (2.13), $\dot{x}$ can be substituted in (2.4) to obtain

$$F(x,\dot{x}) = Kx + CA\omega\sqrt{1-x^2/A^2} \tag{2.14}$$

Rearranging (2.14) and squaring one gets

$$F^2 + (K^2+C^2\omega^2)x^2 - 2FKx = C^2A^2\omega^2 \tag{2.15}$$

where F is simply $F(x,\dot{x})$. Let f be the restoring force per unit of mass, i.e.:

$$f \equiv \frac{F}{M} \tag{2.16}$$

Substituting (2.16) into (2.15) and using (2.6) yields

$$f^2 + \left[\omega_0^4 + \frac{C^2\omega^2}{M^2}\right]x^2 - 2f\omega_0^2 x = \frac{C^2A^2\omega^2}{M^2} \tag{2.17}$$

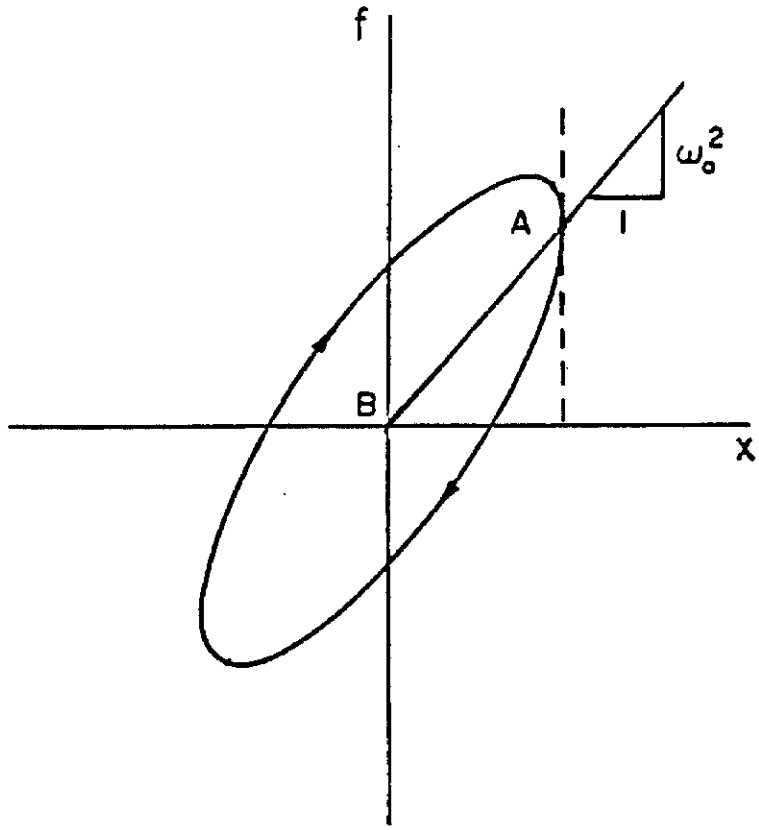

Figure 2.3 Restoring force diagram for the steady-state harmonic response of a linear oscillator.

Equation (2.17) represents an ellipse in the f-x plane. Figure 2.3 depicts this ellipse. Note that the slope of the line A-B is equal to ω_0^2. The area of the ellipse, $\pi C\omega A^2/M$, is equal to the energy dissipated per unit of mass by the oscillator in one cycle. The ellipse is traversed in a clockwise direction as indicated.

Next, consider an earthquake type excitation. Figure 2.4 shows a typical ground acceleration recorded during an earthquake at the basement of a building. Figure 2.5 displays the restoring force behavior for the same linear oscillator subjected now to the earthquake excitation. It is noted that the slope of the line between the origin and the point of maximum displacement in each of the subellipses remains constant and equal to ω_0^2. This is not surprising since the slope of the semi-major axis of the ellipse for the case of harmonic excitation was independent of the frequency of the excitation.

2.2.3 Restoring Force Diagrams and Earthquake Records

Let equation (2.1) be rewritten in the following form

$$\frac{F(x,\dot{x})}{M} = -(\ddot{x} + \ddot{z}) = \ddot{y} \qquad (2.18)$$

The left hand side is the restoring force per unit of mass, f, as defined in (2.16).

Since the earthquake records provide both, $\ddot{z}(t)$ and $\ddot{y}(t)$, it is possible to determine $f(x,\dot{x})$ on a discrete set of points. Moreover, it is possible to plot $f(x,\dot{x})$ as a function of x, and obtain the restoring force diagram corresponding to a particular mode of the response of the

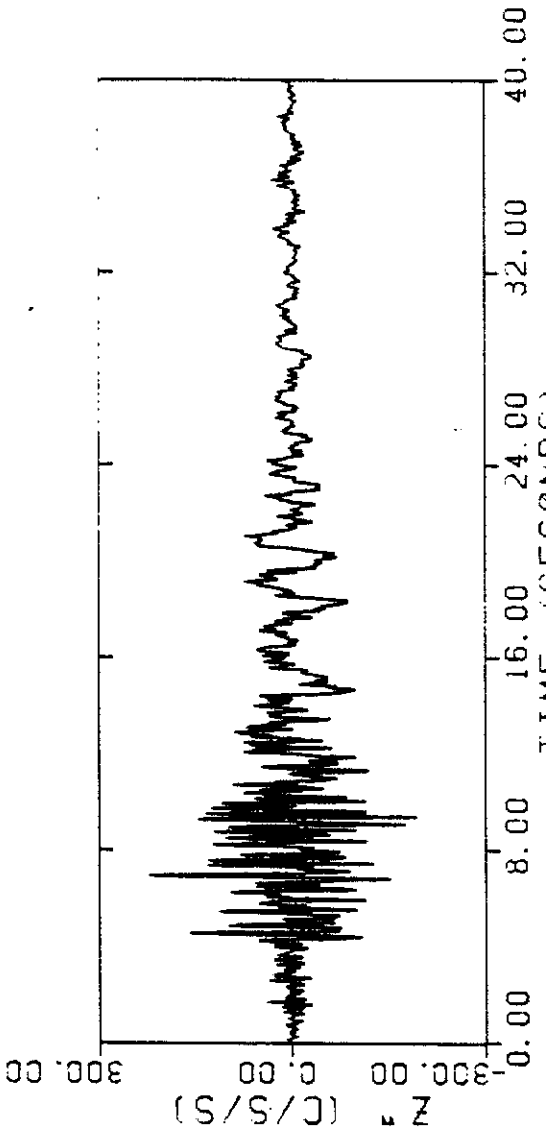

Figure 2.4 Typical ground acceleration time history

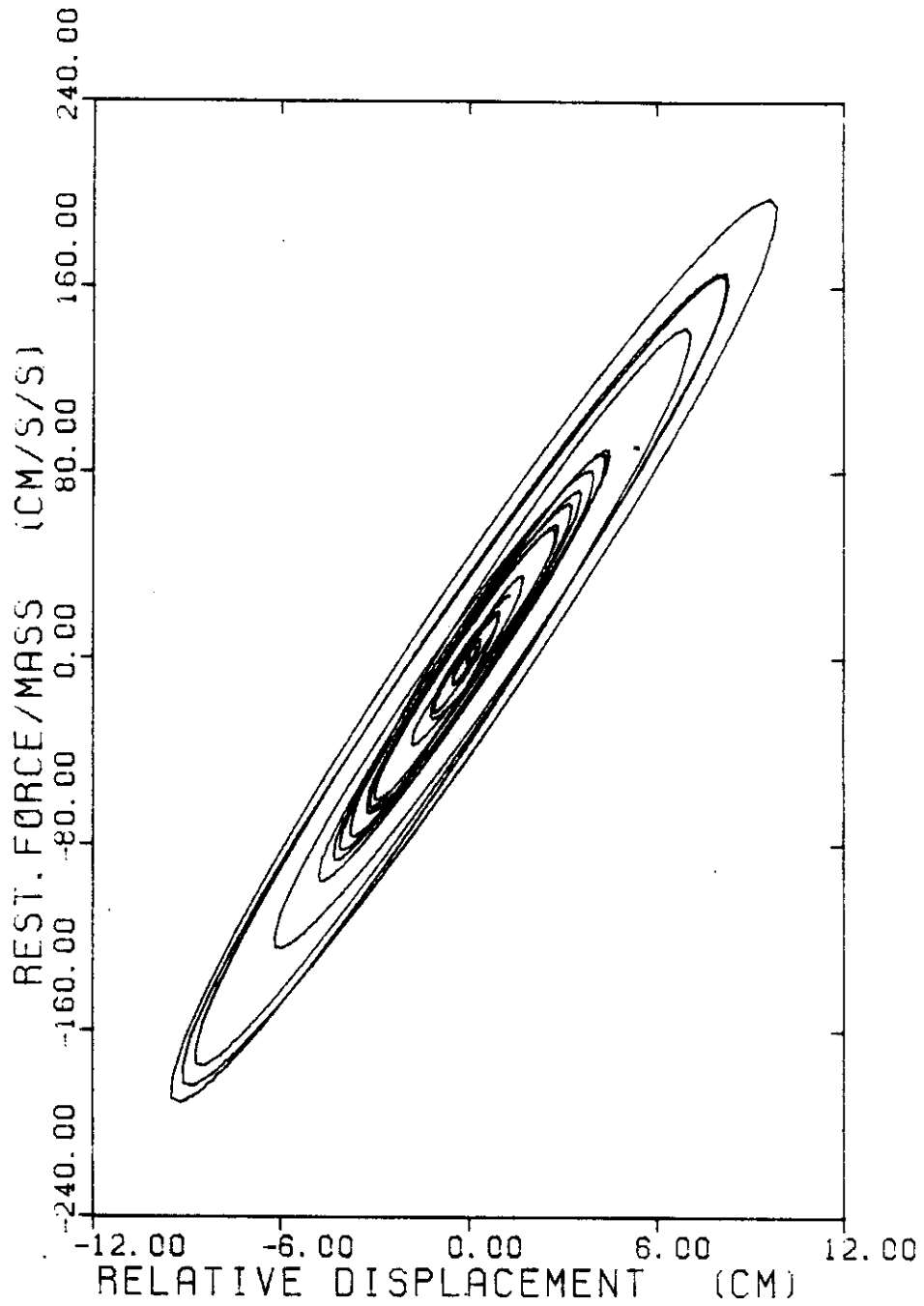

Figure 2.5 Restoring force diagram for the case of a linear oscillator subjected to earthquake excitation.

building under consideration. This interesting idea was first exploited by Iemura and Jennings [3]. It provides a useful mechanism for visualizing the characteristics of the restoring force as a function of x. This approach will be used to examine the restoring force behavior of several buildings.

2.3 COMPUTATION OF THE RESTORING FORCE DIAGRAMS

Several restoring force diagrams showing the structural behavior of different buildings have been examined as part of this research. The discussion presented herein will be illustrated with examples taken from the following reinforced concrete structures:

1) Bank of California Building, 15250 Ventura Blvd. N11E and N79W component (CIT Vol. II, files H115 and H117). This structure was extensively damaged during the San Fernando earthquake of 1971. McVerry [1] showed that it was not possible to fit a linear model to the response of this structure. A more exhaustive analysis of the performance of this building can be found in [1], [5] and [10].

2) Holiday Inn Building, 8244 Orion. N00W and S90W component (CIT Vol. II, files D062 and D064). This building was also seriously damaged during the San Fernando earthquake [1], [5], [10]. Again, linear modelling failed to match the response of the structure.

3) Imperial County Services Building. E-W component (CIT Vol. II, files Z002.N90E.TR4 and Z002.N90E.TR13). The failure of this building during the 1979 Imperial Valley earthquake has been the subject of many engineering reports [6], [7]. As expected from the degree of structural

damage, analysis of the record show that the response of this building was markedly nonlinear [7], [12].

2.3.1 Elimination of the Influence of Higher Modes

Consider the N11E component of the Bank of California building. Figure 2.6 shows the restoring force diagram obtained from the earthquake records following the approach indicated in Section 2.2.3. It is clear from this figure that it is rather difficult to extract any conclusions regarding the general nature of the restoring force. One of the reasons for this is the presence of a number of modes of response in the time history of the structure. Recalling that it was assumed that the transfer function between the relative displacement of the roof of the building (x) and the ground acceleration ($\ddot{z}$) could be represented as a SDOF oscillator, it was decided to apply a low pass filter to the data. The motivation for this operation is to be able to observe more clearly the features of the fundamental mode, which is normally the mode that dominates the response. The low pass filtering operation essentially removes all frequencies larger than the cutoff frequency of the filter. Figure 2.7 shows an ideal low pass filter and its effect on a typical response signal.

In practice, there are several ways to perform the low pass filtering operation. In the present investigation, a nonrecursive low pass filter using a Fourier series approximation was used. This technique has been described in detail by Blimchikoof and Zvenev [11].

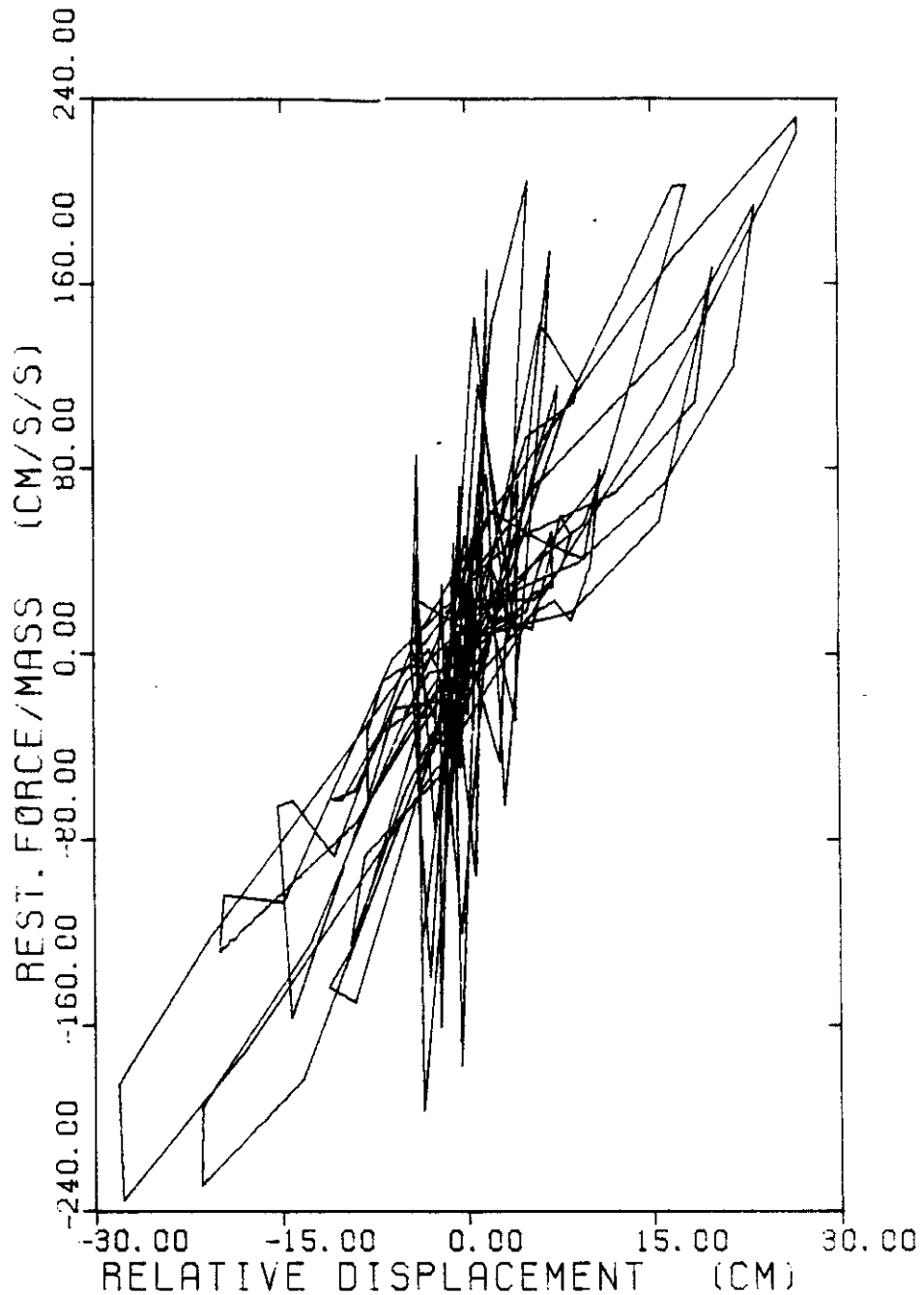

Figure 2.6 Bank of California building, N11E component. Restoring force diagram obtained directly from the earthquake records.

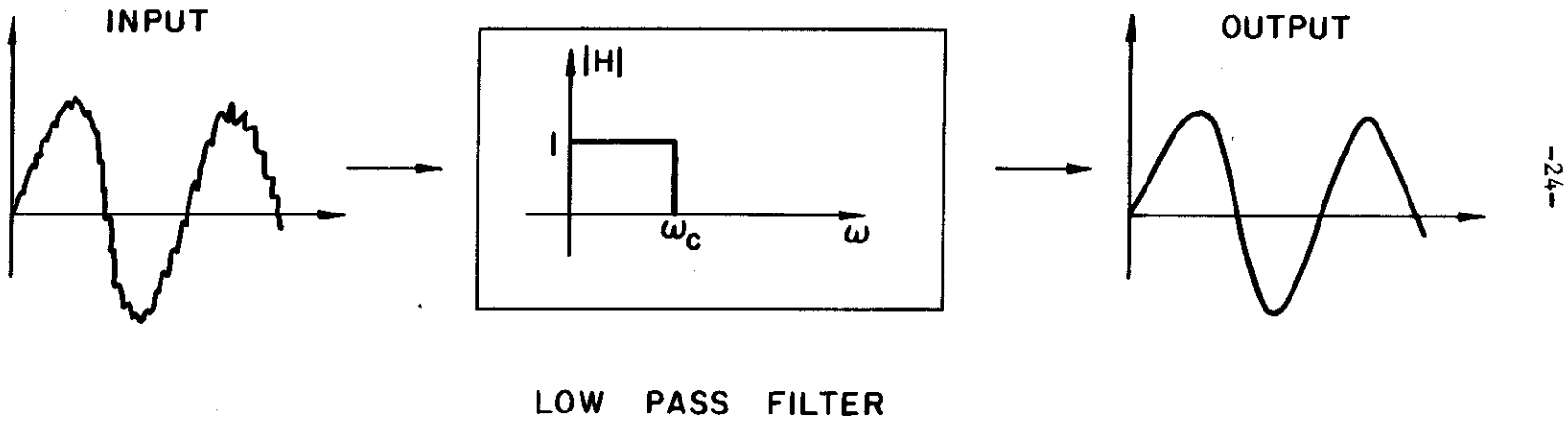

Figure 2.7 Ideal low pass filter and its effect on a given signal.

The determination of the appropriate cutoff frequency was made by inspection of the Fourier amplitude spectrum of the response acceleration [8]. This is shown for the Bank of California record (N11E component) in Figure 2.8. This figure suggests an appropriate cutoff frequency of 1Hz to eliminate the influence of higher modes on the earthquake data.

Figure 2.9 depicts the new version of the restoring force diagram corresponding to the N11E component of the Bank of California, after low pass filtering the earthquake records. A comparison with Figure 2.6 is almost self explanatory. In Figure 2.9 one can easily observe a consistent pattern of structural behavior, namely stiffness degradation, while in Figure 2.6 it was not possible to detect this phenomenon. Further consideration of this matter will be presented in Section 2.4.1.

The example quite clearly shows the advantage of low pass filtering of the data. By means of this technique, one can easily examine the relationship between the restoring force and the relative displacement. Otherwise, the interpretation of the restoring force diagrams is very difficult.

2.3.2 Synchronization of the Records

When computing the restoring force per unit of mass and the relative displacement of the roof with respect to the first floor, it is necessary that both records be synchronized. This means, that the record at the roof and the record at the first floor should have the same time origin, and maintain the same time progression throughout the

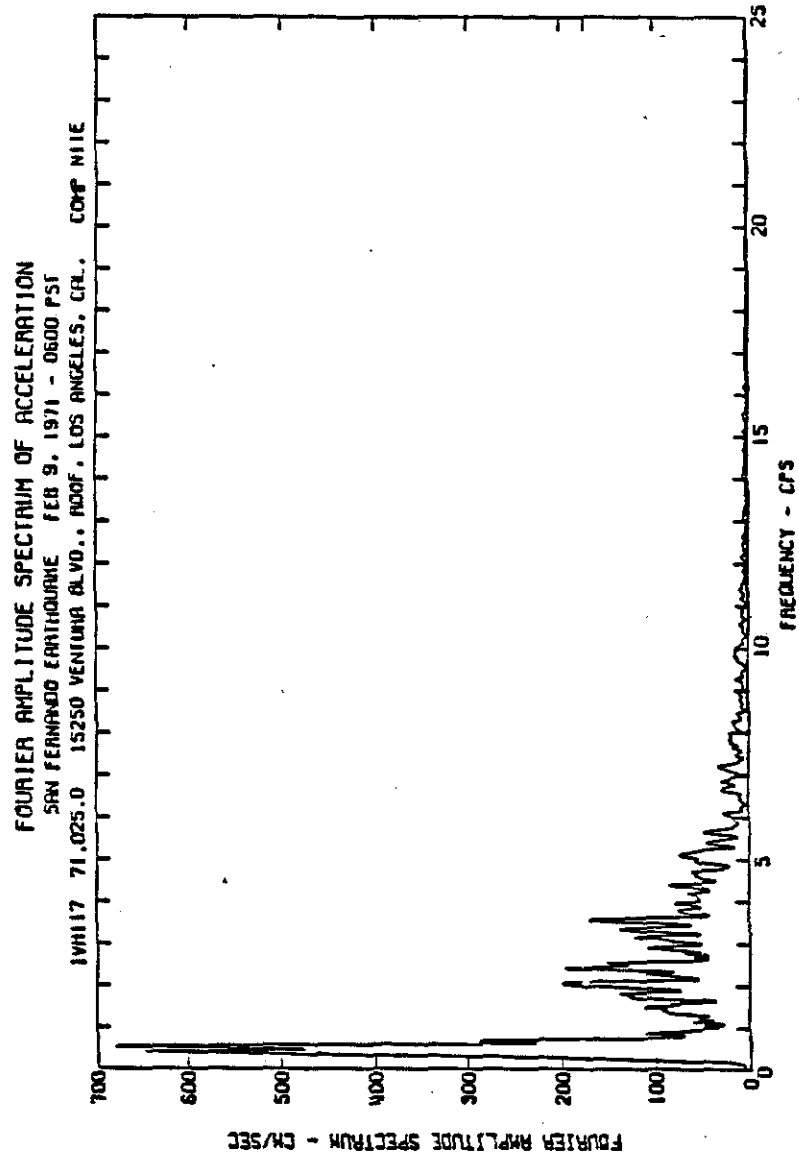

Figure 2.8 Bank of California building, N11E component. Fourier amplitude spectrum of acceleration.

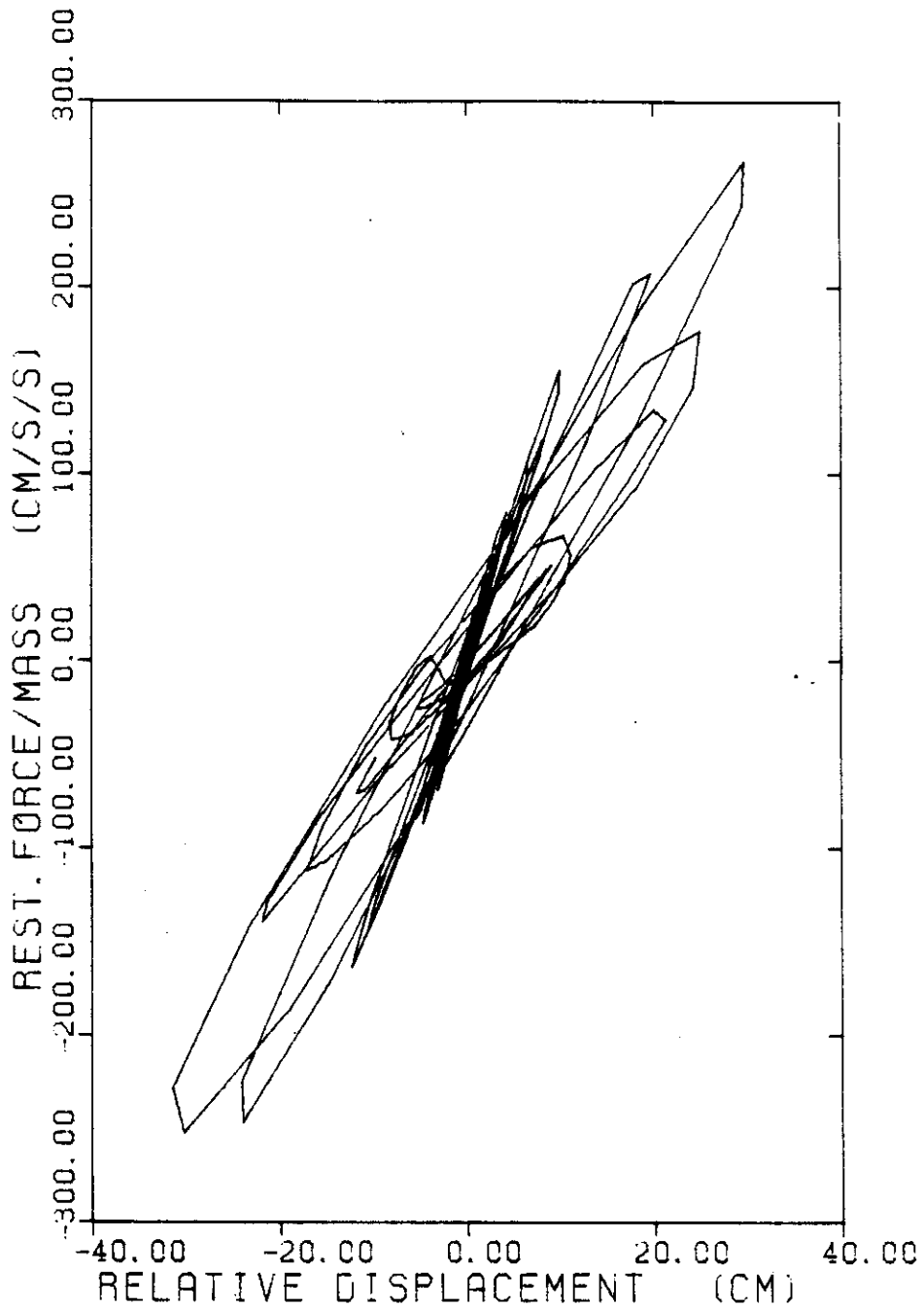

Figure 2.9 Bank of California building, N11E component. Restoring force diagram after low pass filtering the acceleration and displacement records.

entire record. Unfortunately, these conditions are not always satisfied. The records may not be synchronized due to the fact that both instruments did not start recording at precisely the same time, or as a consequence of the digitization process. This problem has also been described by McVerry and Beck [13] and Iemura and Jennings [3] as it related to the response of Millikan library during the San Fernando earthquake.

To find out whether this problem is present, it is helpful to examine the restoring force behavior within a small time window; usually between 3 to 5 seconds depending on the natural period of the structure. To clarify this point, consider again the N11E component of the Bank of California. Figure 2.10 displays the restoring force diagram corresponding to the time interval between 32 and 36 seconds. It is seen that the direction of the hysteresis loop is negative, i.e., counterclockwise rather than clockwise. This is not physically possible, since it would indicate that the structural system is putting energy into motion instead of dissipating energy while oscillating. This observation suggests that there is a shift of one record with respect to the other. To correct this problem, the appropriate shift, Δt, must be determined.

One way to determine the appropriate time shift, is to plot the restoring force diagram for several values of Δt and select the smallest Δt (in absolute value) that makes the negative loops become positive. This approach was employed in this example, and a value of $\Delta t = 0.07$

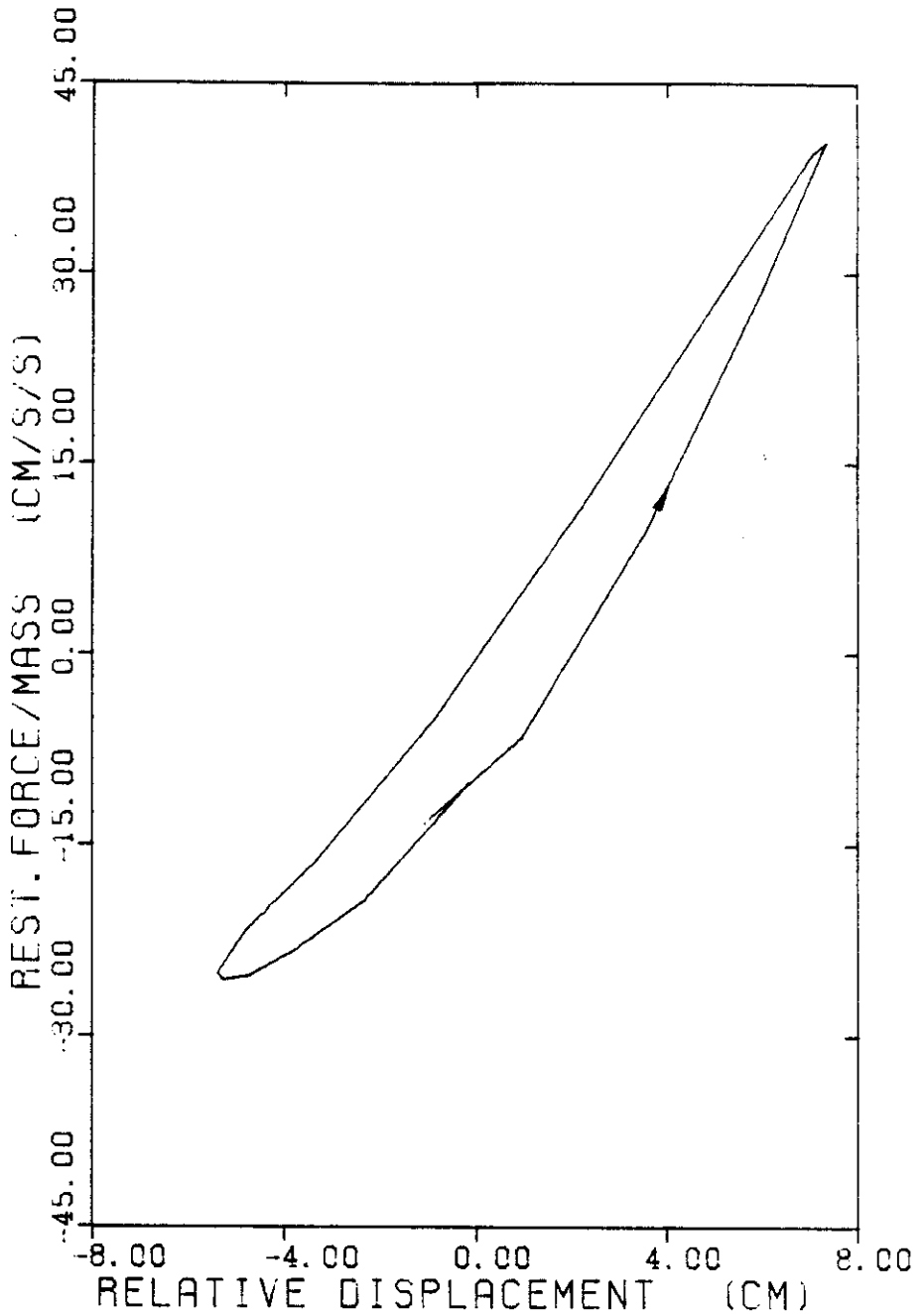

Figure 2.10 Bank of California building, N11E component. Restoring force diagram for the time interval 32-36 seconds.

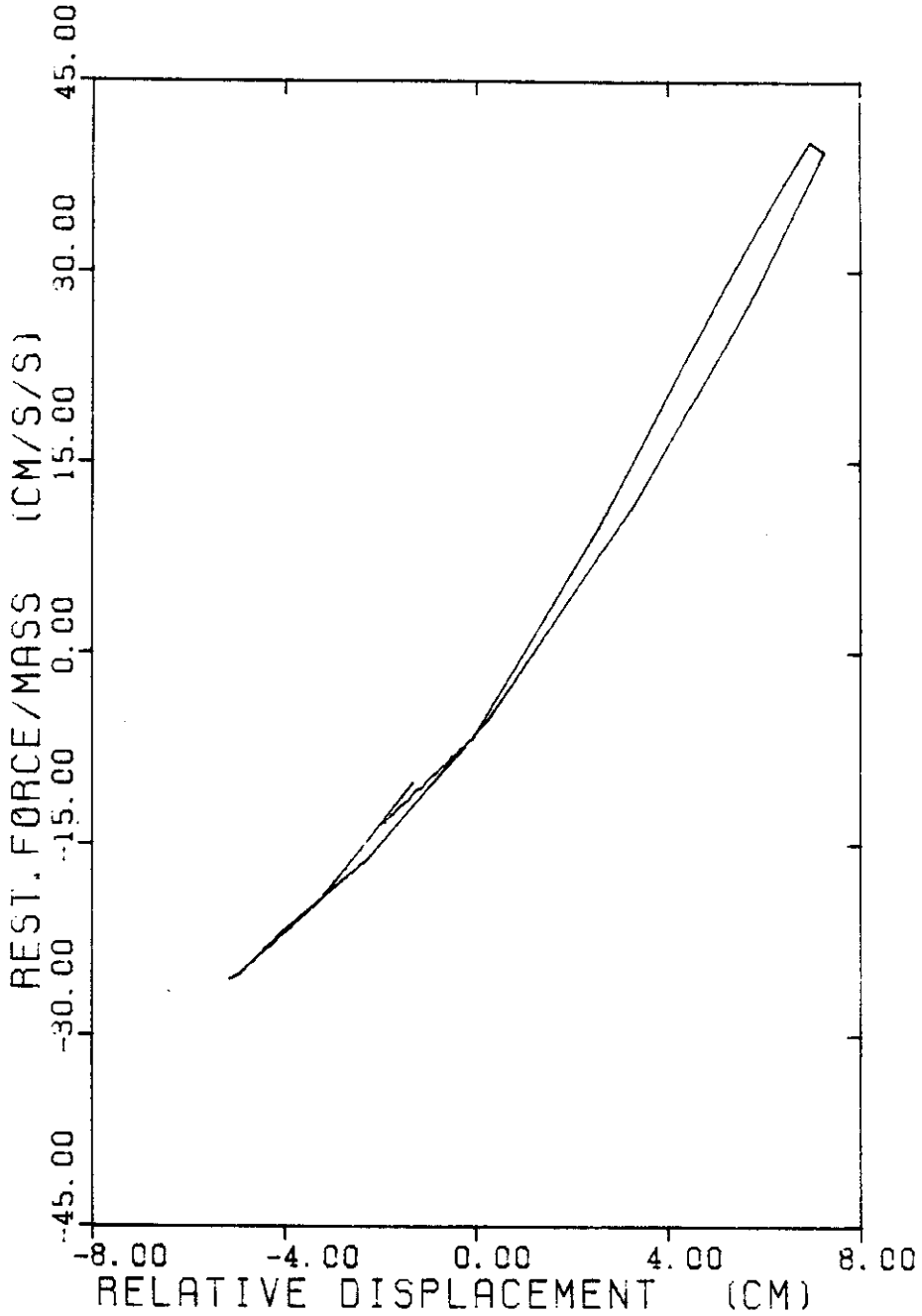

Figure 2.11 Bank of California building, N11E component. Restoring force diagram for the time interval 32-36 seconds after synchronizing the records.

seconds was obtained. Figure 2.11 shows the restoring force diagram given by the corrected records.

In this particular case, the shift was applied only to the last portion of the record, 32-40 seconds. The reason was the following. During the digitization process this record was cut into 8 second segments [9], and then enlarged. Since no evidence of negative loops appeared in the first portion of the record, and since 32 is a multiple of 8, it is reasonable to assume that the error was introduced at this time; probably when matching the end of the third segment with the beginning of the fourth segment.

Figure 2.12 shows the complete restoring force diagram, once the time shift correction has been applied. As far as the general appearance of the hysteresis loops is concerned, no significant difference can be detected between this diagram and the diagram depicted in Figure 2.9. However, in future computations this correction can be important. More will be said about this point in Chapter 5.

2.3.3 Long Period Errors

Long period errors can totally change the appearance of the restoring force diagrams and lead to misleading results. As a general recommendation, records should not be assumed to be free of this source of error unless carefully checked. Several authors have studied this problem including Berg and Housner [14] and Boyce [15] among others. However, its treatment has not yet been standarized.

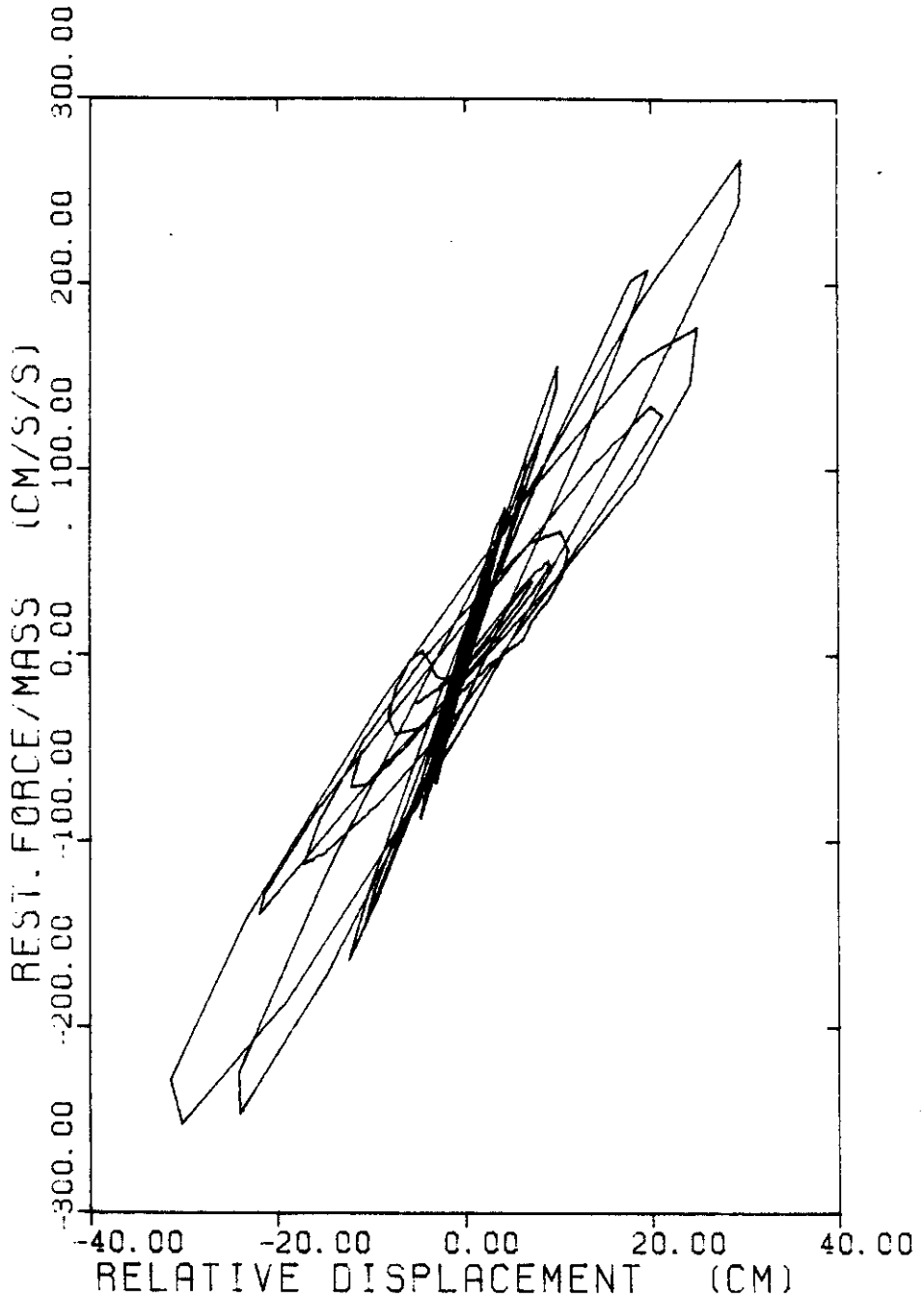

Figure 2.12 Bank of California building, N11E component. Corrected version of the restoring force diagram.

Consider, for example, the N00W component of the Holiday Inn Orion. The restoring force behavior as a function of the relative displacement is shown in Figure 2.13(a). This diagram was plotted after low pass filtering the digitized data with a cutoff value of 1.0 Hz.

A simple inspection of this figure suggests some strange characteristics. One notes the presence of a displacement drifting behavior of obscure physical interpretation. This is particularly apparent in the intervals of 25-30 seconds and 30-35 seconds as shown in Figure 2.13(b) and 2.13(c).

To better understand this behavior, the time history of the response was also plotted (Figure 2.14). The existence of a long period signal can be detected from this figure. When this record was originally processed, it was high pass filtered with an Ormsby filter having a cutoff frequency of 0.07 cps and a rolloff termination frequency of 0.05 cps [9]. According to Figure 2.14, a higher cutoff value would possibly have been more appropriate. This, since the period of the noise can be approximately estimated from this figure around 10 seconds.

To determine the appropriate cutoff frequency, the uncorrected data were treated as follows: a nonrecursive high pass Fourier type filter was applied using several cutoff values. Then, the corresponding restoring force-relative displacement diagrams were plotted. The smallest cutoff frequency that eliminated the displacement drifting behavior from the restoring force diagram was considered to be the

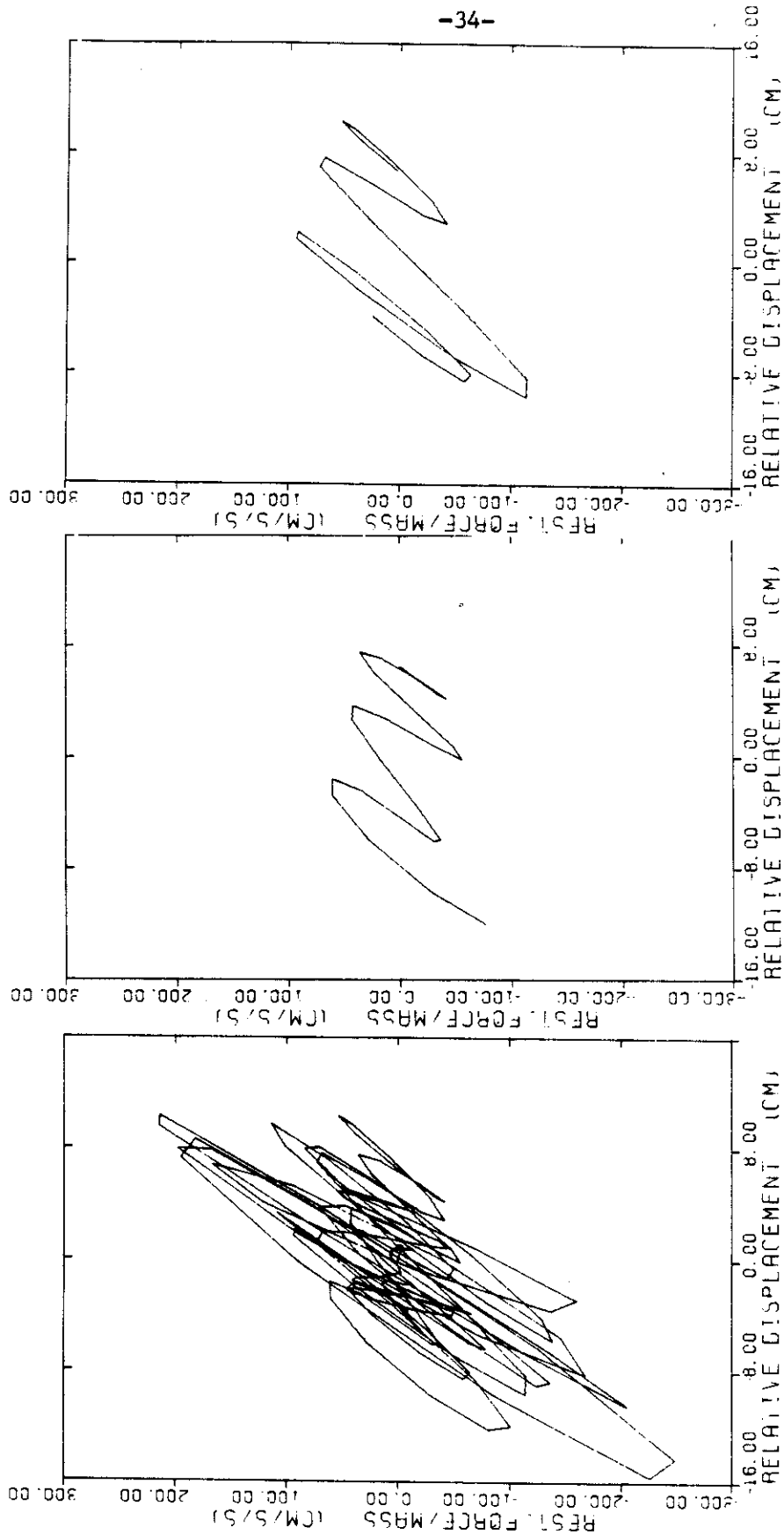

Figure 2.13 Holiday Inn building, NOOW component. Restoring force diagram for three different time intervals (a) 0.0-40.0 seconds (b) 25.0-30.0 seconds (c) 30.0-35.0 seconds

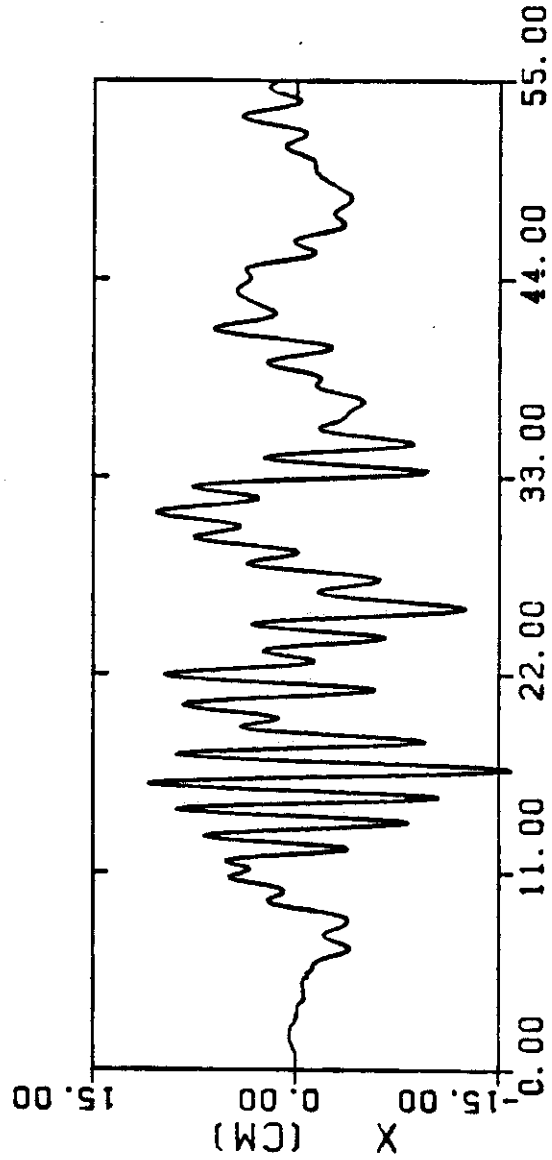

Figure 2.14 Holiday Inn building, N00W component. Time history of the response.

appropriate cutoff value. In this case, the value chosen was 0.57 Hz, which corresponds to a period of 1.75 seconds.

Figures 2.15 and 2.16 show the corrected version of the restoring force diagram and the time history of the response, after applying the high pass filter. The difference between these figures and those corresponding to the uncorrected case (Figures 2.13 and 2.14) is quite evident.

In view of the importance of this correction, another example will be discussed. Figure 2.17(a) depicts the restoring force behavior, corresponding to the E-W component of the Imperial County Services Building. The digitized data were previously low pass filtered using a cutoff value of 1.8 Hz, as recommended in Section 2.3.1. Here, the problem is not as clear as it was in the Holiday Inn case. However, it is possible to detect the same displacement drifting behavior already mentioned. This is apparent in the interval between 0.0 and 7.4 seconds and 24.0 and 30.0 seconds as shown in Figures 2.17(b) and 2.17(c).

After applying a high pass filter with a cutoff value of 0.33 Hz, these problems disappear. Figure 2.18 shows the corrected version of the restoring force diagram.

More than twenty other records of the San Fernando earthquake were examined to detect the presence of long period noise using the approach described above, i.e., investigating the presence of a displacement drifting behavior in the restoring force diagram. In many cases this problem seems to be serious, and the original cutoff frequency of 0.07 Hz would have to be increased. The determination of the

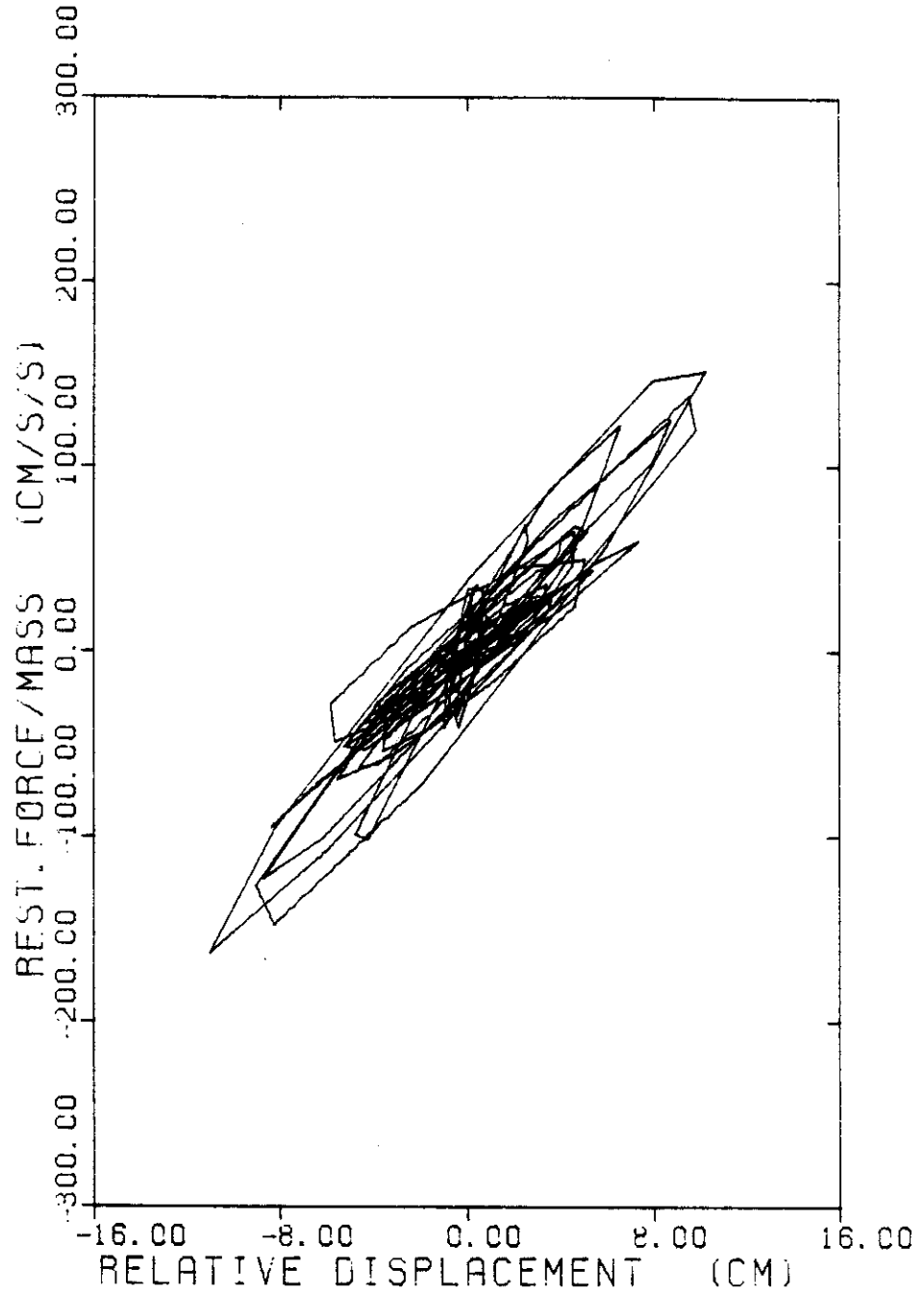

Figure 2.15 Holiday Inn building, N00W component. Corrected version of the restoring force diagram.

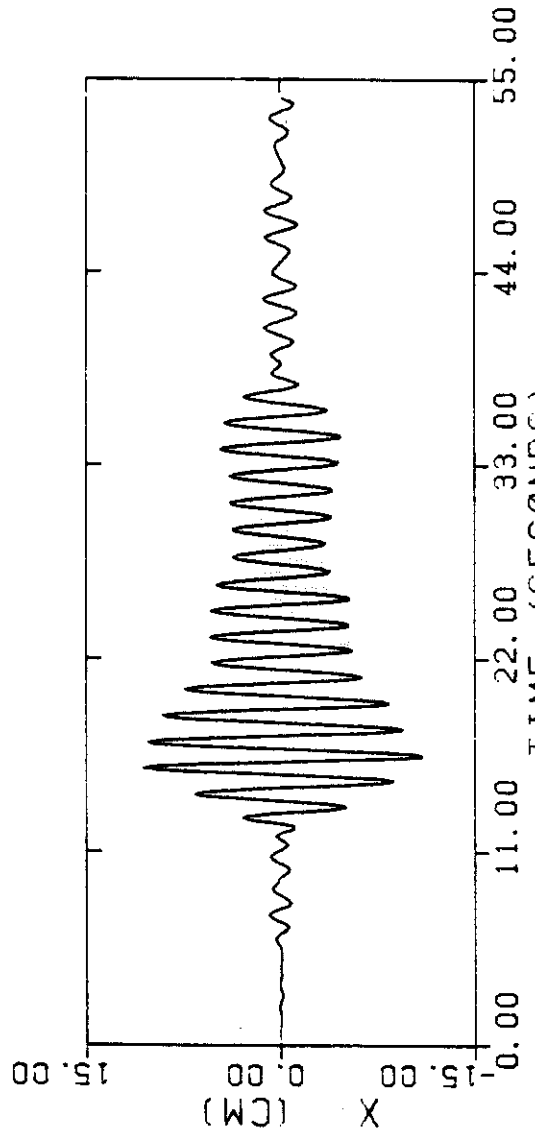

Figure 2.16 Holiday Inn building, N00W component. Corrected version of the time history of the response.

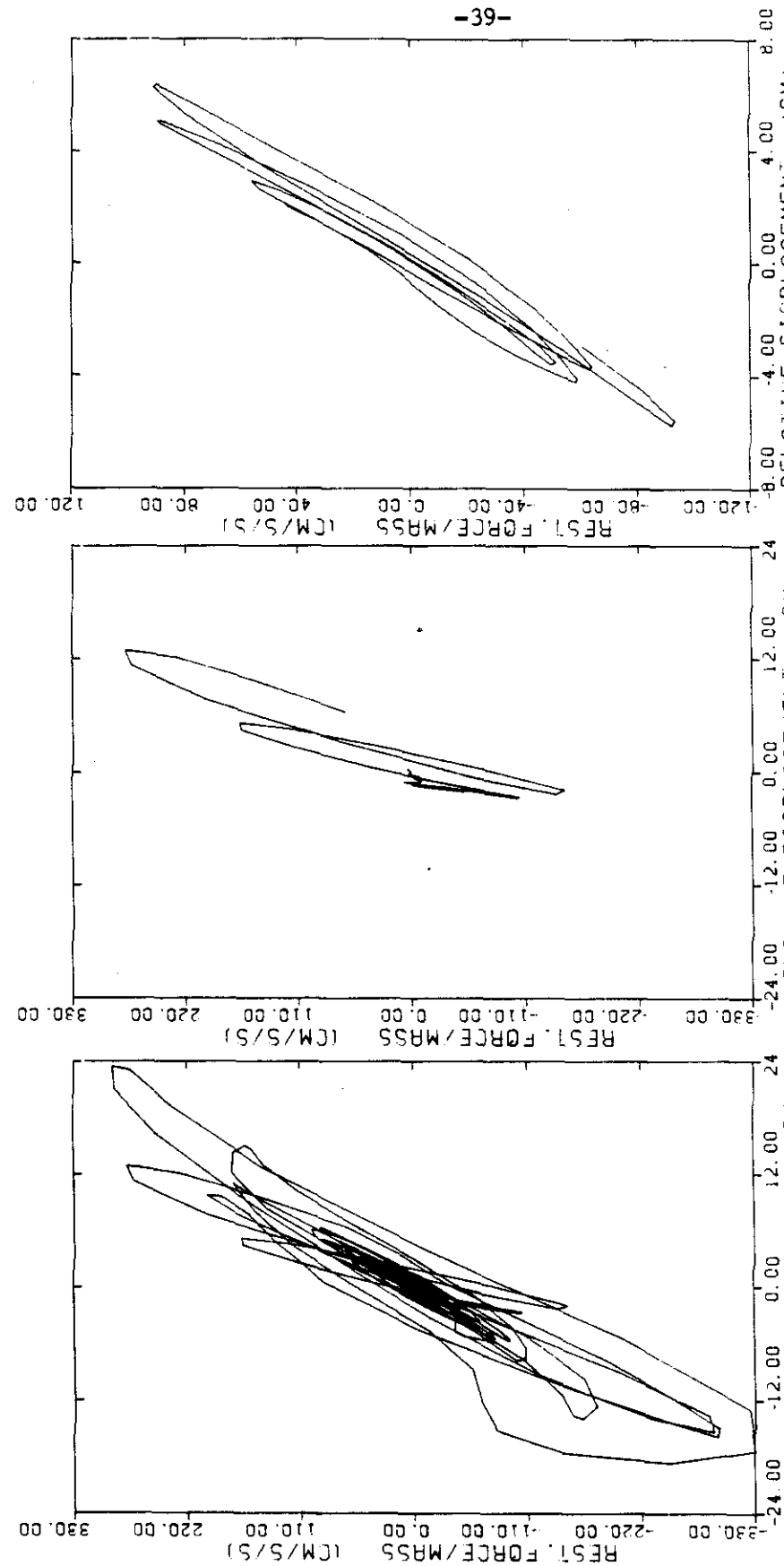

Figure 2.17 Imperial County Services building. Restoring force diagram for three different time intervals (a) 0.0-40.0 seconds (b) 0.0-7.4 seconds (c) 24.0-30.0 seconds.

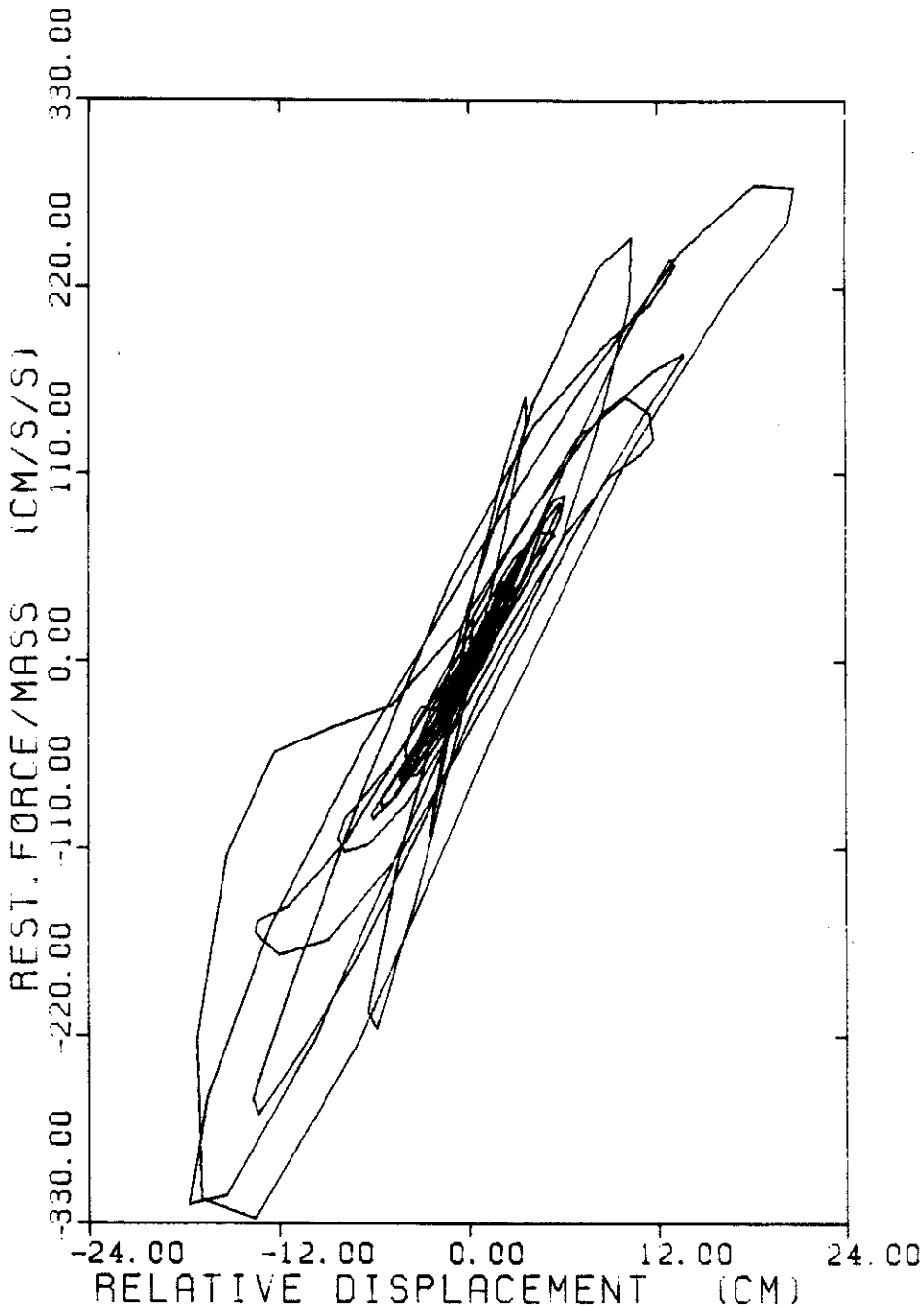

Figure 2.18 Imperial County Services building. Corrected version of the restoring force diagram.

appropriate cutoff value to high pass filter the data in each case, can be done following the procedure previously outlined. Some of the records severely affected by this situation were:

- Holiday Inn Marengo
- 4867 Sunset Boulevard
- 420 North Boxbury
- 533 Freemont Street
- 120 North Robertson
- 468 Wilshire Boulevard

This problem will not be considered in greater detail herein since it is not the aim of this thesis to fully study the long period error problem. However, it is important to mention that this point deserves more attention and research.

2.4 CHARACTERISTICS OF STRUCTURAL BEHAVIOR

Figure 2.19 shows the fully corrected version of the restoring force diagrams, corresponding to the five cases examined in this study. These diagrams can be considered descriptive of the structural behavior of reinforced concrete buildings, under moderate to high loading.

2.4.1 Observations from the Restoring Force Diagrams

Examination of the restoring force diagrams presented in Figure 2.19, leads to the conclusion that one of the most important features of the structural behavior of the buildings under consideration

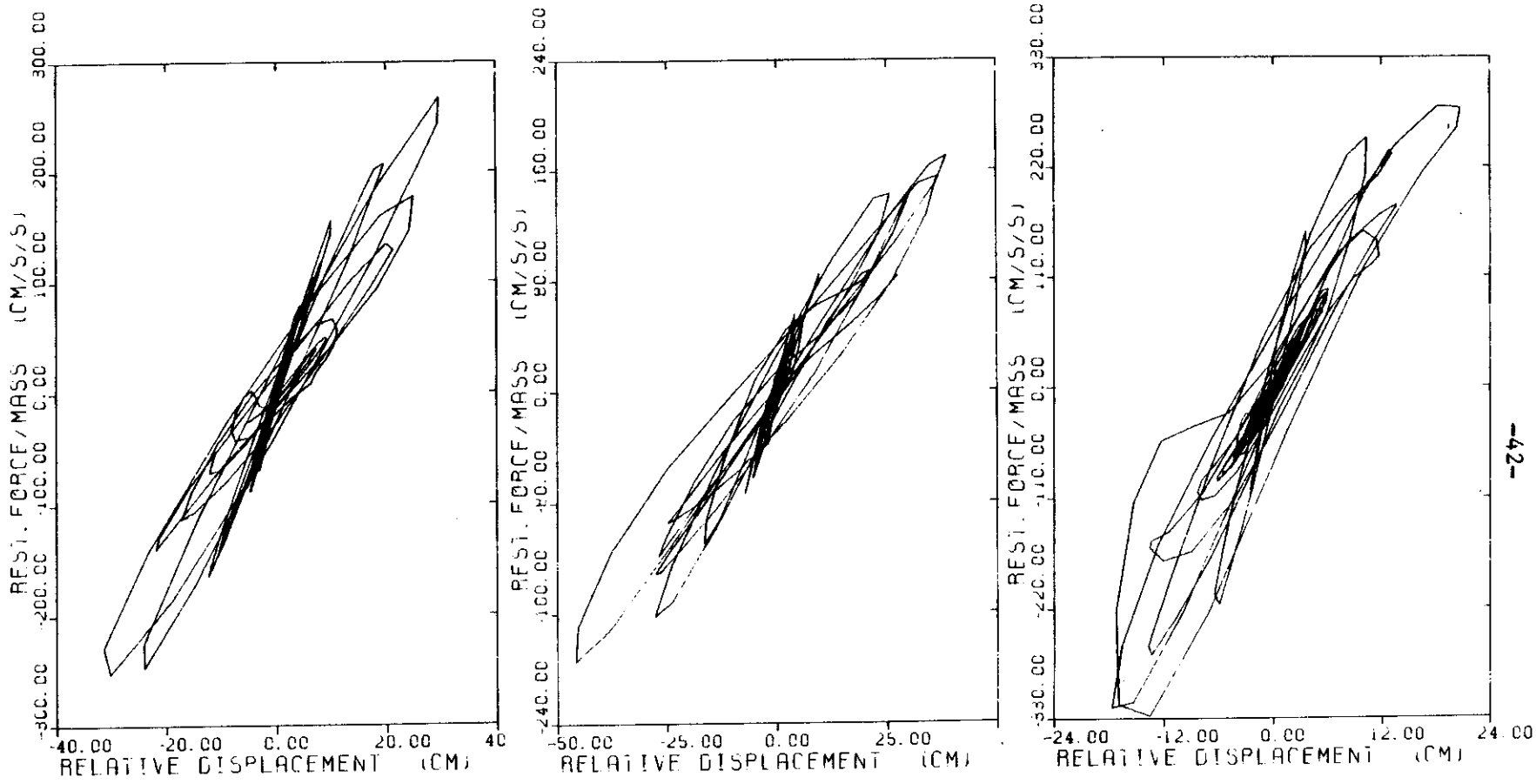

Figure 2.19 Corrected version of the restoring force diagram for the buildings under consideration (a) Bank of California building, N11E component (b) Bank of California building, N79W component (c) Imperial County Services building, E-W component.

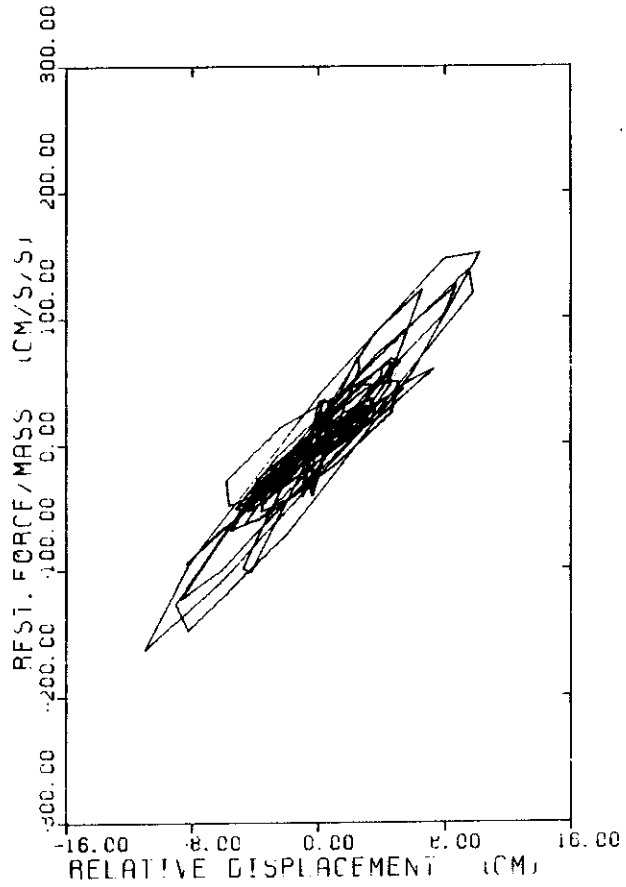

(d)

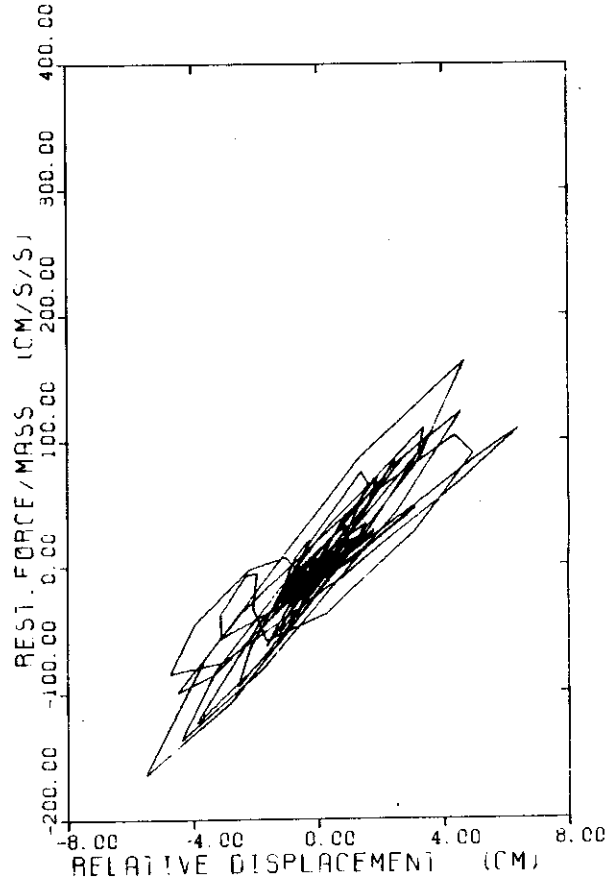

(e)

Figure 2.19 (Continued)
(d) Holiday Inn building, N00W component and (e) Holiday Inn building, S90W component.

is the loss of stiffness with cyclic loading. For conceptual purposes define the effective stiffness (per unit of mass) as,

$$K_{eff} = \frac{f(x_i)}{x_i} \tag{2.19}$$

where x_i is either a local minimum or a local maximum of the relative displacement x and $f(x_i)$ is the corresponding value of the restoring force per unit of mass. This is sometimes referred as the secant stiffness. Figure 2.20 illustrates this concept. Intuitively, K_{eff} provides an estimation of the "equivalent linear stiffness" of a given hysteresis loop.

It is noted, that the loss of stiffness in these structures is apparent from the fact that K_{eff} decreases when the absolute value of x increases. It seems, in Figure 2.19, as if the hysteresis loops were rotating with respect to the origin. The stiffness reduction observed results from yielding, cracking, or other forms of "failure" of structural members.

As an illustration, consider in more detail the restoring force diagram corresponding to the N11E component of the Bank of California (Figure 2.19(a)). It is observed that the effective stiffness is more or less constant during the initial oscillations (x smaller than approximately 5 cm). However, when the amplitude of oscillation starts to exceed this value, a progressive decrease in effective stiffness takes place. Finally, as the amplitude of oscillation decays after reaching its maximum value, the value of the effective stiffness tends

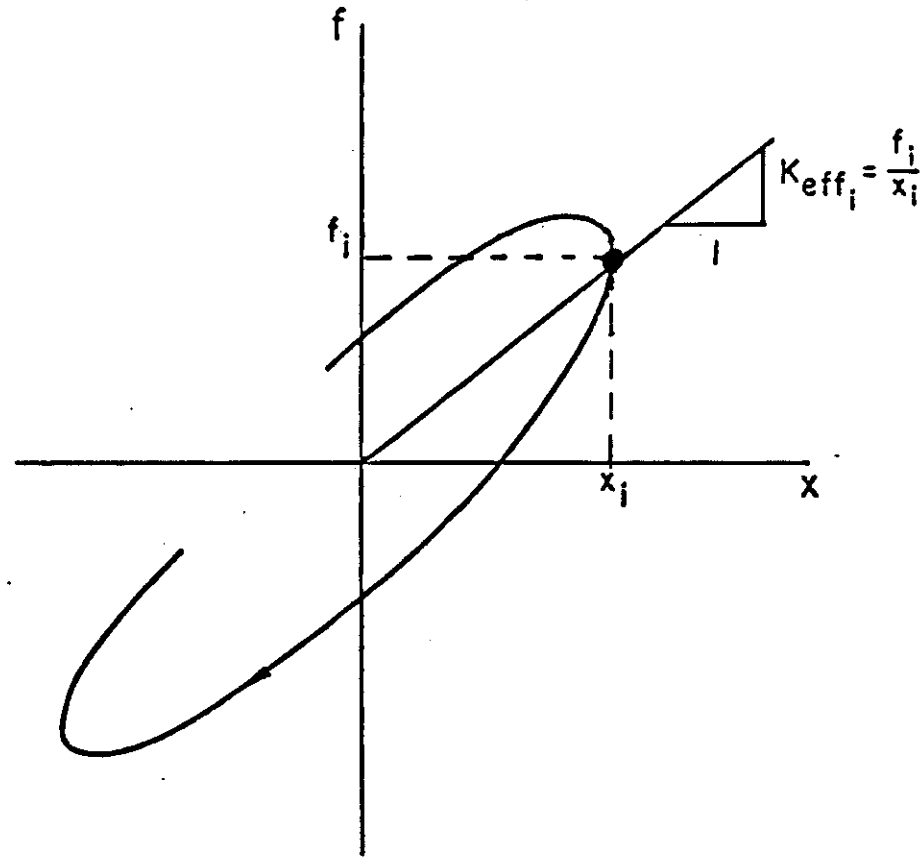

Figure 2.20 Graphical interpretation of the effective stiffness concept.

to become constant. However, the final value of the effective stiffness is clearly smaller than its initial value. Thus, permanent stiffness degradation has taken place.

A comparison between the restoring force diagram of Figure 2.19(a) and that of a linear system (Figure 2.5) is enlightening. Indeed, one can easily observe the difference between linear behavior, and the behavior exhibited by the structures under study herein. In the case of linear behavior the effective stiffness is constant, while for the buildings under consideration the effective stiffness decreases with increasing x. Moreover, the stiffness lost is nonrecoverable.

It might be argued that this finding regarding the loss of stiffness of structures subjected to strong earthquake excitation is nothing new. In fact, several papers have already addressed this point [1],[2],[3] and [6] among others. But the approach taken here, i.e., through the restoring force diagram, allows one not only to visualize and quantify this phenomenon, but also gives a useful insight into the physics of the system.

Finally, it is important to mention, that the restoring force behavior observed during strong earthquake excitation cannot be fully studied by means of standard vibration tests. The load applied in the standard forced vibration test, excites the structure only in the linear range. The restoring force diagrams of Figure 2.19, show that buildings can exceed the linear response range by a considerable margin without

collapsing. Therefore an estimation of building performance under severe ground shaking based solely on data collected from a standard vibration test can be more than a little misleading.

2.4.2 Stiffness Degradation

In the previous section stiffness degradation has been described in a more or less qualitative fashion. In order to present this effect in a more quantitative manner, a slightly different approach will be introduced.

Consider Figure 2.21. This figure shows what can be considered as a typical time history of the response of a building. This example corresponds to the N00W component of the Holiday Inn Orion. It can be observed that the general pattern of the curve is the following: 1) A sequence of increasing amplitude oscillations until a maximum X_{max} is reached and, 2) An almost monotonic decay of the response. Making use of the effective stiffness, K_{eff}, as defined in (2.19), one can therefore analyze the variation of the structural properties of the building during the earthquake. In fact, one can determine from the earthquake records K_{eff} as a function of the amplitude of the oscillation on a discrete set of points; and observe the variation of K_{eff} while x increases until X_{max}, and then decays.

Figure 2.22 depicts the effective stiffness diagrams for the Bank of California, Holiday Inn Orion and Imperial Valley Services buildings. It is observed from these diagrams that the initial value of the effective stiffness, K_0, and the final value, K_f, are remarkably

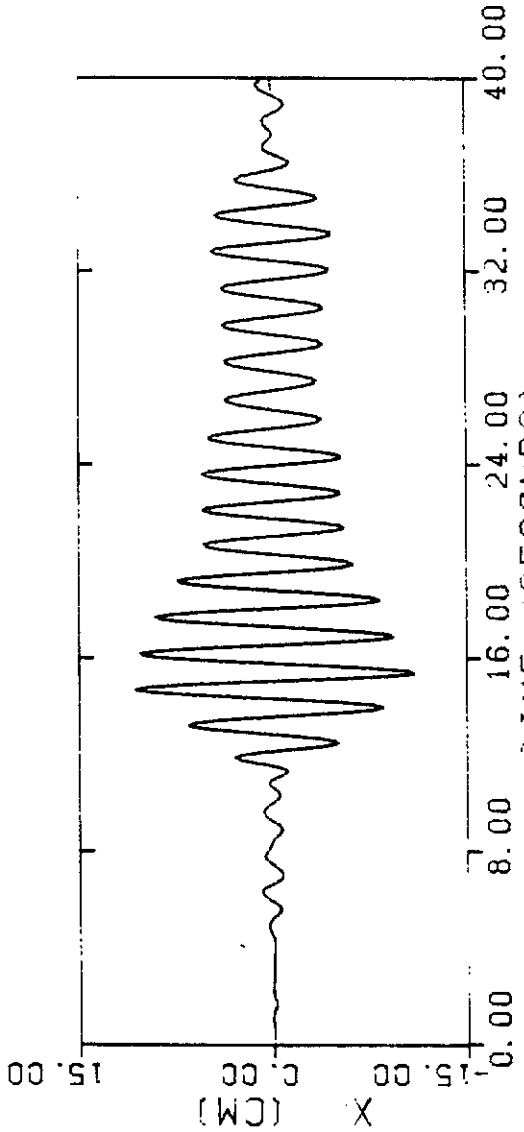

Figure 2.21 Typical time history of the earthquake response of a building.

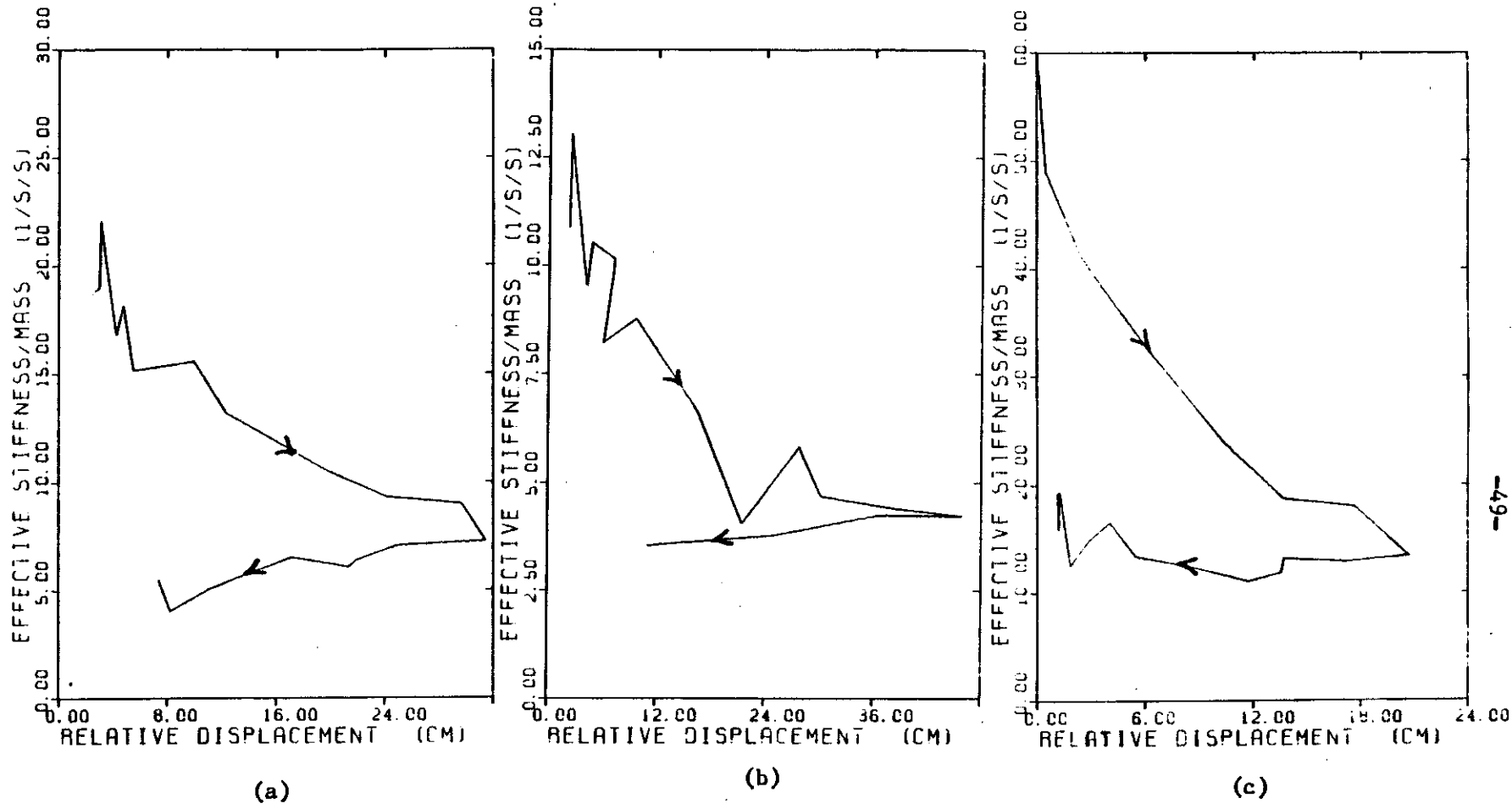

Figure 2.22 Effective stiffness diagrams for the buildings under study. The vertical axis corresponds to the effective stiffness per unit of mass and the horizontal axis corresponds to the absolute value of the relative displacement. By estimating the intersection of these curves with the vertical axis, one can determine K_0 and K_f. (a) Bank of California building, N11E component (b) Bank of California building, N79W component (c) Imperial County Services building.

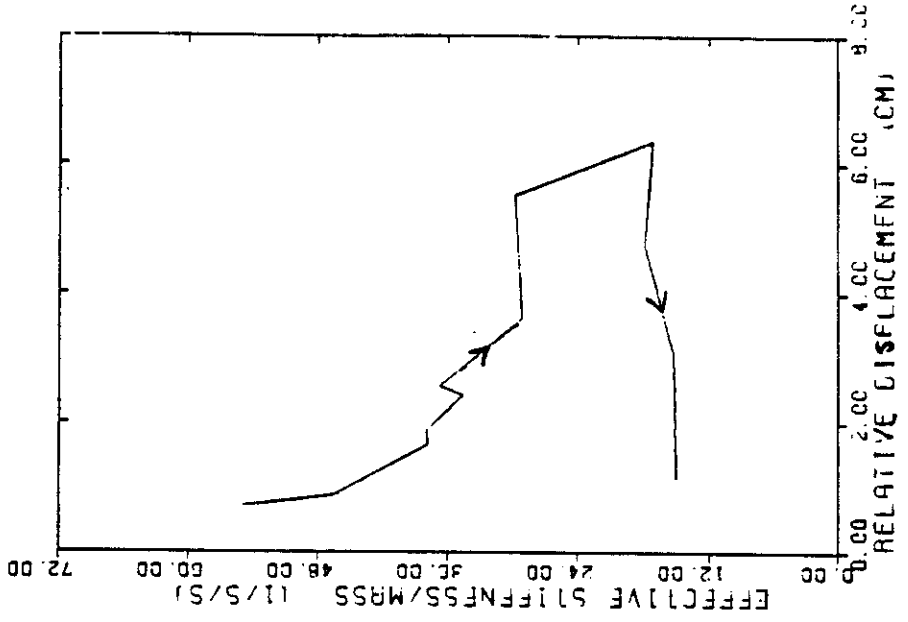

(d)

(e)

Figure 2.22 (Continued)
(d) Holiday Inn building, N00W component and (e) Holiday Inn building, S90W component.

different. This means that the structure does not totally recover its initial stiffness after experiencing the maximum amplitude oscillation. In other words, the structure has suffered permanent deterioration. This is in clear contrast with the case of linear behavior, in which K_{eff} is constant.

The difference between K_0 and K_f is associated with the stiffness lost. This point will be considered in more detail in Chapter 4.

2.5 SUMMARY AND CONCLUSIONS

A general procedure for the analysis and treatment of earthquake records obtained from instrumented buildings exhibiting strong hysteretic behavior has been introduced. Following the procedure outlined in the previous sections, it is possible to determine the restoring force behavior corresponding to the seismic response of these structures.

The earthquake response of several reinforced concrete buildings subjected to a strong ground acceleration has been studied. The difference between the restoring force behavior of these structures, and that of a linear oscillator is very clear. It has been found that one of the most important features of the response of the structures under consideration is stiffness degradation. The restoring force diagrams and the effective stiffness diagrams determined from the earthquake records allow one to visualize and quantify this effect.

An appropriate physically motivated model to estimate the dynamic response of reinforced concrete buildings should be able to represent

the features observed herein. These findings will be considered in evaluating existing structural models and in formulating a new model.

REFERENCES

[1] McVerry, G.H., "Frequency Domain Identification of Structural Models from Earthquake Records," Earthquake Engineering Research Laboratory Report No. EERL 79-02, California Institute of Technology, Pasadena, California, October 1979.

[2] Beck, J.L., "Determining Models of Structures from Earthquake Records," Earthquake Engineering Research Laboratory Report No. EERL 78-01, California Institute of Technology, Pasadena, California, June 1978.

[3] Iemura, H. and Jennings, P.C., "Hysteretic Response of a Nine-Story Reinforced Concrete Building," International Journal of Earthquake Engineering and Structural Dynamics, Vol. 3, pp. 183-201, 1974.

[4] Thomson, W.T., Theory of Vibrations with Applications, 2nd Edition, Prentice-Hall, 1981.

[5] Murphy, L.M., "San Fernando, California, Earthquake of February 9, 1971," Vol. 1, Part A, U.S. Department of Commerce, National Oceanic and Atmospheric Administration (NOAA), Washington, D.C., 1973.

[6] Pauschke, J.M., Oliveira, C.S., Shah, H.C. and Zsulty, T.C., "A Preliminary Investigation of the Dynamic Response of the Imperial County Services Building During the October 15, 1979 Imperial Valley Earthquake," The John A. Blume Earthquake Engineering Center, Department of Civil Engineering, Stanford University, Report No. 49, January 1981.

[7] Rojahn, C. and Mark, P.N., "An Analysis of Strong-Motion Data from a Severely Damaged Structure -- The Imperial County Services Building," El Centro, California," recorded by the California Division of Mines and Geology Strong-Motion Network, The Imperial Valley, California Earthquake of October 15, 1979, Geology Survey Professional Paper 1254, U.S. Dept. of the Interior, 357-375. U.S. Government Printing Office, Washington, D.C., 1982.

[8] California Institute of Technology, "Analysis of Strong Motion Earthquake Accelerograms," Earthquake Engineering Research Laboratory Report No. EERL-74-100, California Institute of Technology, Pasadena, California, January 1974.

[9] Trifunac, M.D. and Lee, V., "Routine Computer Processing of Strong-Motion Accelerograms," Earthquake Engineering Research Laboratory Report No. EERL 73-03, California Institute of Technology, Pasadena, California, October 1973.

[10] Foutch, D.A., Housner, G.W., and Jennings, P.C., "Dynamic Response of Six Multistory Buildings During the San Fernando Earthquake," Earthquake Engineering Research Laboratory Report No. EERL 75-02, California Institute of Technology, Pasadena, California, October 1975.

[11] Blimchikoff and Zvenev, Filtering in the Time and Frequency Domain, John Wiley and Sons, 1979.

[12] Kreger, M. and Sozen, M., "A Study of the Causes of Column Failures in the Imperial County Services Building During the 15 October 1979 Imperial Valley Earthquake," Report UILU-ENG-83-2013, Civil

Engineering Studies, Structural Research Series No. 509, University of Illinois at Urbana-Champaign, Urbana, Illinois, August 1983.

[13] McVerry, G.H. and Beck, J.L., "Structural Identification of JPL Building 180 Using Optimally Synchronized Earthquake Records," Earthquake Engineering Research Laboratory Report No. EERL 83-01, California Institute of Technology, Pasadena, California, August 1983.

[14] Berg, G.V. and Housner, G.W., "Integrated Velocity and Displacement of Strong Earthquake Ground Motion," Bull. Seis. Soc. Amer., Vol. 51, No. 2, 1961.

[15] Boyce, W.H., "Integration of Accelergrams," Bull. Seis. Soc. Amer., Vol. 60, No. 1, 1970.

CHAPTER III

ANALYTICAL MODELS FOR STRUCTURAL BEHAVIOR

3.1 INTRODUCTION

The purpose of this chapter is to evaluate and discuss some of the models most commonly used in structural dynamics. This will be done mainly against the backdrop of the conclusions drawn in Chapter 2 regarding the restoring force behavior of reinforced concrete buildings. Finally, in Section 3.4, a new model will be introduced. This new model is based upon the observations presented in Section 2.4 concerning the restoring force behavior of actual buildings. It is intended to be used primarily to estimate the earthquake response of reinforced concrete structures subjected to severe ground shaking.

3.2 THE LINEAR MODEL

Consider the equation of motion of a SDOF oscillator

$$\ddot{x} + f(\dot{x}, x) = a(t) \tag{3.1}$$

where $f(x,\dot{x})$ is the restoring force per unit of mass due to relative displacement, x, and relative velocity, $\dot{x}$; and $a(t)$ is the excitation. The system is said to be linear if $f(x,\dot{x})$ can be expressed as

$$f(x,\dot{x}) = \omega_0^2 x + 2\omega_0 \zeta \dot{x} \tag{3.2}$$

where ω_0 is the natural frequency of the system; and ζ represents the

fraction of critical damping. In this case the stiffness of the system is constant, and the energy is dissipated only by means of the viscous damper.

The linear model has been widely used in structural dynamics. Recent research by Beck [1] and McVerry [2], has demonstrated that the linear model can give a satisfactory approximation of the earthquake response of buildings under certain conditions. Normally, these conditions amount to the assumption that the structure under consideration does not suffer important damage. In the case of buildings exhibiting significant damage, it has been found that linear models give very poor approximations. An illustrative example, that shows the limitations of the linear model, is the N11E component of the Bank of California. This was one of the most damaged buildings during the San Fernando earthquake [3]. McVerry [2] showed that it was not possible to approximate the entire response by means of a single linear model with constant coefficients. Moreover, by dividing the record in two segments (0.0-20.48 seconds and 19.0-39.48 seconds), he concluded that there was a very significant variation in the linear model parameters during the earthquake. The fundamental period of the linear model corresponding to the first segment was 1.74 seconds, while that in the second segment was increased to 2.35 seconds. This represents a decrease of almost 50% in terms of the linear stiffness of the system. These findings are in agreement with the features observed in the restoring force diagram and the effective stiffness diagram presented in the previous chapter.

Similar characteristics can be observed in the behavior of the Holiday Inn and Imperial County Services Buildings. It is not surprising that a linear model fails to give a good approximation in the cases, since the basic assumption of constant stiffness and damping is clearly violated.

3.3 REVIEW OF SOME NONLINEAR MODELS

Several nonlinear models have been proposed to describe structural behavior under cyclic loading. These models represent an attempt to overcome the limitations of the linear model for strong excitations. Some of these models will be briefly discussed in the following sections. The emphasis will be placed on the relationship between the restoring force and the relative displacement.

3.3.1 The Elastoplastic Model

The governing equation in the case of the elastoplastic model is (3.1), where the restoring force per unit of mass, f, is given by the diagram of Figure 3.1(a).

Figure 3.1(b) shows an idealized physical system that exhibits elastoplastic behavior. This system consists of a linear spring with stiffness K in series with a Coulomb or slip damper which has a maximum allowable force of f*.

Due to its simplicity, this model has gained some popularity among analysts. However, it does not do a very good job of representing the restoring force behavior observed in Chapter 2.

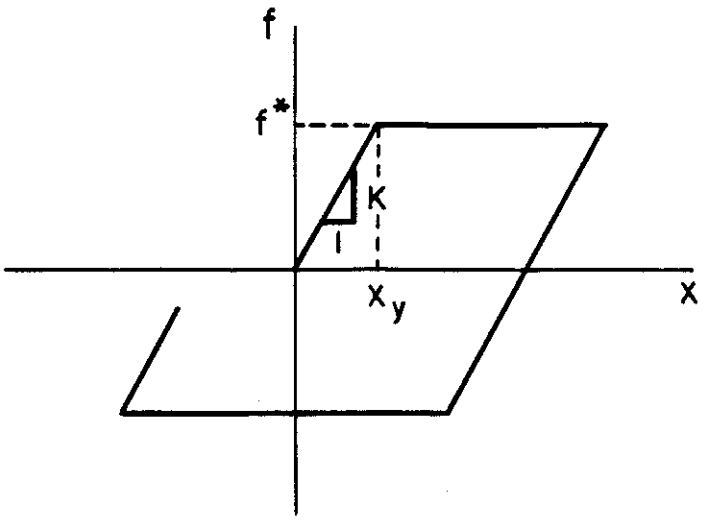

(a)

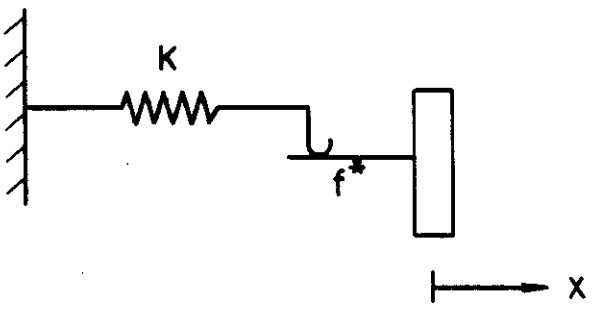

(b)

Figure 3.1 Elastoplastic model. (a) Restoring force diagram and (b) Idealized physical system.

To illustrate this point, consider the response of an elastoplastic system with unitary mass and a restoring force f given by the diagram of Figure 3.2(a), subjected to the E-W component of the ground acceleration recorded at the Imperial County Services Building. Figure 3.2(b) shows the restoring force diagram corresponding to this case and Figure 3.2(c) the effective stiffness diagram. The restoring force behavior exhibited by this model is considerably different in general appearance from that observed in Figure 2.19(c). One notes that in the case of the elastoplastic model, even though the effective stiffness decreases when x exceeds Xy, the system eventually recovers its initial stiffness. This is apparent in Figure 3.2(b) by the fact that one can hardly distinguish between the small amplitude oscillations that occurred at the beginning and at the end of the excitation. On the contrary, in the hysteresis loops presented in Figure 2.19(c), for example, one can clearly distinguish the difference in the period of the initial and final oscillations. In other words, the elastoplastic system does not adequately represent the stiffness degradation phenomenon that characterizes the behavior of the type of structures under consideration.

3.3.2 The Bilinear Hysteretic Model (BLH)

This model is very similar to the elastoplastic model except for the addition of an additional linear spring. The governing equation is (3.1) where f is given by the diagram of Figure 3.3(a). Figure 3.3(b)

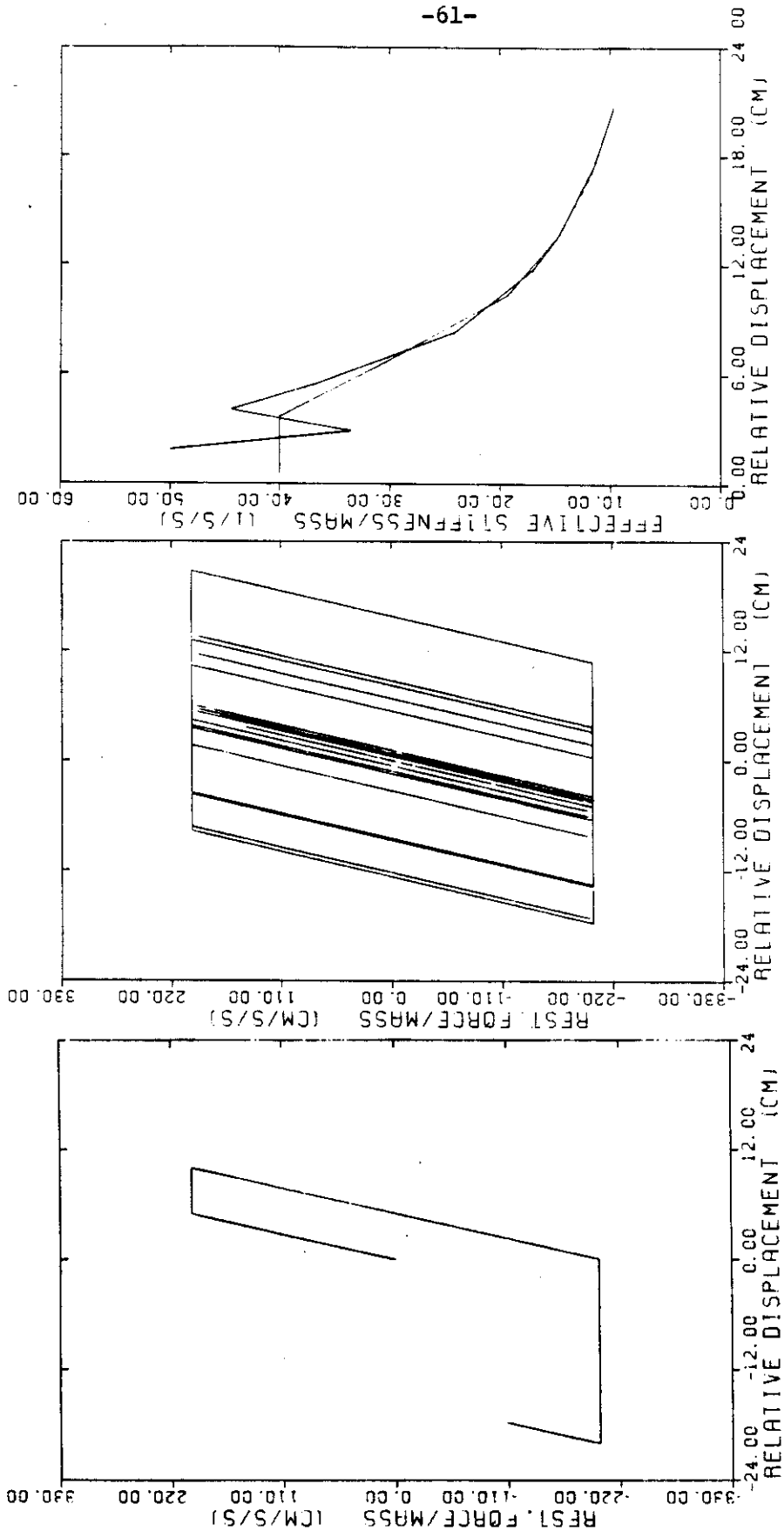

Figure 3.2 Response of an elastoplastic system to the ground acceleration recorded at the Imperial County Services building. (a) Restoring force - relative displacement relationship for the system (b) Restoring force diagram (c) Effective stiffness diagram.

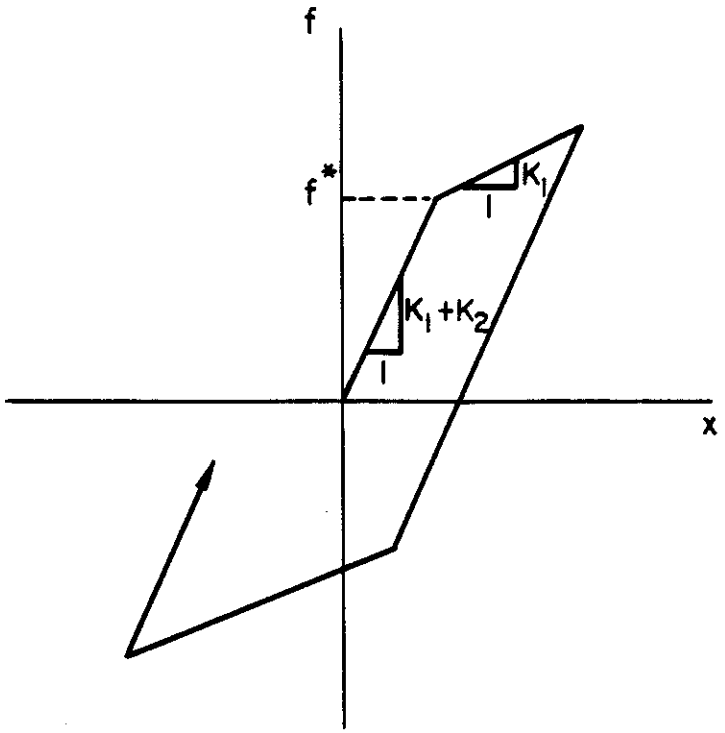

(a)

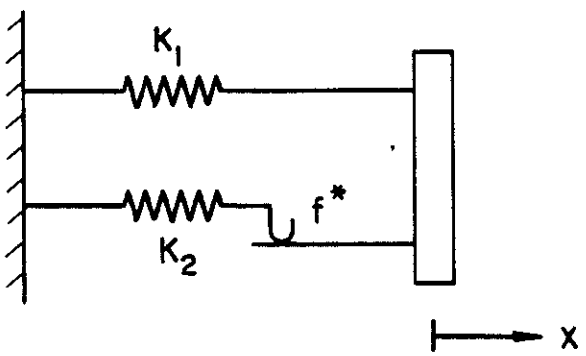

(b)

Figure 3.3 Bilinear hysteretic system. (a) Restoring force-relative displacement relationship (b) Idealized physical system.

shows an idealized physical system that behaves according to this model. In a sense, one can say that this model is a refinement of the elasto-plastic model.

Except for general reduction in stiffness, the BLH model has the same general characteristics exhibited by the elastoplastic model. It is therefore unable to adequately represent deterioration. Iemura and Jennings [4], showed that it was not possible to model the E-W response of Millikan Library during the San Fernando earthquake using a simple time invariant BLH model. Other discouraging results regarding the capabilities of this approach have been reported by Otani [5] and Saiidi [6]. Using experimental data they have demonstrated that this model does not do an adequate job of representing the restoring force behavior of concrete structures, and gives a poor estimation of the time history of the response.

3.3.3 Johnston's Model

Johnston's model [7] represents an attempt to characterize the deteriorating properties of concrete. Figure 3.4 shows the relationship between the restoring force per unit of mass, f, and the relative displacement, x, in this case. This model was proposed after studying the behavior of beam-column assemblies subjected to cyclic loading.

Some satisfactory results using this model and experimental data have been reported by Saiidi [6]. But no research considering actual earthquake records has yet been undertaken.

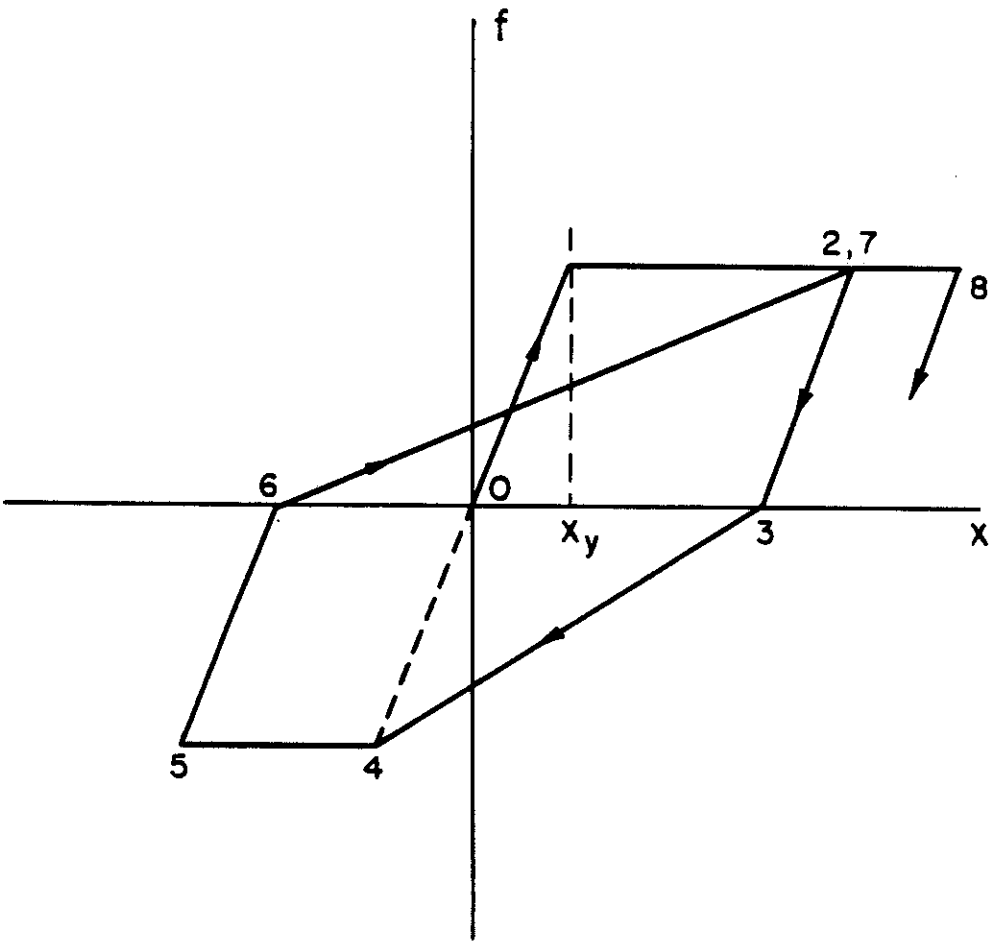

Figure 3.4 Restoring force diagram for Johnston's model.

Figure 3.5 shows several restoring force diagrams generated using the time history of response of the Bank of California (N11E component) and Johnston's model. Comparing these results with Figure 2.19(a), one notes that for small values of the yielding displacement (Xy equal to 5 cm for example), this model underestimates the restoring force for large amplitudes. On the other hand, for large values of Xy (Xy equal to 18 cm), the model tends to overestimate the energy dissipated after the peak amplitude is reached. This is clear in Figure 3.5(c) from the fact that the area within the hysteresis loops corresponding to the final part of the excitation is greater compared to that observed in Figure 2.19(a).

The physical interpretation of the rules presented in Figure 3.4 to determine the restoring force is uncertain. This is due to the fact that the model is not based on any particular physical analogy. However, in spite of this drawback, the Johnston's model represents a major advance compared to the BLH and elastoplastic models, in that it introduces the most important feature of the hysteretic response of reinforced concrete structures; i.e., stiffness degradation.

3.3.4 The Distributed-Element Model

This model consists of a system composed of a series of elasto-plastic elements as indicated in Figure 3.6 [8]. Each elastoplastic element consists of a linear spring with stiffness K/N in series with a Coulomb or slip damper that has a maximum allowable force of f_i/N. N is

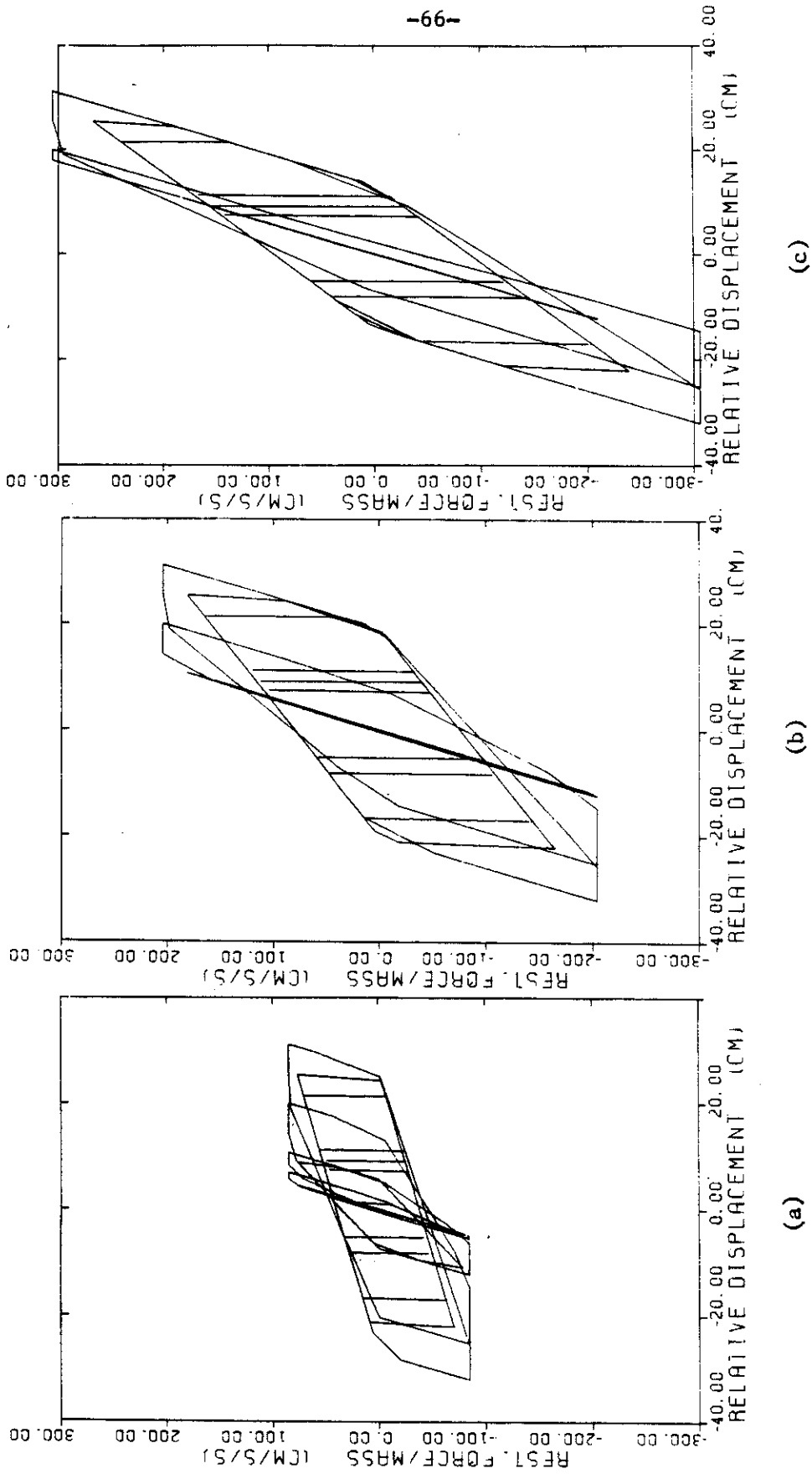

Figure 3.5 Restoring force diagram generated using the time history of response of the Bank of California (N11E component) and Johnston's model. The value of the initial stiffness is 17 sec^{-2}. (a) X_y = 5 cm (b) X_y = 12 cm and (c) X_y = 18 cm.

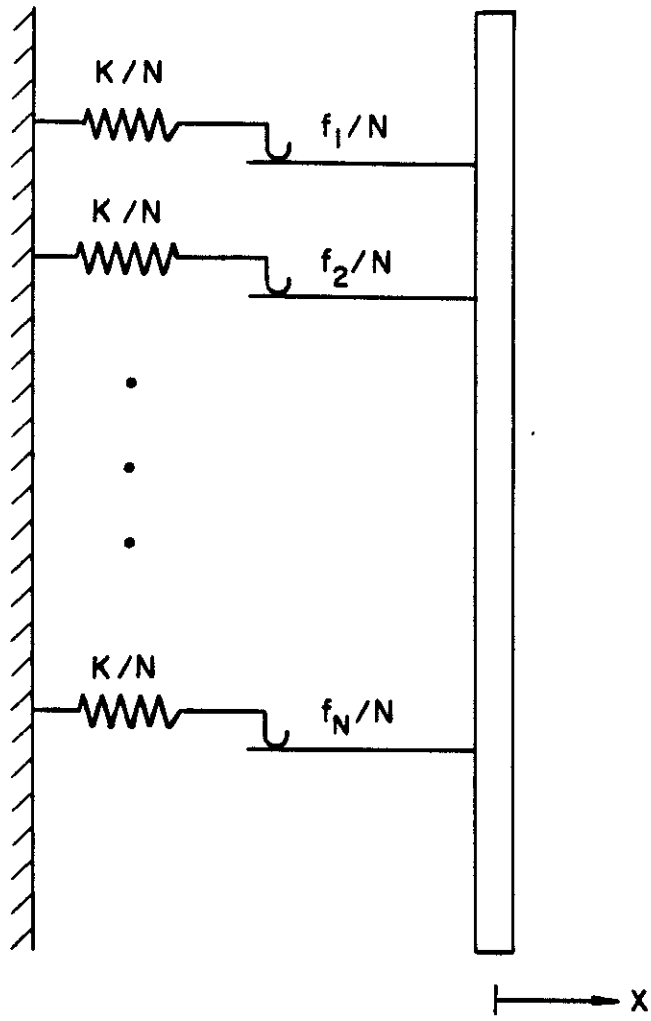

Figure 3.6 The Distributed-Element model

the number of elements. The restoring force-relative displacement relationship for a typical elastoplastic element is shown in Figure 3.7.

If the number of elements N, becomes very large, the system will tend to exhibit a restoring force diagram like the one shown in Figure 3.8. It is important to notice that this is a physically motivated model, since it can be built by using an array of linear springs and slip dampers.

The distributed-element model has two attractive features. First, it is relatively easy to relate it to a system whose structural behavior is known and second, it is easy to visualize how variations in the parameters of the model are reflected in the nature of the hysteretic behavior exhibited. These points are discussed in more depth in [8] and [9].

Although the distributed-element model can describe with sufficient accuracy the hysteretic behavior of a large variety of structures, it does not include the stiffness degradation phenomenon. However, it will provide the basis for developing a more general model taking into account deterioration.

3.3.5 Other Models

Several other nonlinear models have been proposed to describe the relationship between the restoring force and relative displacement in structures subjected to cyclic loading.

Takeda et al. [10] have introduced a model based on sixteen different rules depending on the loading or unloading regime. Some

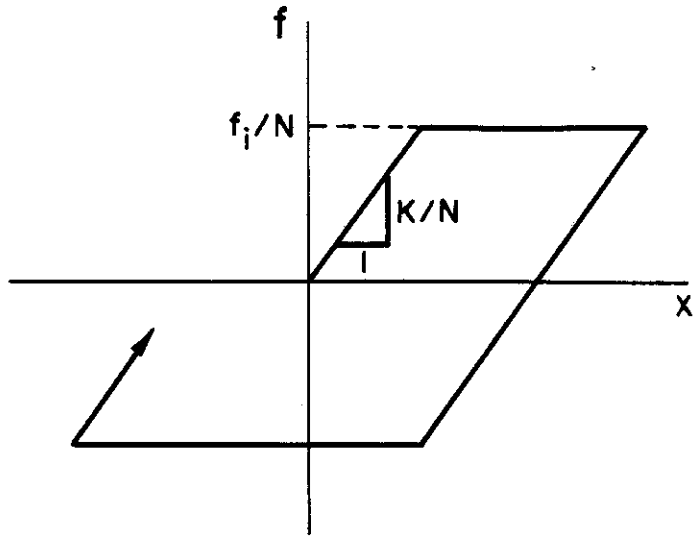

Figure 3.7 Restoring force-relative displacement relationship for a typical elastoplastic element of the Distributed-Element model.

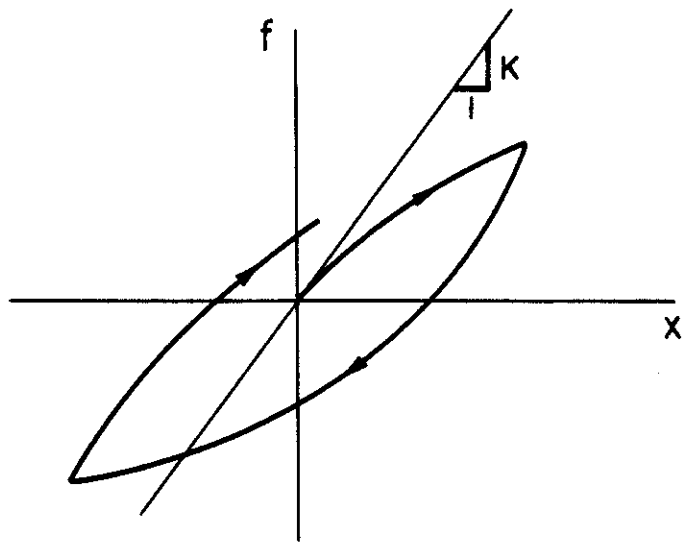

Figure 3.8 Distributed-Element model. Typical restoring force diagram for the case in which N becomes very large.

satisfactory results using experimental data have been reported [6]. Despite this, the complexity of some of the rules of this model represents a major inconvenience.

Sina [6] proposed another model which is a complicated version of Johnston's model without any significant improvement; at least, according to experimental results presented by Saiidi [6].

Toussi and Yao [11], [12] have chosen to express the restoring force as a polynomial expression of the form

$$f(x,\dot{x}) = f_s(x) + f_d(\dot{x}) \tag{3.3}$$

where

$$f_s(x) = a_0 + a_1 x + \ldots + a_q x^q \tag{3.4}$$

and

$$f_d(\dot{x}) = b_0 + b_1 \dot{x} + \ldots + b_m \dot{x}^m \tag{3.5}$$

The expression for the "spring force" violates (at least theoretically) the condition required in order to exhibit stiffness degradation. This, since $f_s(x)$ does not take into account the history of deformation; i.e., it will always give the same contribution to the restoring force for a particular value of x.

Masri and Caughey [13] have suggested a nonparametric identification technique for general nonlinear problems. In this case, the restoring force f is expanded using a Chebyshev polynomial approximation of the form

$$f(x,\dot{x}) = \sum_{i=0}^{P} \sum_{j=0}^{Q} c_{ij} T_i(x) T_j(\dot{x}) \qquad (3.6)$$

As far as representing stiffness degradation is concerned, this approach has the same disadvantage that Toussi's model has. However, it introduces a fairly new idea; the system identification is performed by approximating the restoring force rather than the time history of the response. This approach will be discussed in more depth in the next chapter.

Several other models have been suggested, [14], [15], [16], [17], [18] among others, but space limitations prevent a detailed discussion of each.

3.3.6 Conclusions

A brief discussion of some of the most important nonlinear models used in structural dynamics has been presented. The models considered for this purpose cover a broad spectrum, from relatively simple but not very realistic models (elastoplastic), to very sophisticated models (Takeda's). This review is not intended to be exhaustive. It does, however, show that there is still room for improvement in the modeling of the deteriorating behavior of reinforced concrete structures.

3.4 THE DETERIORATING - DISTRIBUTED - ELEMENT MODEL

A new model, called the deteriorating - distributed - element (DDE)

model is herein introduced. This model shows promise in describing the restoring force behavior of reinforced concrete structures subjected to cyclic loading.

3.4.1 General Description of the DDE Model

The DDE model consists of four types of elements, arranged in parallel as shown in Figure 3.9. The four categories of elements are the following:

(i) Linear Element

The linear element consists of a linear spring with a characteristic constant K_e.

(ii) Elastoplastic Element

The elastoplastic element consists of a linear spring with a constant K_{ep}, in series with a slip damper which has a maximum allowable force equal to $K_{ep}Xy_{ep}$. That is, if the value of the relative displacement x is less than Xy_{ep}, the elastoplastic subelement behaves linearly. Accordingly, Xy_{ep} is called the yielding displacement of the elastoplastic element. The restoring force diagram for this kind of subelement was already shown in Figure 3.7 (in this case K/N would be equivalent to K_{ep}, and f_i/N would be equivalent to $K_{ep}Xy_{ep}$).

(iii) Deteriorating Element

The deteriorating element is similar to the elastoplastic element except for the fact that it "breaks" when the relative displacement exceeds a certain limit. This element consists of a linear spring with constant K_i, in series with a slip damper that has a maximum allowable

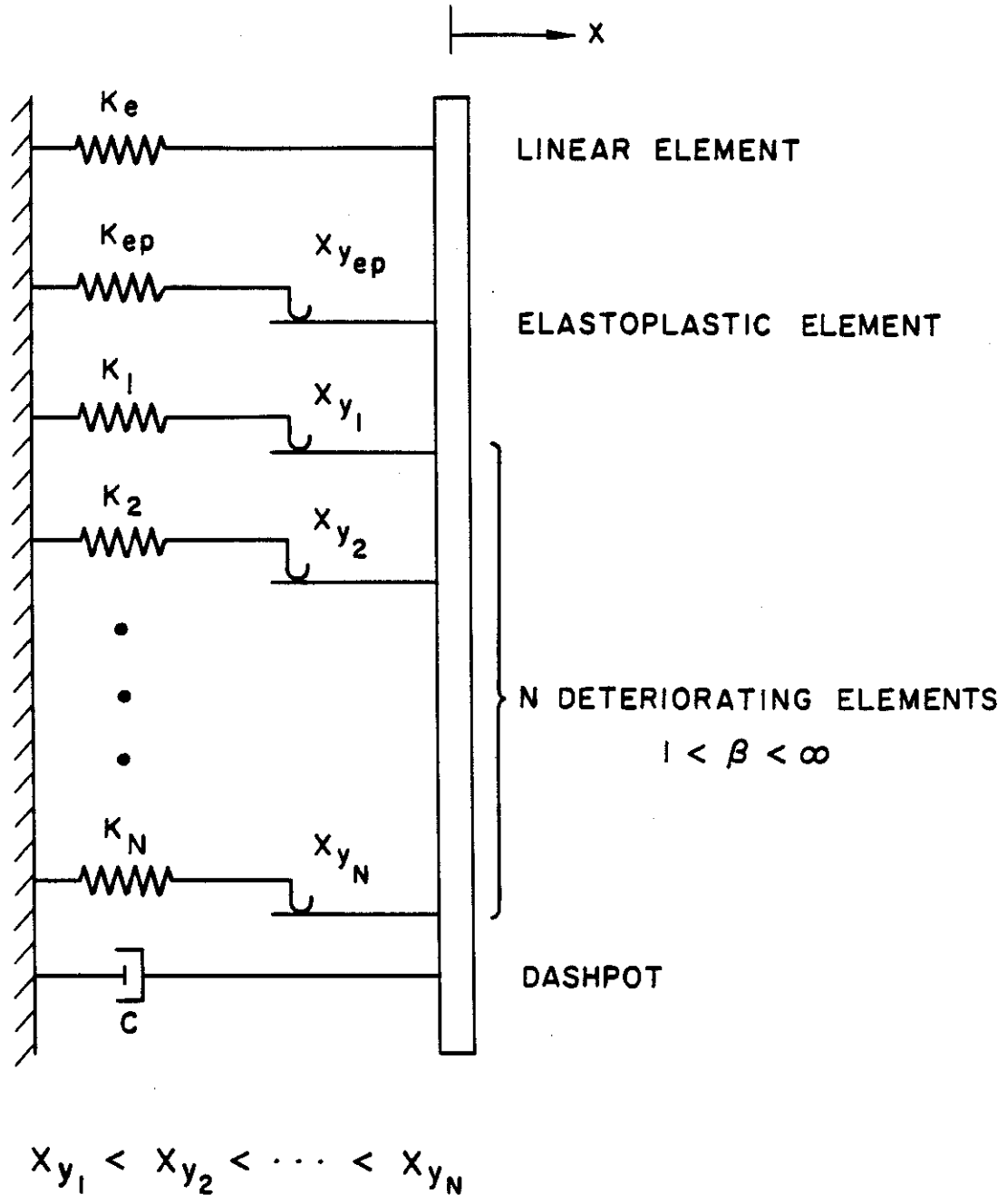

Figure 3.9 The Deteriorating-Distributed-Element (DDE) model.

force equal to $K_i Xy_i$. Xy_i is the yielding displacement. It is assumed that the spring "breaks" if the relative displacement becomes larger than βXy_i. When the spring "breaks", the contribution of this element to the total restoring force becomes zero. At least in principle, the factor β can be any number larger than 1. If $\beta = 1$, the deteriorating element behaves like a linear spring until it "breaks". If $\beta \rightarrow \infty$, the deteriorating element behaves like the elastoplastic element presented in (ii). The restoring force-displacement relationship for this type of element is shown in Figure 3.10.

(iv) Viscous Damper

This element can be considered as a dashpot which contributes to the restoring force with a value equal to $C\dot{x}$.

The complete DDE model, as shown in Figure 3.9, consists therefore of one linear element, one elastoplastic element, N deteriorating ele-

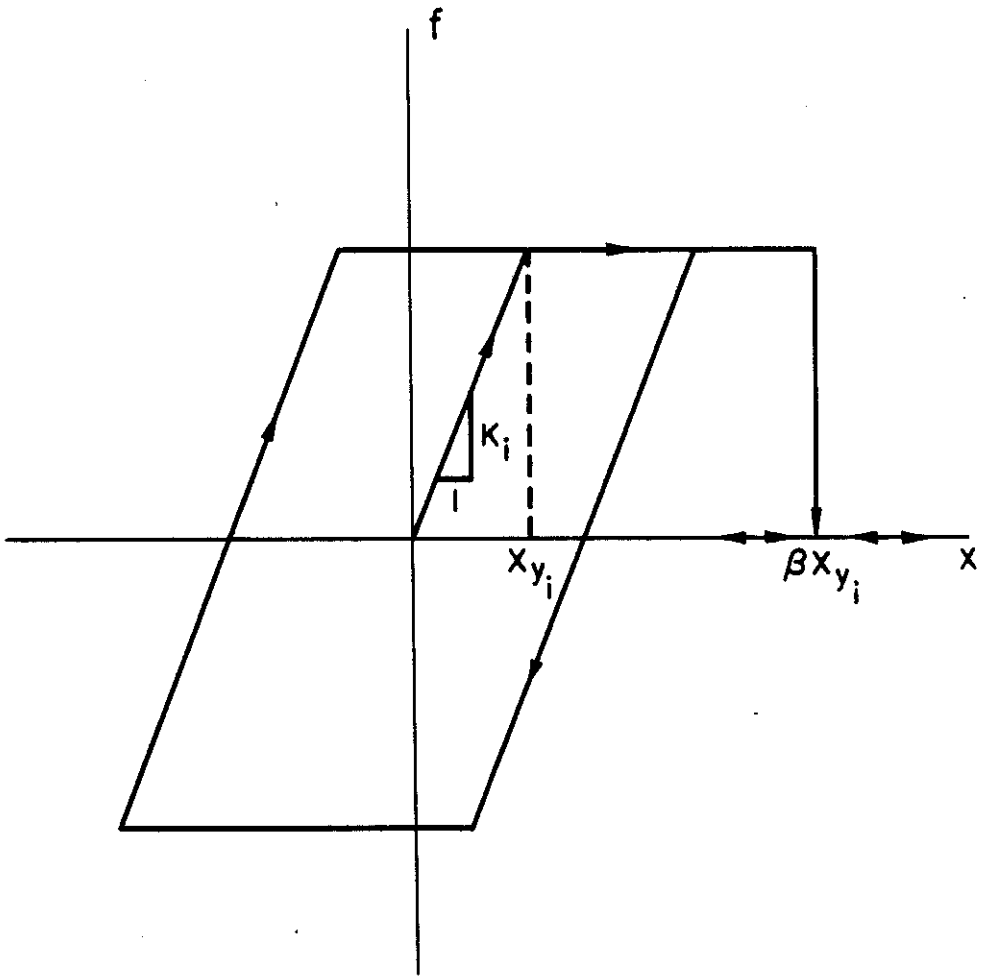

Figure 3.10 Typical restoring force-relative displacement relationship for a deteriorating element. The element "breaks" when it reaches a displacement equal to βXy_i or $-\beta Xy_i$.

ments and a dashpot. The N deteriorating elements deserve some further discussion.

The deteriorating elements account for the loss of stiffness of the structure with large amplitude oscillations. This phenomenon, as observed in the effective stiffness diagrams is rather continuous. Indeed, the larger the displacement the more stiffness the structure loses. According to this observation, it seems more appropriate to include several deteriorating elements rather than only one. Notice also (Figure 3.9) that the deteriorating elements have been arranged so that $Xy_1 < Xy_2 < \ldots < Xy_N$. Since these element "break" when the displacement exceeds the value βXy_i, they will "break" in ascending order. In that regard, the stiffness degradation phenomenon as represented by the DDE model, is a gradual process. The question of how many deteriorating elements must be included in the model, will be considered in Chapter 5.

The coefficient β, which relates the yielding displacement Xy_i in a deteriorating element and the displacement at which the element "breaks" could be considered as a parameter of the model. Accordingly, it could be determined in the system identification process. However, to keep the model as simple as possible, it was decided in this study to assign an a priori numerical value to β so as to reduce the number of free parameters to be determined. In this case the value chosen was 2. Any decision regarding the value of β is, in a way, a little arbitrary. Nevertheless, an a posteriori justification will be offered in Chapter 5

taking into account the results obtained when matching the response of the structures considered in this study.

The type of restoring force diagram characteristic of this model, is discussed in Section 3.4.4.

3.4.2 Physical Motivation

When a structural model is proposed, the only real proof of its validity consists in testing it against real data, namely, earthquake records. However, before appealing to this argument, one should be able to justify (at least from an intuitive point of view) the decisions made regarding the general form of the model. This section represents an attempt to do this.

Assume that a building is oscillating as a consequence of an input ground acceleration. The total restoring force associated with this motion, will result from the contribution made by each one of the structural members of the building. Each member will, in principle, exhibit a different behavior since properties like equivalent linear stiffness or yielding displacement, for example, will not necessarily be the same for all the members. Having this in mind, one can speculate that the structural members can be divided into three different groups as far as the restoring force is concerned.

The first group of structural members will consist of those members that have behaved linearly, i.e., within the elastic regime. The contribution to the total restoring force made by these elements may be represented by means of a linear spring K_e. A second group of

structural members will be those that have experienced deformations beyond the elastic limit, but not large enough to produce significant deterioration. The combined effect of these members may be represented by the elastoplastic element of the model. Finally, a third group of structural members will be those that have suffered deterioration, i.e., stiffness degradation. The behavior of these members may be represented by the N deteriorating elements of the model. The viscous damper accounts for the energy dissipated through mechanisms not considered in the yielding elements.

3.4.3 Relationship Between K_i and X_i

Each of the deteriorating elements is completely defined in terms of two parameters; the spring stiffness K_i, and the yielding displacement Xy_i. Therefore, since there are N deteriorating elements, there will be 2N parameters to be determined in an identification problem.

In order to investigate whether one can establish a relationship between K_i and Xy_i (and consequently reduce the number of variables), consider the following argument. Let a section of a beam be deformed under the action of a bending moment M, as shown in Figure 3.11. It may be assumed that the moment is resisted by a large number of axial fibers arranged in parallel. Assume also, that each fiber behaves as an elastoplastic subelement with a yielding displacement equal to x_y. If θ is the net rotation of the end planes of the beam section, the elongation of a typical fiber i will be,

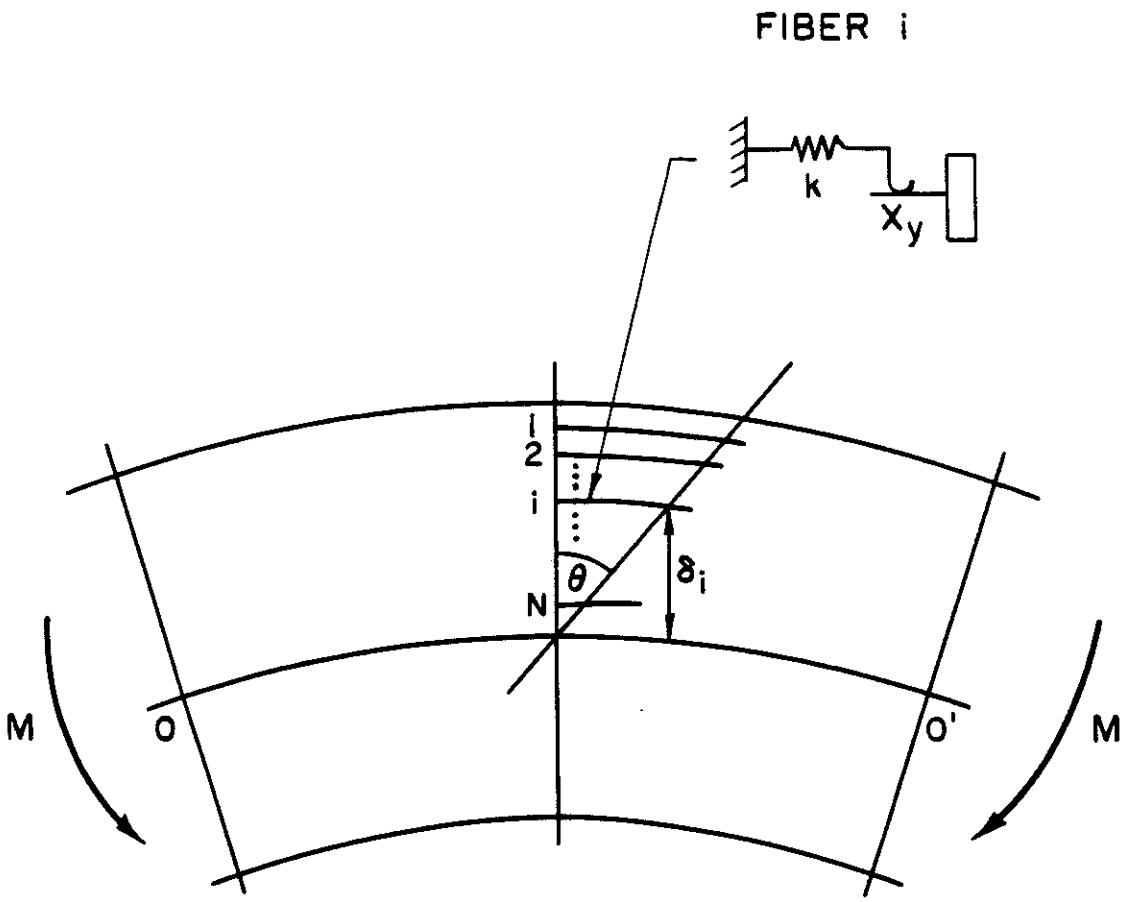

Figure 3.11 Idealized representation of a section of a beam deformed under the action of a moment.

$$x_i = \delta_i \theta \tag{3.7}$$

where x_i is the elongation and δ_i is the distance between the i^{th} fiber and the neutral axis of the section, 0-0'. The moment M_i, resisted by this fiber is

$$M_i = (kx_i)\delta_i = k\delta_i^2\theta \tag{3.8}$$

or more simply

$$M_i = k_i^*\theta \tag{3.9}$$

where

$$k_i^* = k\delta_i^2 \tag{3.10}$$

Let θy_i be the rotation angle such that the i^{th} fiber reaches its yielding displacement x_y. Then

$$\theta y_i = \frac{x_y}{\delta_i} \tag{3.11}$$

Note that $\theta y_1 < \theta y_2 < \ldots < \theta y_N$. From (3.11)

$$\delta_i^2 = \frac{x_y^2}{\theta y_i^2} \tag{3.12}$$

substituting this expression for δ_i^2 in (3.10) yields

$$k_i^* = k \frac{x_y^2}{\theta y_i^2} \tag{3.13}$$

It has been shown, therefore, that the stiffness k_i^* is proportional to $1/\theta y_i^2$. In the same fashion, one may assume that when a force F is applied in the DDE model, each deteriorating element will resist with a stiffness K_i proportional to $1/Xy_i^2$. Recall that in the DDE model the deteriorating elements have been arranged so that $Xy_1 < Xy_2 < \ldots < Xy_N$, and since in this analysis $\theta y_1 < \theta y_2 < \ldots < \theta y_N$, the analogy between the two cases is straightforward. Therefore, K_i in each of the deteriorating elements will be considered to be proportional to $1/Xy_i^2$.

It will be assumed that the following relationship holds, for the N deteriorating elements of the DDE model presented in Figure 3.9,

$$K_i = \frac{A}{Xy_i^2} \qquad i=1,2,\ldots,N \tag{3.14}$$

where K_i is the linear spring stiffness; Xy_i is the yielding displacement of the element and A a proportionality constant that needs to be determined. Relationship (3.14) implies that each deteriorating element spring can store the same amount of elastic energy at yield. This reduces the number of parameters associated with the N deteriorating

elements, initially equal to 2N, to N+1.

3.4.4 Hysteresis Loops Generated by the DDE Model

The DDE model presented in Section 3.4.1 and shown in Figure 3.9 is intended to represent the features of the restoring force behavior observed in Chapter 2. Indeed, it is based upon these observations. It is interesting, therefore, to explore whether the hysteresis loops generated by the DDE model reflect the qualitative nature of the restoring force behavior observed in Chapter 2.

Figure 3.12(a) shows a typical DDE model. This system consists of 20 deteriorating elements, a linear element, an elastoplastic element and a viscous damper. The numerical value of each of the parameters is indicated in Figure 3.12(a). The response of an oscillator having a unitary mass and a restoring force given by the system of Figure 3.12(a) was determined. The input acceleration used was the N79W component of the Bank of California. Figure 3.12(b) depicts the restoring force diagram corresponding to this case. A comparison between this figure and Figure 2.19(b), for example, shows that the restoring force -- relative displacement relationship is very similar in both cases. In fact, Figure 3.12(b) reveals clearly the stiffness degradation phenomenon that has been discussed in Chapter 2.

3.5 SUMMARY AND CONCLUSIONS

A model has been proposed to represent the restoring force behavior of reinforced concrete buildings subjected to earthquake excitation. This is a physically motivated model based upon the conclusions

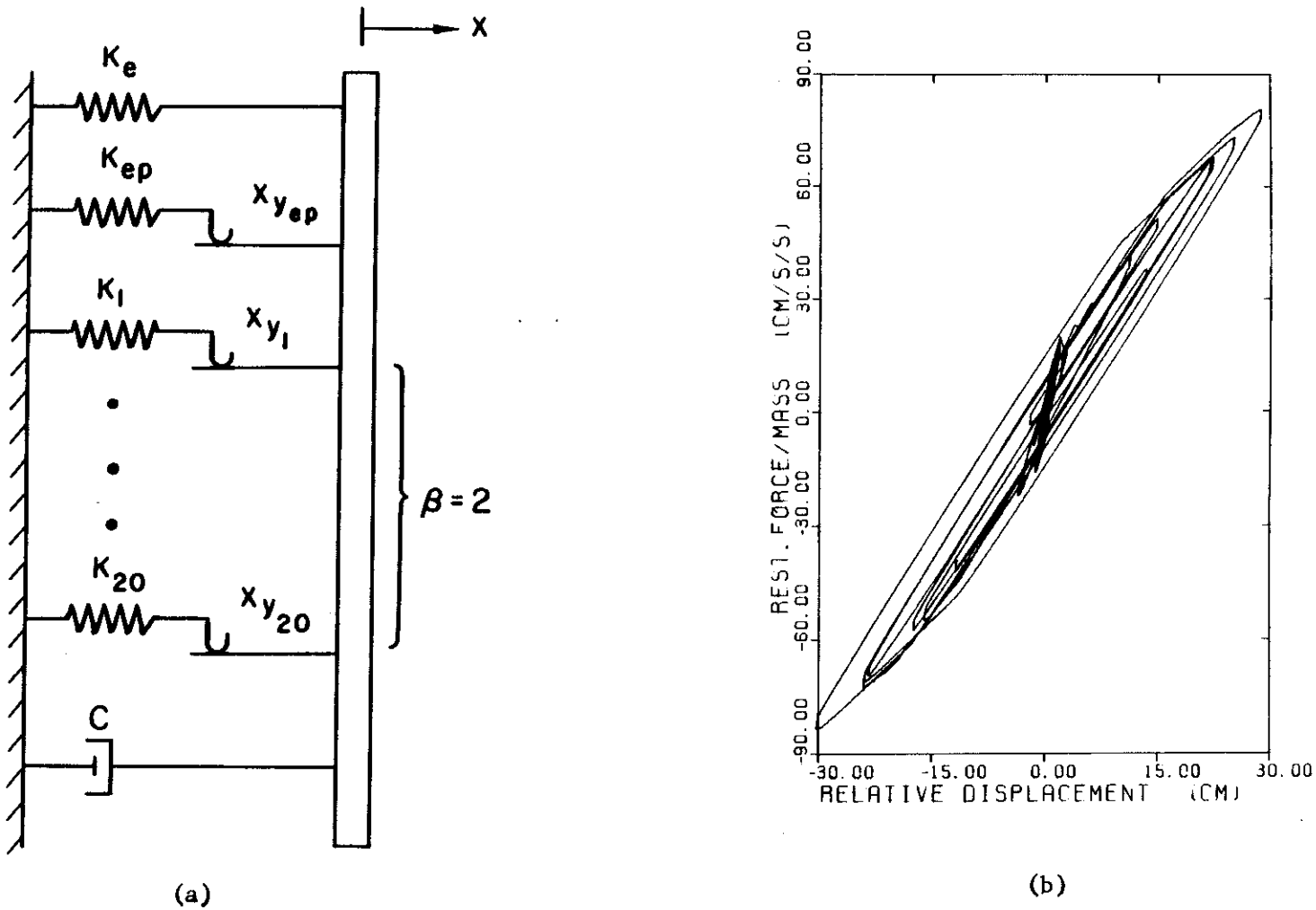

(a) (b)

Figure 3.12 Typical restoring force diagram generated by a DDE model (a) DDE model consisting of 20 deteriorating elements. The parameters of the model are Xy_1 = 1 cm, Xy_2 = 2 cm, ... , Xy_{20} = 20 cm, A = 6 cm^2/sec^2, K_e = 2.0 sec^{-2}, K_{ep} = 1.0 sec^{-2}, Xy_{ep} = 20 cm and C = 0.5 sec^{-1} (b) restoring force diagram.

drawn in Chapter 2 after studying several earthquake records corresponding to actual buildings. The model suggested is intended to be used for estimating the response of structures subjected to strong ground acceleration when deformations are produced beyond the elastic limit. For small oscillations, the DDE model coincides with the linear model since all of the elements behave like linear springs.

REFERENCES

[1] Beck, J.L., "Determining Models of Structures from Earthquake Records," Earthquake Engineering Research Laboratory Report No. EERL 78-01, California Institute of Technology, Pasadena, California, June 1978.

[2] McVerry, G., "Frequency Domain Identification of Structural Models from Earthquake Records," Earthquake Engineering Research Laboratory Report No. EERL 79-02, California Institute of Technology, Pasadena, California, October 1979.

[3] Blume, J.A., "Bank of California, 15250 Ventura Boulevard, Los Angeles," in 'San Fernando, California, Earthquake of February 9, 1971' , L.M. Murphy (ed.), Vol. I, Part A, 327-357, U.S. Dept. of Commerce, National Oceanic and Atmospheric Administration (NOAA), Washington, D.C., 1973.

[4] Iemura, H. and Jennings, P.C., "Hysteretic Response of a Nine-Story Reinforced Concrete Building," International Journal of Earthquake Engineering and Structural Dynamics, Vol. 3, 1974, pp. 183-201.

[5] Otani, S., "Nonlinear Dynamic Analysis of 2-D Reinforced Concrete Building Structures," Third Canadian Conference on Earthquake Engineering, Vol. 2, 1979, pp. 1009-1037.

[6] Saiidi, M., "Influence of Hysteresis Models on Calculated Seismic Response of R/C Frames," Proceedings of the Fifth World Conference on Earthquake Engineering, Vol. 5, Rome, Italy, 1973, pp. 423-430.

[7] Clough, R.W. and Johnston, S.B., "Effect of Stiffness Degradation on Earthquake Ductility Requirements," Proceedings, Japan Earthquake Engineering Symposium, Tokyo, Japan, October 1966, pp. 227-232.

[8] Iwan, W.D., "A Distributed-Element Model for Hysteresis and Its Steady-State Dynamic Response," Journal of Applied Mechanics, Vol. 33, No. 4, Trans. ASME, Vol. 88, Series E, Dec. 1966, pp. 893-900.

[9] Iwan, W.D., "On a Class of Models for the Yielding Behavior of Continuous and Composite Systems," Journal of Applied Mechanics, Vol. 34, No. 3, September 1967, pp. 612-617.

[10] Takeda, T., Sozen, M.A., and Nielsen, N.N., "Reinforced Concrete Response to Simulated Earthquakes," ASCE, Journal of the Structural Division, Vol. 96, December 1970, pp. 2557-2573.

[11] Toussi, S. and Yao, J., "Identification of Hysteretic Behavior for Existing Structures," Report CE-STR-80-19, School of Civil Engineering, Purdue University, December 1980.

[12] Toussi, S. and Yao, J., "Hysteretic Identification of Multi-Story Buildings," Report CE-STR-81-15, School of Civil Engineering, Purdue University, May 1981.

[13] Masri, S.F. and Caughey, T.K., "A Nonparametric Identification Technique for Nonlinear Dynamic Problems," Journal of Applied Mechanics, Vol. 46, June 1979, pp. 433-447.

[14] Wen, Y.-K., "Method for Random Vibration of Hysteretic Systems," ASCE, Journal of the Engineering Mechanics Division, Vol. 102, April 1976, pp. 249-263.

[15] Saiidi, M. and Sozen, M., "A Naive Model for Nonlinear Response of Reinforced Concrete Buildings," Proceedings of the Seventh World Conference on Earthquake Engineering, Istanbul, Turkey, 1980, Vol. 7, pp. 8-14.

[16] Muguruma, M., Tominaga, M. and Watanabe, F., "Response Analysis of Reinforced Concrete Structures Under Seismic Forces," Proceedings of the Fifth World Conference on Earthquake Engineering, Rome, Italy, 1974, Vol. 1, pp. 1389-1392.

[17] Aoyama, H., "Simple Nonlinear Models for the Seismic Response of Reinforced Concrete Buildings," Proceedings of the Review Meeting U.S.-Japan Cooperative Research Program in Earthquake Engineering , Tokyo, Japan, 1976, pp. 291-309.

[18] Atalay, B. and Penzien, J., "Inelastic Cyclic Behavior of Reinforced Concrete Flexural Members," Proceedings of the Sixth World Conference on Earthquake Engineering, New Delhi, India, 1977, Vol. III, pp. 3062-3068.

CHAPTER IV

SYSTEM IDENTIFICATION OF HYSTERETIC STRUCTURES

4.1 INTRODUCTION

The purpose of this chapter is to present a new system identification algorithm to be used with the DDE model introduced in Chapter 3. This algorithm is based on the information obtained from the restoring force diagram and the effective stiffness diagram. Section 4.2 very briefly discusses the traditional approach to the problem of identifying a structural system to facilitate a comparison with the approach herein introduced.

4.2 TRADITIONAL APPROACH

A simplified version of the typical identification problem that arises in structural dynamics is the following: the response x(t) of a real system, (a building for example), to an input ground acceleration a(t) has been recorded. It is assumed that the behavior of the system can be modeled by a certain type of differential equation which is completely determined in terms of some parameters. Assume these parameters are $p_1,\ldots,p_g$. The system identification problem consists therefore in determining the appropriate numerical value for the parameters $p_1,\ldots,p_g$.

The traditional way of solving this problem requires the definition of an error in terms of x(t). That is, a real positive number that quantifies the degree of agreement between the response of the real

system, $x(t)$, and that predicted by the model $x^*(t)$. Some common definitions for the error ε are

$$\varepsilon = \int_0^T |x(t) - x^*(t)|dt \tag{4.1}$$

or

$$\varepsilon = \int_0^T (x(t) - x^*(t))^2 dt \tag{4.2}$$

where T is the time interval for which data are available. Therefore, a natural way to determine the parameters $p_1, \ldots, p_g$ of the model is to choose those values that make ε a minimum. This problem is outlined in Figure 4.1.

It is important to realize that since the minimization of ε is carried out numerically, the function ε (which depends on the parameters $p_1, \ldots, p_g$) needs to be evaluated at several points. Accordingly, each time it is necessary to solve a differential equation to determine the new response $x^*(t)$ predicted by the model. This point will be crucial when evaluating the algorithm proposed in Section 4.3.

The traditional approach in the case of linear systems, with some minor modifications, has been successfully used by several authors, [1],[2].

4.3 A NEW SYSTEM IDENTIFICATION ALGORITHM BASED ON THE RESTORING FORCE

It will be assumed that a decision has been made regarding the

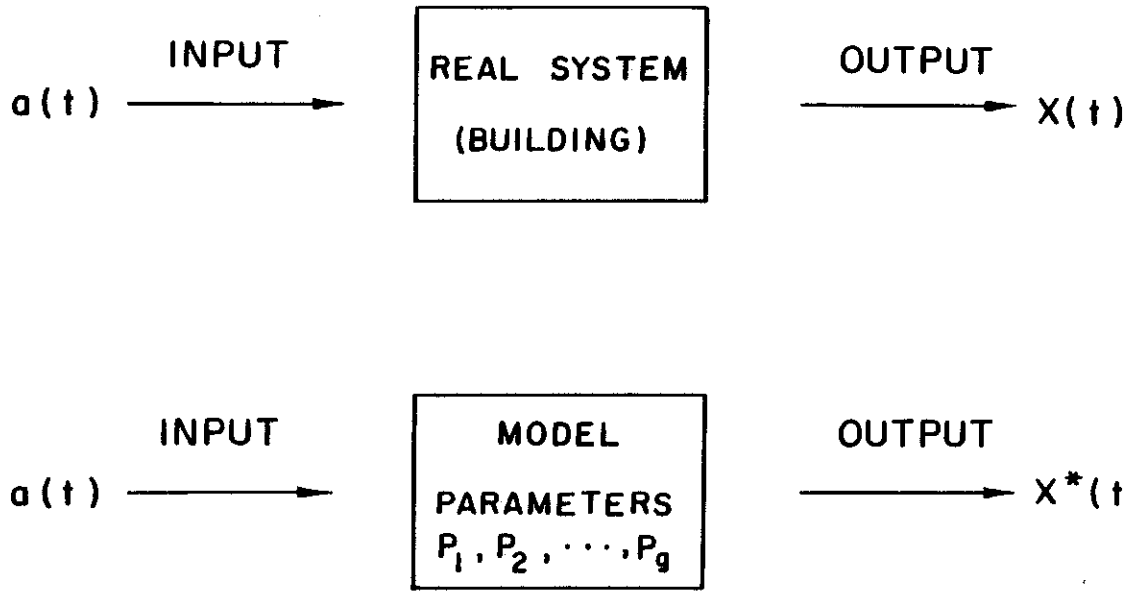

$$\epsilon = \int_0^T [X(t) - X^*(t)]^2 \, dt$$

CHOOSE $P_1, P_2, \cdots, P_g$ SO TO MINIMIZE ϵ .

Figure 4.1 Schematic Representation of a Typical System Identification Problem.

number of deteriorating elements to include in the DDE model, i.e., N. The next step is to determine $Xy_1, \ldots, Xy_N$, the yielding displacement of each of the deteriorating elements.

Let X_{max} be the maximum relative displacement of the roof (in absolute value) determined from the earthquake records for the building under consideration. Since the behavior of the building is essentially unknown for oscillations with amplitude exceeding X_{max}, it is natural to take Xy_n equal to X_{max}. On the other hand, for simplicity, it is convenient to take the values $Xy_1, \ldots, Xy_N$ equally spaced. This simplification leads to the choice

$$Xy_i = \frac{i}{N} X_{max} \qquad \text{for} \quad i=i,\ldots,N \tag{4.3}$$

Therefore, the parameters of the DDE model that remain to be determined are (see Figure 3.9), K_e, K_{ep}, Xy_{ep}, C and A. Recall that A links Xy_i and K_i for each of the deteriorating elements according to (3.14) and remember also that $\beta=2$.

4.3.1 Determination of A

The value of A in the DDE model can be determined directly from the effective stiffness diagram. Assume that this diagram has been computed and K_0 and K_f have been estimated for the building under consideration. Then, one may proceed as follows. Since K_0 is the value associated with the initial stiffness of the structural system, K_0 can be related to the parameters of the DDE model by the relationship

$$K_0 = K_e + K_{ep} + \sum_{i=1}^{N} K_i \tag{4.4}$$

Furthermore, using equation (3.14), equation (4.4) can be rewritten as

$$K_0 = K_e + K_{ep} + A\sum_{i=1}^{N} \frac{1}{Xy_i^2} \tag{4.5}$$

This equation establishes that the initial stiffness of the DDE model is equal to the summation of the contribution of the elastic element, the elastoplastic element and the N deteriorating elements.

The final stiffness of the system, K_f, can be expressed, in terms of the DDE model, as the summation of the contribution of the linear element, the elastoplastic element and those deteriorating elements that are not "broken" after experiencing a displacement equal to X_{max}. The deteriorating elements that have not "failed" are those for which $2Xy_i \geq X_{max}$. Assuming then that the deteriorating elements $\ell+1, \ell+2, \ldots, N$ have not failed, one obtains

$$K_f = K_e + K_{ep} + A \sum_{i=\ell+1}^{N} \frac{1}{Xy_i^2} \tag{4.6}$$

Subtracting equation (4.5) from equation (4.6) leads to

$$K_f - K_0 = A\sum_{i=1}^{\ell} \frac{1}{Xy_i^2} \tag{4.7}$$

the summation on the right hand side includes all the deteriorating elements that are "broken" after experiencing a displacement equal to X_{max}, i.e., those for which $2Xy_i \leq X_{max}$.

Finally, from equation (4.7) one obtains

$$A = \frac{K_f - K_0}{\sum_{i=1}^{\ell} \frac{1}{Xy_i^2}} \tag{4.8}$$

This relationship allows A to be determined from the effective stiffness diagram.

4.3.2 Definition of the Error

The method presented herein is based upon matching the restoring force behavior observed during the earthquake rather than the time history of the response. It is expected that a model able to capture the features of the restoring force, should naturally give a good approximation of the time history of the response, x(t). Therefore, an error in terms of the restoring force diagram will be defined.

It will be assumed that the viscous damping coefficient, C, is small and can be neglected when defining the error in terms of the restoring force. This means, that the contribution to the total restoring force made by the term $C\dot{x}$, is small compared to the contribution made by the elastic, elastoplastic and deteriorating elements of the DDE model.

The motivation for this assumption is that the viscous damping coefficient should not control the large amplitude oscillations. Therefore, a value of the order of 1% or 2% of critical damping is expected

to be appropriate for C and accordingly it can be neglected when defining the error. It must be understood, however, that the value of the viscous damping coefficient C in the DDE model is not zero in general. Section 4.3.5 deals with its determination.

Assume that the restoring force diagram corresponding to the structure considered is given by a discrete set of points (x_i, f_i) $i=1,\ldots,q$ where x_i is the relative displacement and f_i the corresponding value of the restoring force per unit of mass. Consider a typical hysteresis loop, such as the one shown in Figure 4.2. The intersections with the vertical axis, of each hysteresis loops of the restoring force diagram, can be determined using the points (x_i, f_i) and linear interpolation. Let g_j and g_{j+1} be the values of the restoring force at these points. The value of the restoring force for the maximum positive displacement in the loop and the maximum negative displacement in the loop can likewise be determined. Let these values be h_s and h_{s+1} as shown in Figure 4.2.

Each hysteresis loop is, therefore, characterized by four points. Assume that the restoring force diagram given by the DDE model, and for the same time history x(t), is given by the points (x_i, f_i^*) $i=1,\ldots,q$. And conversely, let g_j^*, g_{j+1}^*, h_s^* and h_{s+1}^* be the points that characterized the corresponding hysteresis loops. A natural definition of the error between the two restoring force diagrams would be associated with the differences between the values h_s and h_s^*, and g_j and

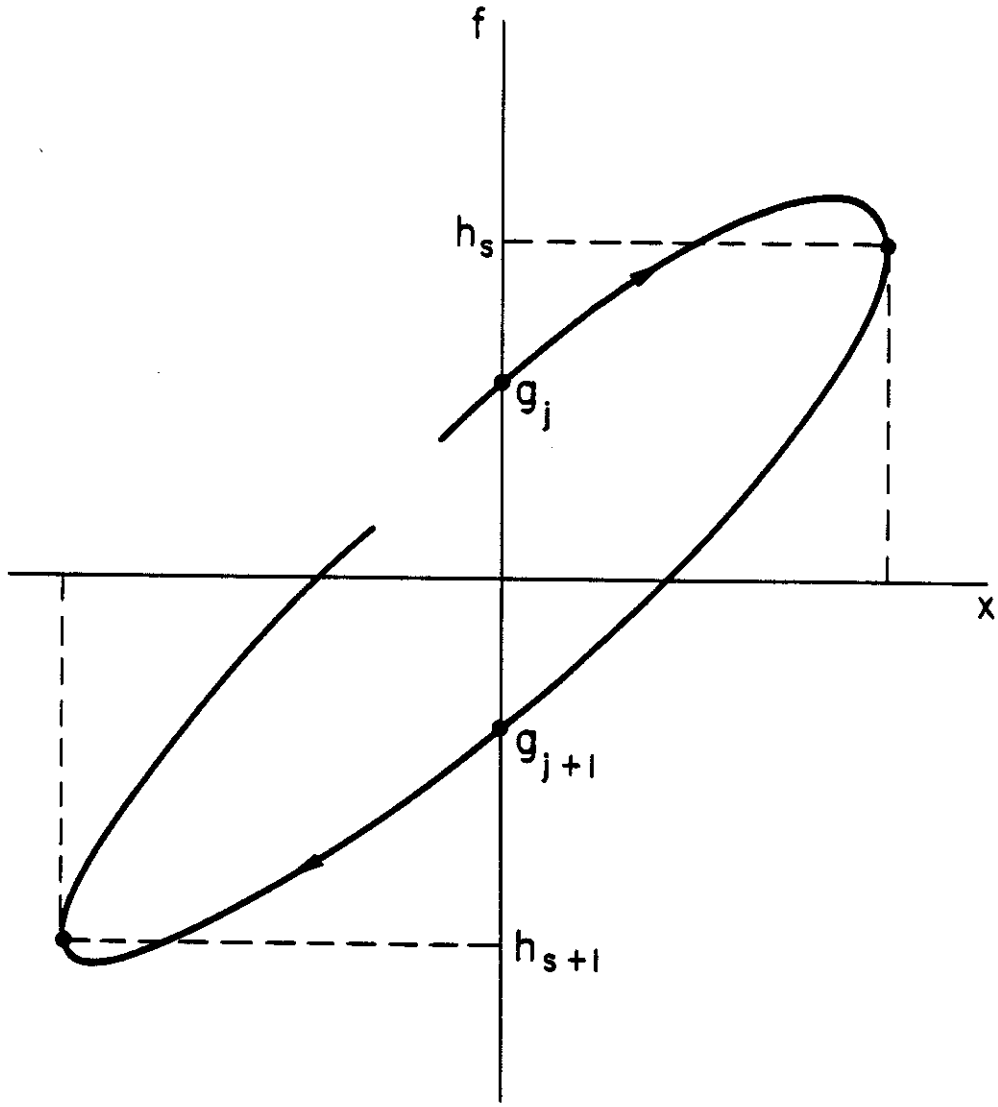

Figure 4.2 Typical Hysteresis loop

g_j^*. Hence, the error, ε, to be used in the system identification process will be defined as

$$\varepsilon = \sum_s |h_s - h_s^*| + B \sum_j | g_j - g_j^*| \qquad (4.9)$$

Both summations include all the necessary points to define the hysteresis loops of the restoring force diagram considered. The factor B, is to homogenize the variance of both populations (h's and g's) so they can be comparable. B is defined as

$$B = \frac{\sum_s h_s^2}{\sum_j g_j^2} \qquad (4.10)$$

Notice that neglecting the viscous damping when determining ε, at least in the case of the h's, should not be important since these values correspond to maximums or minimums of x and therefore the velocity $\dot{x}$ is zero. Consequently, there is no contribution to the restoring force due to viscous damping at these points.

A significant feature of the proposed system identification algorithm is that the evaluation of the error ε, as defined in equation (4.9), does not require the solution of any differential equation. It requires only the determination of (x_i, f_i^*) i=1,..., q i.e., the values of the restoring force f_i^* at each point x_i. The advantage of neglecting the viscous damping when defining the error ε, now becomes apparent. This is in clear contrast to the traditional approach in which each new

evaluation of the error requires a new differential equation to be solved. Accordingly, this new system identification algorithm based on the restoring force is expected to be much more efficient in terms of reducing the amount of computation.

4.3.3 Minimization of the Error ε

Having determined A, and neglecting for the moment the viscous damping coefficient C, the next step in the system identification process is to determine K_e, K_{ep} and Xy_{ep}.

Noting that the error ε defined in equation (4.9) is now a function of K_e, K_{ep} and Xy_{ep} only, the following problem can be formulated to estimate the value of these parameters.

$$\text{Min} \quad \varepsilon = \varepsilon(K_e, K_{ep}, Xy_{ep}) \tag{4.11a}$$

subjected to

$$K_e \geq 0 \quad , \quad K_{ep} \geq 0 \quad \text{and} \quad Xy_{ep} \geq 0 \tag{4.11b}$$

This is a standard nonlinear optimization problem, in which the optimum must be found by means of numerical techniques. Several approaches are available to attack such a problem. A detailed discussion concerning the possible algorithms to be used is beyond the scope of this thesis. For this purpose one can refer to Gallagher [3], Rosen [4], Fletcher [5] or Luenberger [6].

In this investigation, the following numerical technique was

employed to solve the problem formulated by relationships (4.11a) and (4.11b).

(i) Let K_e^o, K_{ep}^o and Xy_{ep}^o be initial guesses for the optimum.

(ii) Keeping K_{ep}^o and Xy_{ep}^o as constants, evaluate ε for several values of K_e i.e., K_e^o, $K_e^o + \delta$, $K_e^o + 2\delta$, ... in which δ is a small positive or negative number. The evaluation of ε continues until a minimum of the function ε has been isolated. That is, until an integer number r has been found such that

$$\varepsilon(K_e^o+r\delta, K_{ep}^o, Xy_{ep}^o) > \varepsilon(K_e^o+(r+1)\delta, K_{ep}^o, Xy_{ep}^o)$$

and (4.12)

$$\varepsilon(K_e^o+(r+1)\delta, K_{ep}^o, Xy_{ep}^o) < \varepsilon(K_e^o+(r+2)\delta, K_{ep}^o, Xy_{ep}^o)$$

(iii) A new approximation for the optimum K_e is computed by passing a parabola through the three points $K_e^o + r\delta$, $K_e^o + (r+1)\delta$ and $K_e^o + (r+2)\delta$ and evaluating the minimum of this parabola analytically. K_e^o is redefined using this new approximation and δ is halved.

(iv) An analogous process to the one described in (ii) and (iii) is carried out considering K_e^o and Xy_{ep}^o as constants and K_{ep} as a variable and afterwards K_e^o and K_{ep}^o as constants and Xy_{ep} as a variable.

(v) Once step (iv) has been completed, a new approximation K_e^o, K_{ep}^o, Xy_{ep}^o to the optimum is obtained. Steps (ii), (iii) and (iv) are repeated until the function ε no longer exhibits a significant decrease.

In order to avoid an indefinite search for a minimum when carrying out the one dimensional minimizations for K_e, K_{ep} and Xy_{ep} some upper bounds for these variables must be defined. For the case of K_e and K_{ep}, K_0 provides a reasonable upper bound. In the same manner X_{max} is a reasonable upper bound for Xy_{ep}.

4.3.4 Determination of the Participation Factor

The participation factor α is defined by analogy to the linear single-degree-of-freedom model. In this case, the participation factor specifies the fraction of the ground acceleration $\ddot{z}(t)$ which excites the fundamental mode. Even though the DDE model is a nonlinear model, one may define the participation factor as in the linear case.

Let

$$\ddot{x} + f(x,\dot{x}) = -a(t) \qquad (4.13a)$$

where

$$a(t) = \alpha\ddot{z}(t) \qquad (4.13b)$$

and $f(x,\dot{x})$ is the restoring force per unit of mass given by the DDE model and $a(t)$ the input acceleration. In order to compute an appropriate value α in a given situation, two approaches may be used:

(a) If the mass distribution matrix of the structure analyzed is known and if there exist earthquake records for at least three different locations in the structure (e.g., the basement, the roof and an intermediate floor), one may assume that

$$\alpha = \frac{\{\phi_1\}^T \mathcal{M} \underline{1}}{\{\phi_1\}^T \mathcal{M} \{\phi_1\}} \tag{4.14}$$

where $\{\phi_1\}$ is the vector shape of the first mode of vibration of the structure computed from the earthquake records and $\mathcal{M}$ is the mass distribution matrix of the structure.

(b) If the information required in (a) is not available, one may assume the value of α used for the first mode of the structure during the design process.

The above recommendations to estimate α are based upon the assumption that a participation factor for the DDE model can be estimated assuming linear behavior, even though the DDE model is a nonlinear model. This hypothesis appears to be verified by the results presented in Chapter 5.

4.3.5 Determination of the Viscous Damping Coefficient

The last parameter of the DDE model to be determined is the viscous damping coefficient C. This parameter can be estimated using the time history of the response. The time history of the response predicted by the DDE model, $x^*(t)$, can be computed for several values of

C and compared to x(t), the time history determined from the earthquake records. The value of C that gives a best fit is selected.

The determination of C by means of this approach requires only a very few computations of the time history of the response; no more than four according to the results shown in Chapter 5.

This is in clear contrast to the traditional approach in which all of the parameters of the model are estimated by minimizing an error which depends on the time history of the response. As a consequence, the time history of the response needs to be determined many times and the amount of computation involved increases considerably compared to the algorithm herein introduced.

As mentioned in Section 4.3.2, it is expected that the viscous damping coefficient will be small; of the order of 1% or 2%. The reason for this is that the large amplitude oscillations of the system are controlled primarily by the energy dissipated through hysteresis. Therefore, the viscous damping is really only important for the small amplitude oscillations corresponding to the final portion of the response record.

4.4 FLOW CHART OF THE COMPLETE SYSTEM IDENTIFICATION PROCESS

A flow chart of the complete system identification process described in Section 4.3, including the earthquake records corrections discussed in Chapter 2, is herein presented.

SYSTEM IDENTIFICATION OF HYSTERETIC STRUCTURES

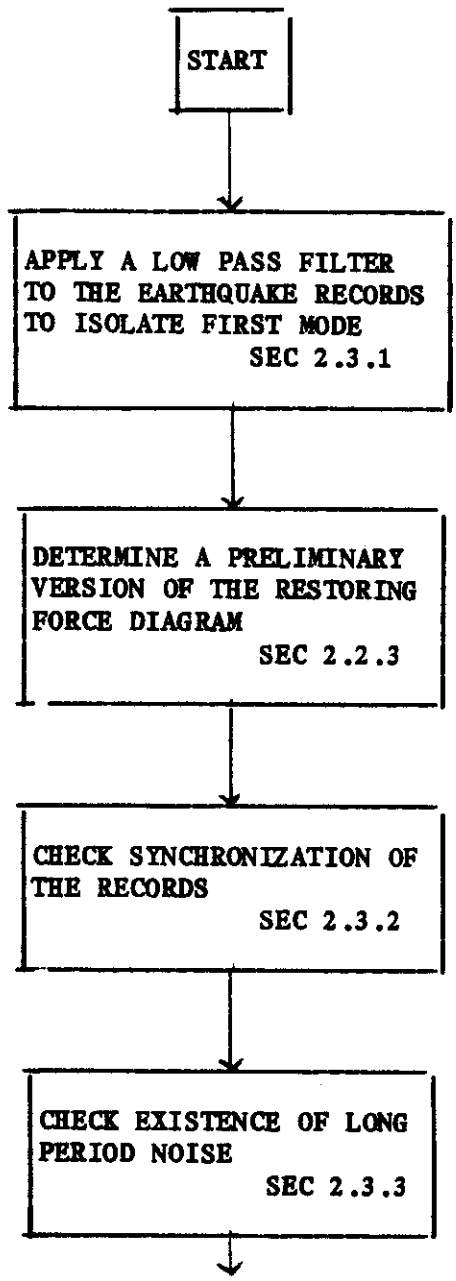

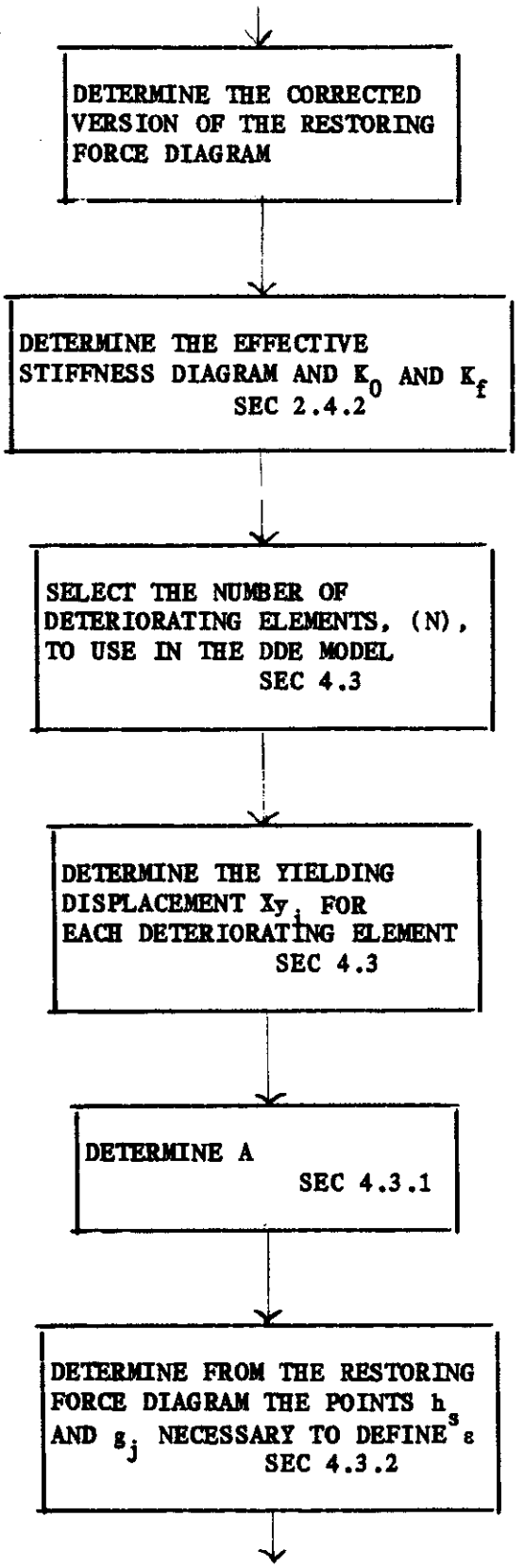
DETERMINE THE CORRECTED VERSION OF THE RESTORING FORCE DIAGRAM
DETERMINE THE EFFECTIVE STIFFNESS DIAGRAM AND K_0 AND K_f SEC 2.4.2
SELECT THE NUMBER OF DETERIORATING ELEMENTS, (N), TO USE IN THE DDE MODEL SEC 4.3
DETERMINE THE YIELDING DISPLACEMENT X_{y_i} FOR EACH DETERIORATING ELEMENT SEC 4.3
DETERMINE A SEC 4.3.1
DETERMINE FROM THE RESTORING FORCE DIAGRAM THE POINTS h_s AND g_j NECESSARY TO DEFINE ε SEC 4.3.2

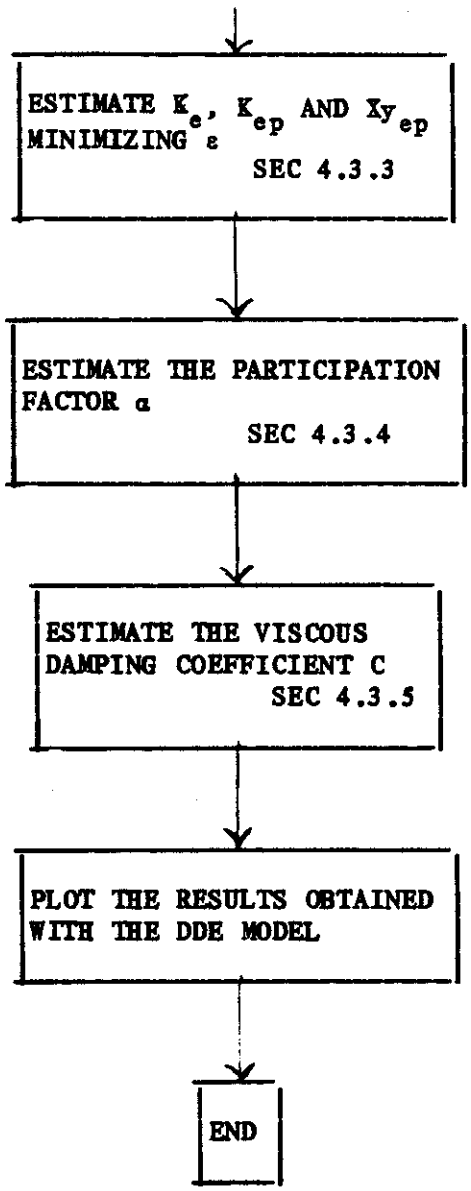
ESTIMATE K_e, K_{ep} AND Xy_{ep} MINIMIZING ε
SEC 4.3.3
ESTIMATE THE PARTICIPATION FACTOR α
SEC 4.3.4
ESTIMATE THE VISCOUS DAMPING COEFFICIENT C
SEC 4.3.5
PLOT THE RESULTS OBTAINED WITH THE DDE MODEL
END

REFERENCES

[1] Beck, J.L., "Determining Models of Structures from Earthquake Records," Earthquake Engineering Research Laboratory Report No. EERL 78-01, California Institute of Technology, Pasadena, California, June 1978.

[2] Beck, J.L. and Jennings, P.C., "Structural Identification Using Linear Models and Earthquake Records," International Journal of Earthquake Engineering and Structural Dynamics, Vol. 8, 145-160, April 1980.

[3] Gallagher, R.H. and Zienkiewicz, O.C. (Ed.), Optimum Structural Design, Theory and Applications, John Wiley and Sons, 1973.

[4] Rosen, J.B. (Ed.), Nonlinear Programming, Academic Press, 1970.

[5] Fletcher, R., Practical Methods of Optimization, John Wiley and Sons, 1980.

[6] Luenberger, D.G., Introduction to Linear and Nonlinear Programming, Addison Wesley, 1973.

CHAPTER V

NUMERICAL EXAMPLES

5.1 INTRODUCTION

This chapter deals with the application of the DDE model introduced in Chapter 3 and the identification algorithm introduced in Chapter 4 to actual earthquake data. Examples from the Bank of California, Holiday Inn and Imperial County Services buildings are presented and discussed.

5.2 THE BANK OF CALIFORNIA BUILDING

The Bank of California building is located at 15250 Ventura Boulevard in the city of Sherman Oaks. Its distance to the epicenter of the San Fernando earthquake of 1971 is approximately 14 miles. The building is a twelve story reinforced concrete moment-resisting structure. Plan dimensions of the floors are 60 X 161 ft except for the first story which is a little larger, 90 X 161 ft. This building stands 159 ft above the street level. During the San Fernando event this structure suffered both structural and nonstructural damage. The structural damage consisted mainly of cracking and spalling of columns and girder stubs. A more detailed description of this building, as well as its performance in the San Fernando earthquake, can be found in the report by Blume [1] and Foutch et al. [2].

5.2.1 Model for the N11E Component

In this first example the calculations will be presented with more detail in order to clarify the steps of the system identification process.

It will be attempted to model the N11E component of the Bank of California building using a DDE model with nine deteriorating elements, i.e., N=9. From the earthquake records, it is found that the maximum relative displacement of the roof, X_{max}, was approximately 29 cm. Accordingly, the yielding displacement for each of the deteriorating elements is determined as follows:

$$Xy_1 = 5cm; \quad Xy_2 = 8cm.; \quad Xy_3 = 11cm.$$
$$Xy_4 = 14cm; \quad Xy_5 = 17cm.; \quad Xy_6 = 20cm.$$
$$Xy_7 = 23cm; \quad Xy_8 = 26cm.; \quad Xy_9 = 29cm.$$

Using the effective stiffness diagram depicted in Figure 2.22(a) one can estimate $K_f - K_0$ as approximately 14 sec^{-2}. Then, by means of equation (4.8) one can estimate A as follows:

$$A = \frac{14}{\left[\frac{1}{5^2} + \frac{1}{8^2} + \frac{1}{11^2} + \frac{1}{14^2}\right]} \frac{cm^2}{sec^2} = 202.9 \frac{cm^2}{sec^2} \qquad (5.1)$$

Note that when applying equation (4.8), f has been taken equal to 4. The reason is that the first four deteriorating elements are expected to "break" since for each of these elements $2Xy_i \leq X_{max}$.

One proceeds to determine K_e, K_{ep} and Xy_{ep} by minimizing the error ε defined in terms of the restoring force diagram shown in Figure 2.19(a). The solution of this optimization problem, as indicated in Section 4.3.3, leads to

$$K_e = 4.75 \text{ sec}^{-2} \; ; \; K_{ep} = 1.3 \text{ sec}^{-2} \text{ and } Xy_{ep} = 9.5 \text{ cm.} \quad (5.2)$$

The next step is the determination of the participation factor α. As mentioned in Section 4.3.4 one possibility for estimating α is by means of relationship (4.14). Three earthquake records corresponding to three different locations in the building (roof, 7^{th} floor and basement) are available in this case. This allows one to estimate the mode shape of the fundamental mode of vibration of the structure, $\{\phi_1\}$, as

$$\{\phi_1\} = \begin{bmatrix} 1.000 \\ 0.575 \end{bmatrix} \quad (5.3)$$

where the first component represents the relative displacement of the roof in the N11E direction and the second component represents the relative displacement of the 7^{th} floor. The mass distribution of this building is given in [1]. This information allows one to determine the mass distribution matrix, , for the case in which the building is considered as a system composed by two lumped masses. One mass is at the roof level and the other is at the 7^{th} floor level. This yields,

$$\mathcal{M} = \begin{pmatrix} 6010 \text{ Kg.} & 0 \\ 0 & 8760 \text{ Kg.} \end{pmatrix} \quad (5.4)$$

Therefore, applying equation (4.14), one obtains

$$\alpha = \frac{\begin{bmatrix}1 & 0.575\end{bmatrix}\begin{bmatrix}6010 & 0\\ 0 & 8760\end{bmatrix}\begin{bmatrix}1\\ 1\end{bmatrix}}{\begin{bmatrix}1 & 0.575\end{bmatrix}\begin{bmatrix}6010 & 0\\ 0 & 8760\end{bmatrix}\begin{bmatrix}1\\ .575\end{bmatrix}} = 1.3 \qquad (5.5)$$

Had the information required to use this approach to estimate α been unavailable, it would have been possible to simply use the value considered for the participation factor in the design process. This value, as reported by Blume [1], is equal to 1.27.

In this particular example there is an additional piece of information concerning the participation factor as a consequence of a study carried out by McVerry [3]. This study presents estimations for the participation factor of the fundamental mode assuming linear behavior and dividing the earthquake records in two segments. For the first segment of the record (0-20.48 seconds) the participation factor is estimated as 1.49. For the second segment of the record (19-39.48 seconds) the participation factor is estimated as 1.52. It is believed that the estimation of the participation factor given by McVerry, although not too different from that obtained using the approaches indicated in Section 4.3.4, is probably more accurate. Therefore, a value of 1.5 is adopted for α.

At this stage, all the parameters of the DDE model have been estimated except the viscous damping coefficient, C. Figure 5.1 shows the time history of the response estimated by the DDE model herein determined assuming the viscous damping coefficient to be zero.

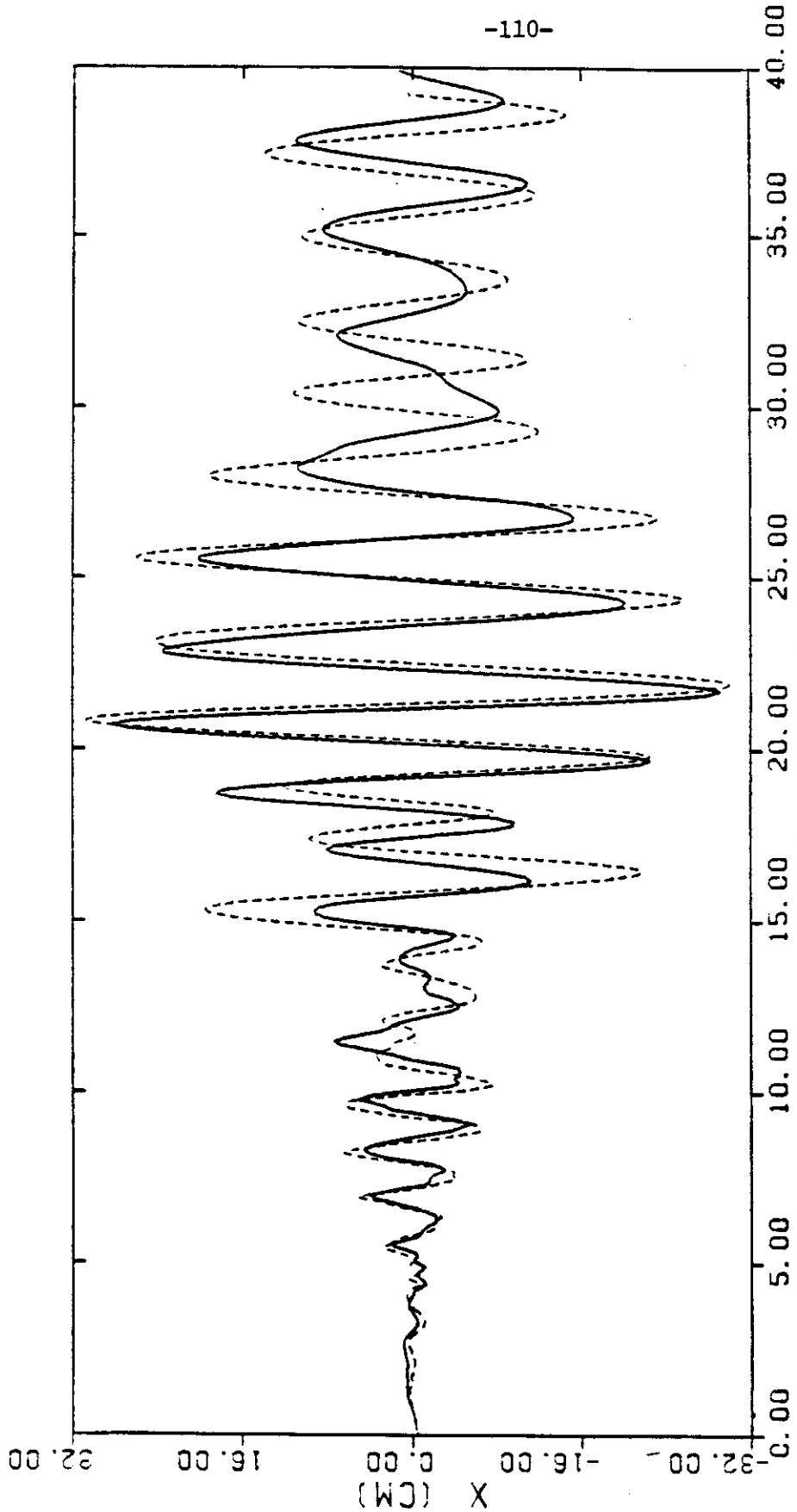

Figure 5.1 Bank of California building, N11E component. Comparison between the actual response (solid line) and the response given by the DDE model with zero viscous damping coefficient (dashed line).

Figure 5.1 allows one to observe that the time history given by this model matches reasonably well the large amplitude peaks. While the larger discrepancies between the actual record and the estimated response correspond to smaller amplitude oscillations. Moreover, one notices in Figure 5.1 that the model somewhat overestimates the amplitude of the peaks mainly in the last portion of the record where the response again becomes nearly linear. This supports the hypothesis made in Section 4.3.5 to the effect that the large amplitude oscillations would be controlled by the energy dissipated through the elasto-plastic and deteriorating elements rather than the energy dissipated through viscous behavior. As a consequence, the viscous damping coefficient C appropriate for this case should be small.

It is found that the value of C that gives an optimum fit in terms of the time history of the response is C = .15 sec^{-1}. Making an analogy with the linear SDOF oscillator, one can quantify the viscous damping coefficient using the expression

$$\zeta = \frac{C}{2\sqrt{K}} \tag{5.6}$$

where ζ is the fraction of critical damping; C is the viscous damping coefficient and K the stiffness coefficient per unit of mass. For the purpose of this computation one can consider K to be equal to the virgin stiffness of the structure. In this case

$$K = K_e + K_{ep} + A \sum_{i=1}^{9} \frac{1}{Xy_i^2} = 21.95 \text{ sec}^{-2} \qquad (5.7)$$

Therefore

$$\zeta = \frac{0.15}{2\sqrt{21.95}} = 1.6\% \qquad (5.8)$$

The estimated values of the parameters of the DDE model are summarized in Table 5.1.

TABLE 5.1

Parameters of the DDE Model. Bank of California Building, N11E Component

K_e $\frac{1}{sec^2}$	K_{ep} $\frac{1}{sec^2}$	Xy_{ep} cm	α	C $\frac{1}{sec}$	A $\frac{cm^2}{sec^2}$
4.75	1.3	9.5	1.5	0.15	202.9

The restoring force diagram corresponding to the model is displayed in Figure 5.2. This diagram clearly shows the stiffness degradation phenomenon already commented in Chapter 2.

Figure 5.3 depicts the time history of the response predicted by the DDE model compared to the actual time history recorded during the earthquake. The agreement between the two curves can be considered good. One notes near t = 30 seconds that the DDE model produces a local positive "peak" that does not appear in the actual record. A similar situation was found by McVerry [3] when trying to fit a linear model for the velocity using the second segment of the record (19.00-39.48

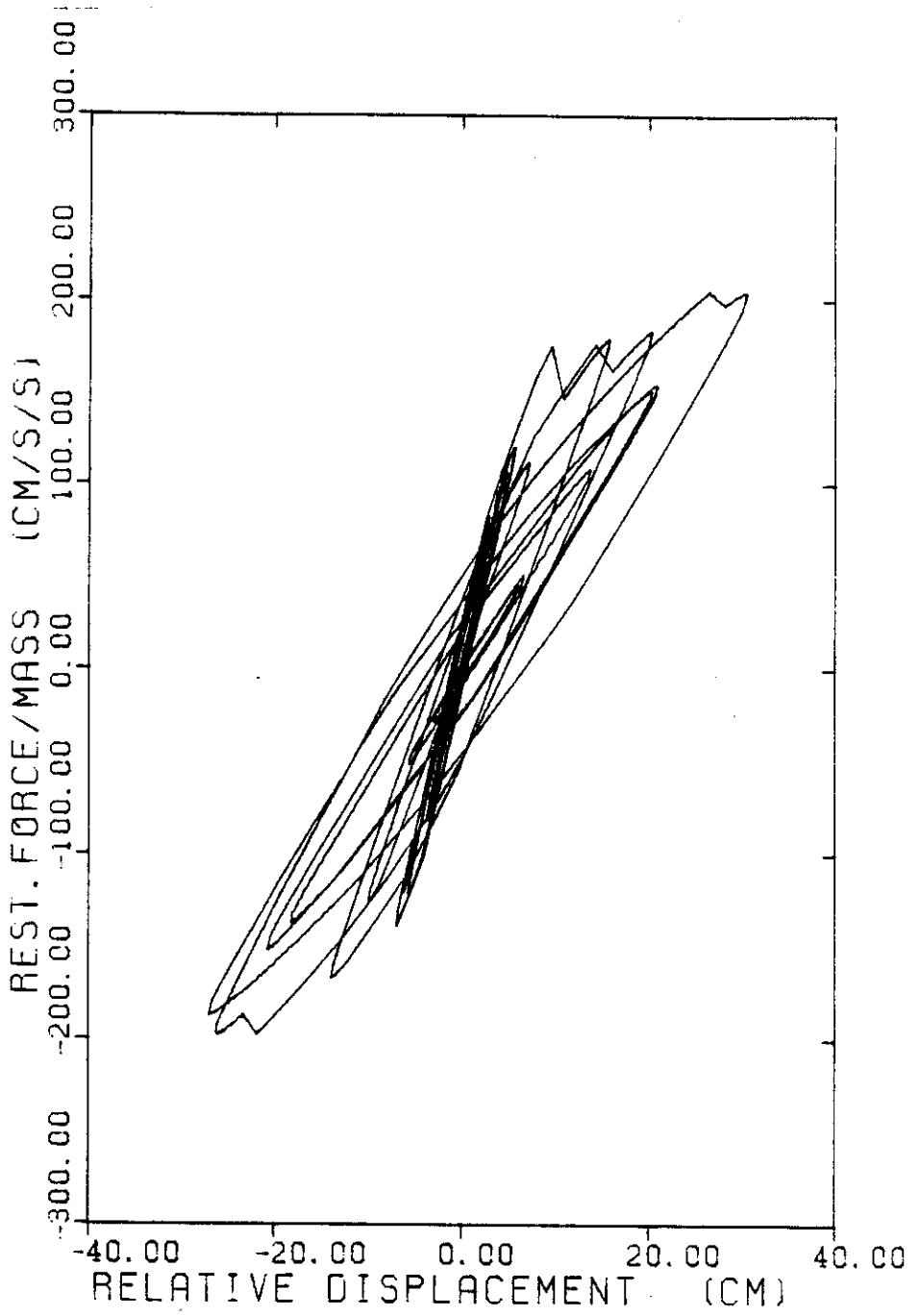

Figure 5.2 Bank of California building, N11E component. Restoring force diagram given by the optimal DDE model.

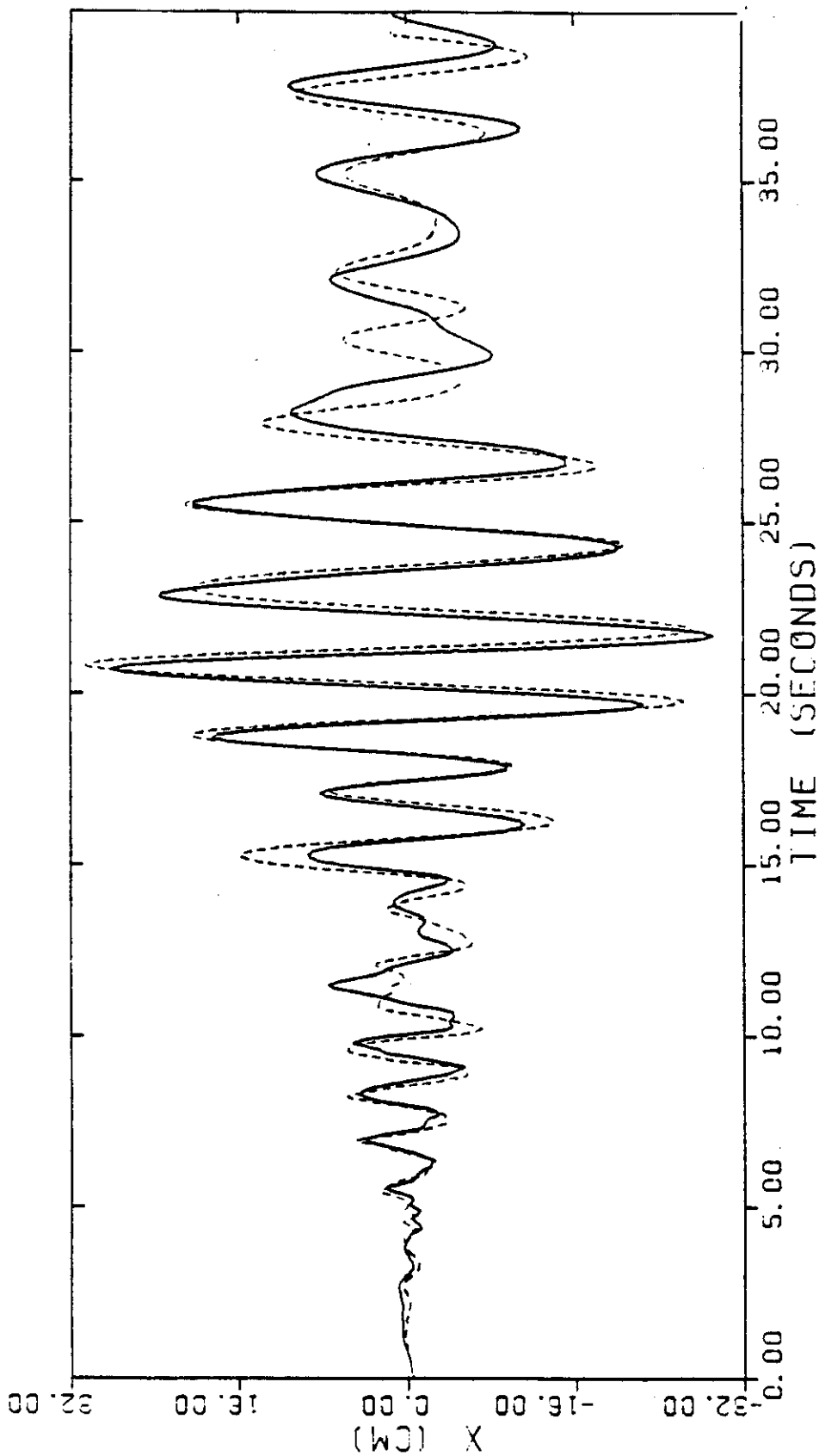

Figure 5.3 Bank of California building, N11E component. Comparison between the actual response (solid line) and the response given by the optimal DDE model (dashed line).

seconds). No physical explanation was found for this phenomenon. Perhaps it is associated with an error during the digitization of the record.

The nonlinear nature of the behavior of this building is clearly reflected in the DDE model. For the small amplitude oscillations that occurred near the beginning of the shaking, the effective stiffness of the system was approximately 21.95 sec^{-2}, as indicated by equation (5.7). In the final portion of the response, however, the effective stiffness of the system for small amplitude oscillations had decreased due to deterioration to a value of approximately

$$K_e + K_{ep} + A \sum_{i=5}^{1} \frac{1}{Xy_i^2} = 8.15 sec^{-2} \qquad (5.9)$$

This represents a decrease of approximately 60% in effective stiffness.

Figure 5.4(a) shows the absolute acceleration of the roof, as obtained from the earthquake records. Figure 5.4(b) shows the approximation given by the one-mode DDE model. It is quite clear that the time history of the absolute acceleration given by the DDE model misses most of the high frequencies of the signal, although the overall behavior is similar to that of the recorded accelerogram. This is due to the fact that the DDE model presented is a one-degree-of-freedom model. Since the acceleration is normally rich in high frequencies, particularly in the initial part of the shaking, one cannot expect the single-degree-of-freedom model to capture the details of the acceleration response.

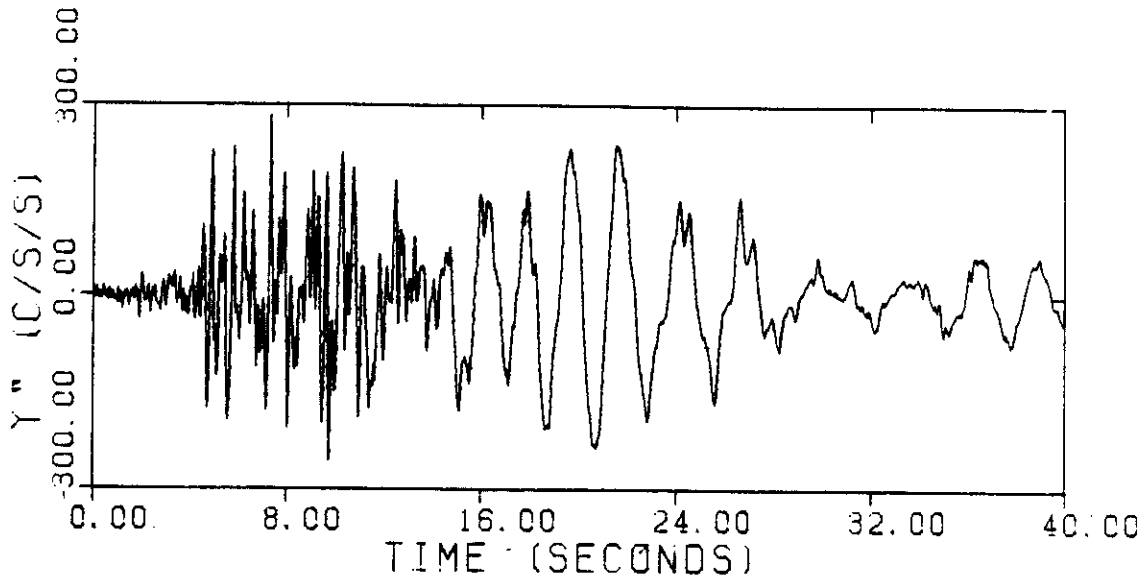

(a)

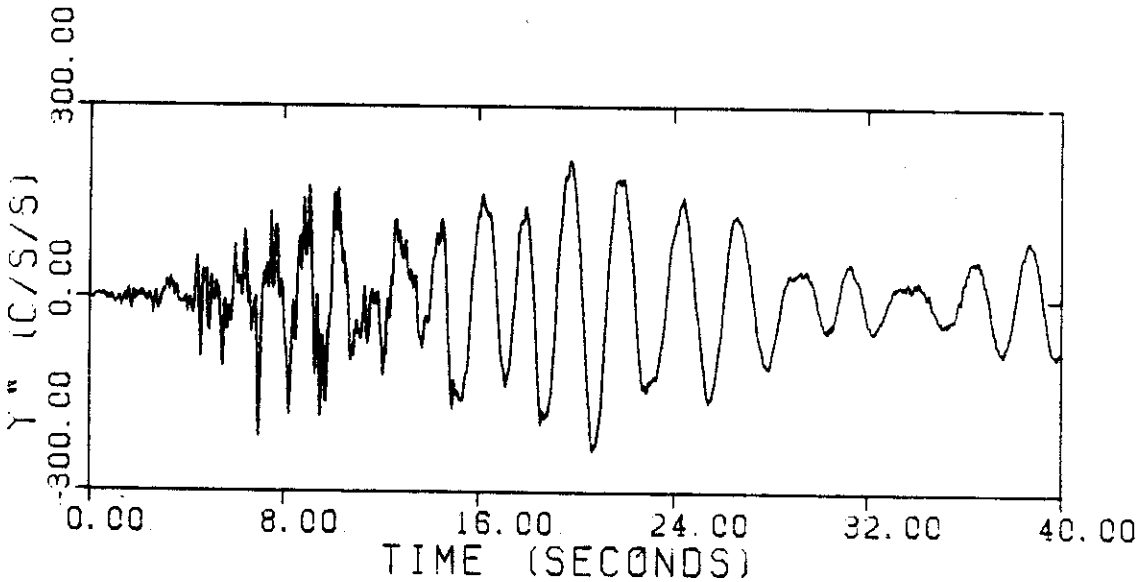

(b)

Figure 5.4 Bank of California building, N11E component. Time history of the absolute acceleration of the roof. (a) actual time history (b) approximation given by the DDE model.

If it is desired to approximate the time history of the acceleration rather than the displacement, more modes should be included. Indeed, each mode of the response could be approximated by a DDE model and the total response determined by combining the contribution of each mode in some logical manner. Further speculations regarding this possibility will be left to be considered in future investigations.

It may be recalled that in this particular case it was necessary to synchronize the final portion of the records (32-40 seconds) by applying a time shift that made the negative hysteresis loops become positive. To investigate the sensitivity of the estimations obtained for K_e, K_{ep} and Xy_{ep} with respect to this correction, it was decided to use the uncorrected version of the restoring force diagram to define the error ε and again solve the minimization problem. No significant difference was found between the values obtained using either the corrected record or the uncorrected record. This does not mean, however, that the correction for synchronization is unnecessary in general. The result described herein, could be simply attributed to the fact that the correction is applied only to the final segment of the records where the amplitude of oscillation is relatively small compared to the peak value. This correction could be much more significant if the model is used for a higher mode of response. Recent research by McVerry and Beck [4] has shown that lack of synchronization between the roof and basements records tends to be more important for higher modes.

5.2.2 Model for the N79W Component

A DDE model with nine deteriorating elements (N=9) is considered, as in the case of the N11E component. The values chosen for the yielding displacements of the deteriorating elements are the following:

Xy_1 = 5cm; Xy_2 = 10cm; Xy_3 = 15cm;
Xy_4 = 20cm; Xy_5 = 25cm; Xy_6 = 30cm;
Xy_7 = 35cm; Xy_8 = 40cm; Xy_9 = 45cm.

The value of the remaining parameters of the DDE model are determined using the effective stiffness diagram of Figure 2.22(b) and the restoring force diagram shown in Figure 2.19(b).

The calculations follow the routine already described for the case of the N11E component.

TABLE 5.2

Parameters of the DDE Model. Bank of California Building, N79W Component

K_e $\frac{1}{sec^2}$	K_{ep} $\frac{1}{sec^2}$	Xy_{ep} cm	α	C $\frac{1}{sec}$	A $\frac{cm^2}{sec^2}$
2.5	0.99	26.3	1.3	0.095	140

Table 5.2 shows the estimated values of the parameters of the DDE model. The value assumed for the participation factor of the first mode during the design process was 1.29 [1]. Accordingly, a value of 1.3 was adopted.

Figure 5.5 shows the time history of the response predicted by the DDE model assuming a viscous damping coefficient equal to zero. Figure 5.6 shows the time history of the response predicted by the DDE model using the optimum value of the viscous damping coefficient. The approximation given by the model fairly well matches the response recorded during the earthquake. The viscous damping coefficient ($C=0.095$ sec.$^{-1}$) corresponds to a fraction of critical damping of 1.3%. This value was estimated as in section 5.2.1.

Figure 5.7 depicts the restoring force diagram given by the model. This figure clearly shows the stiffness degradation phenomenon that characterized the earthquake response of this structure. In this case four deteriorating elements failed. This represents a decrease of approximately 65% in effective stiffness.

Figure 5.8(a) shows the absolute acceleration of the roof determined from the earthquake records and Figure 5.8(b) shows the estimation obtained by means of the DDE model. Again, it is observed that the model, although giving a reasonable overall approximation, fails to represent the high frequency signal that dominates the acceleration record for the time interval between 0. and 16. seconds. One must realize, however, that this is not so much a weakness of the model itself but of the single-degree-of-freedom approximation.

5.2.3 Comparison with Linear Modeling

An attempt was made to model the time history of the response of the Bank of California in each direction using a linear SDOF model.

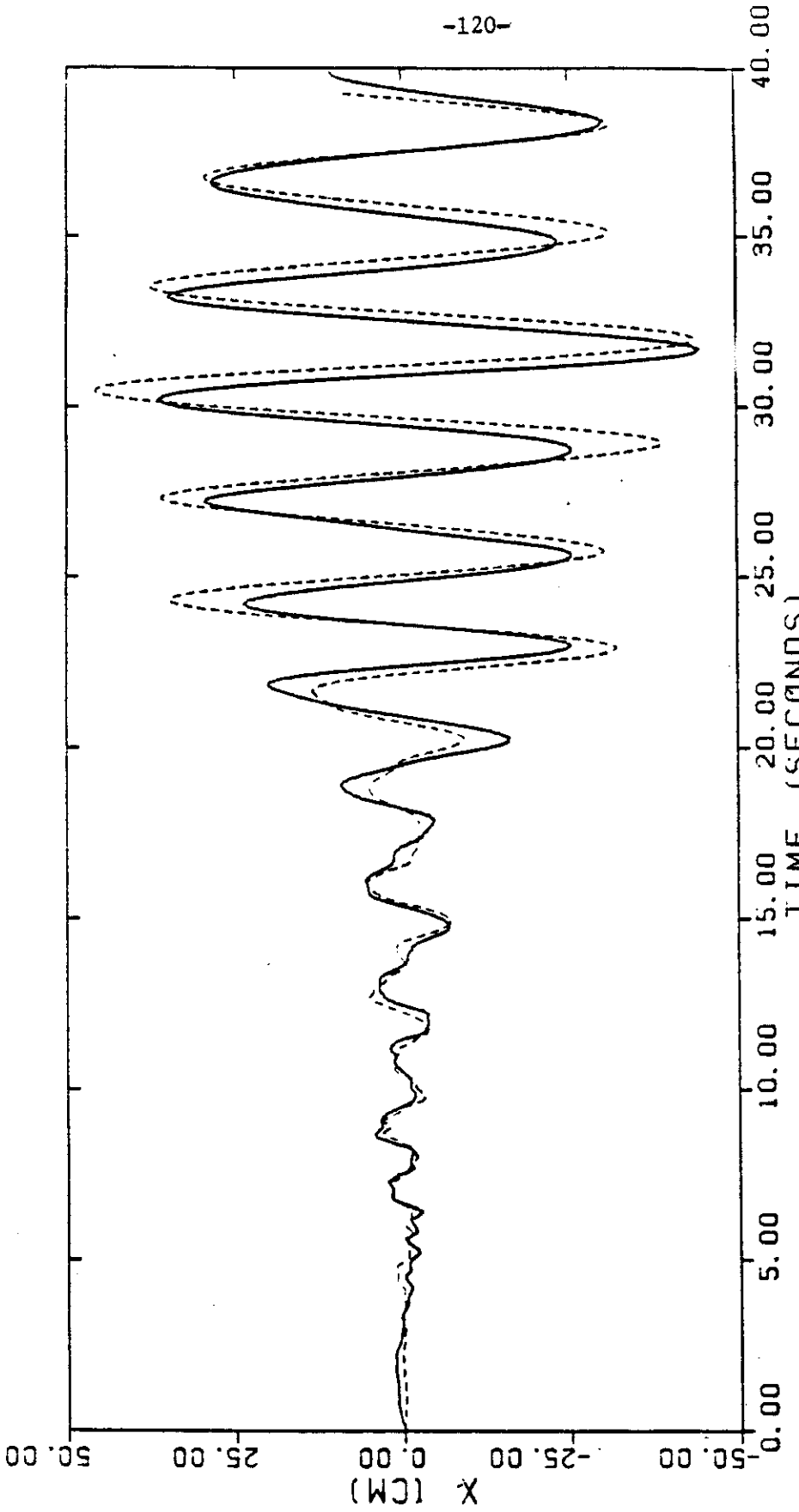

Figure 5.5 Bank of California building, N79W component. Comparison between the actual response (solid line) and the response given by the DDE model with zero viscous damping coefficient (dashed line).

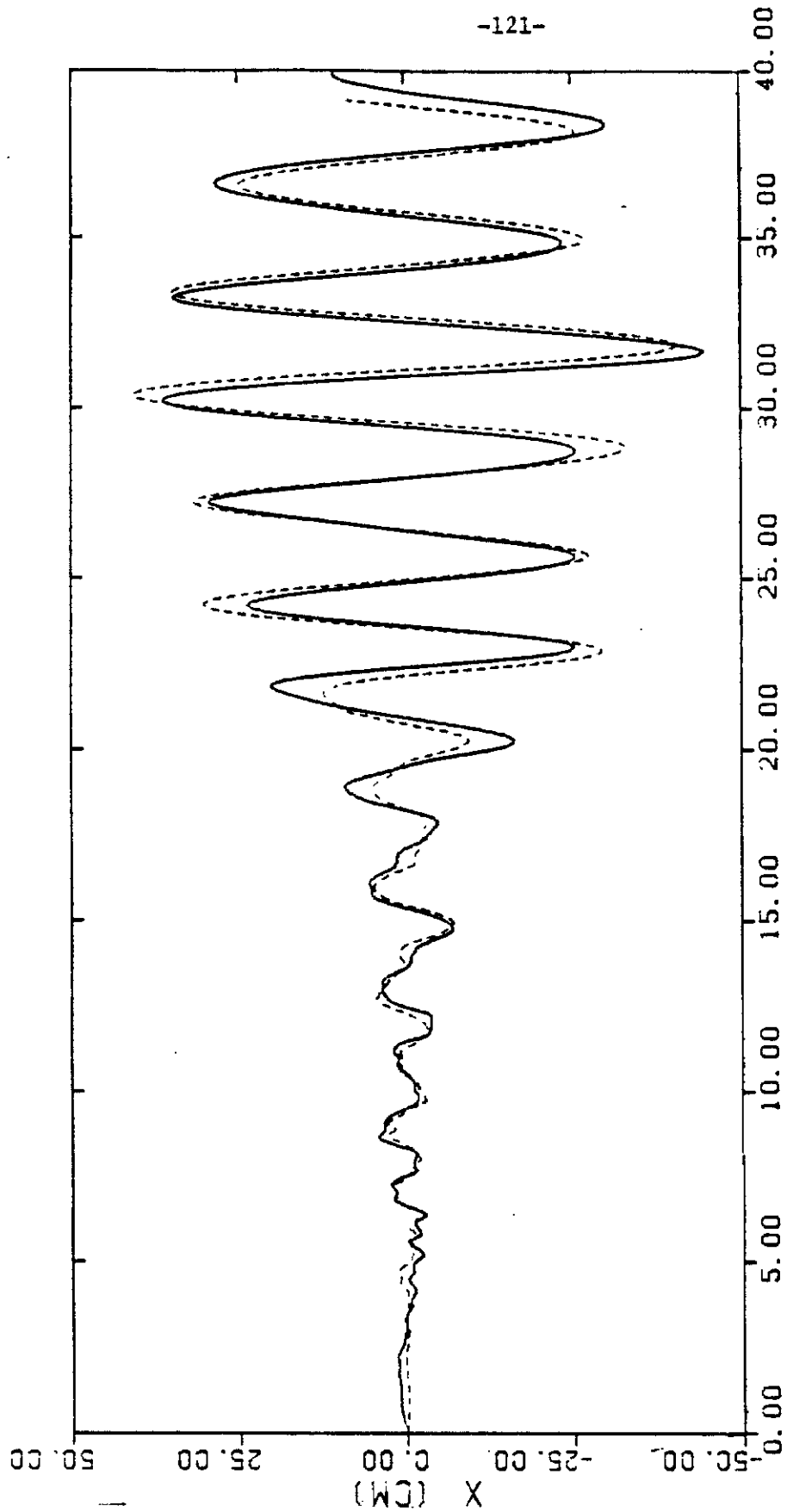

Figure 5.6 Bank of California building, N79W component. Comparison between the actual response (solid line) and the response given by the optimal DDE model (dashed line).

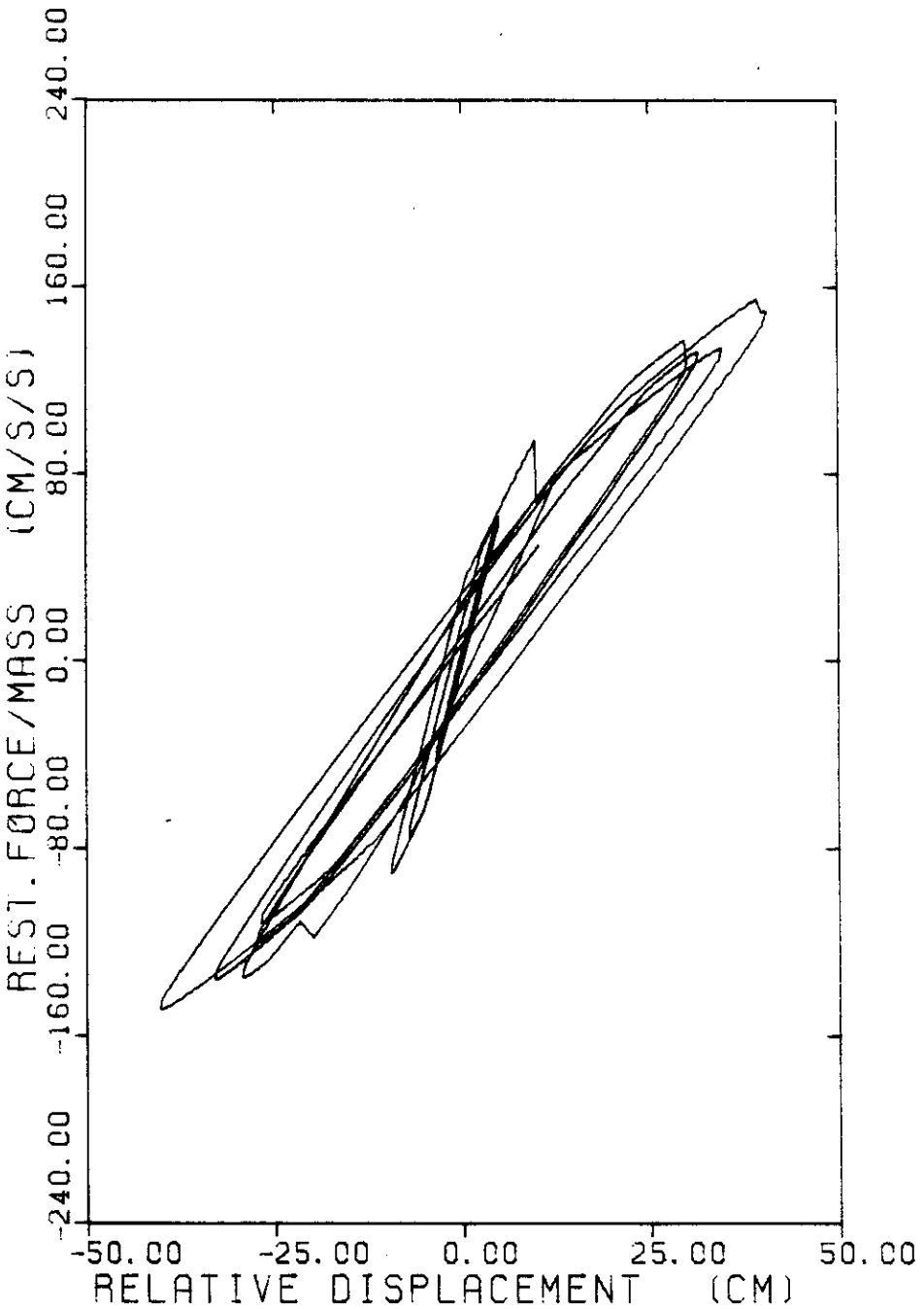

Figure 5.7 Bank of California building, N79W component. Restoring force diagram given by the optimal DDE model.

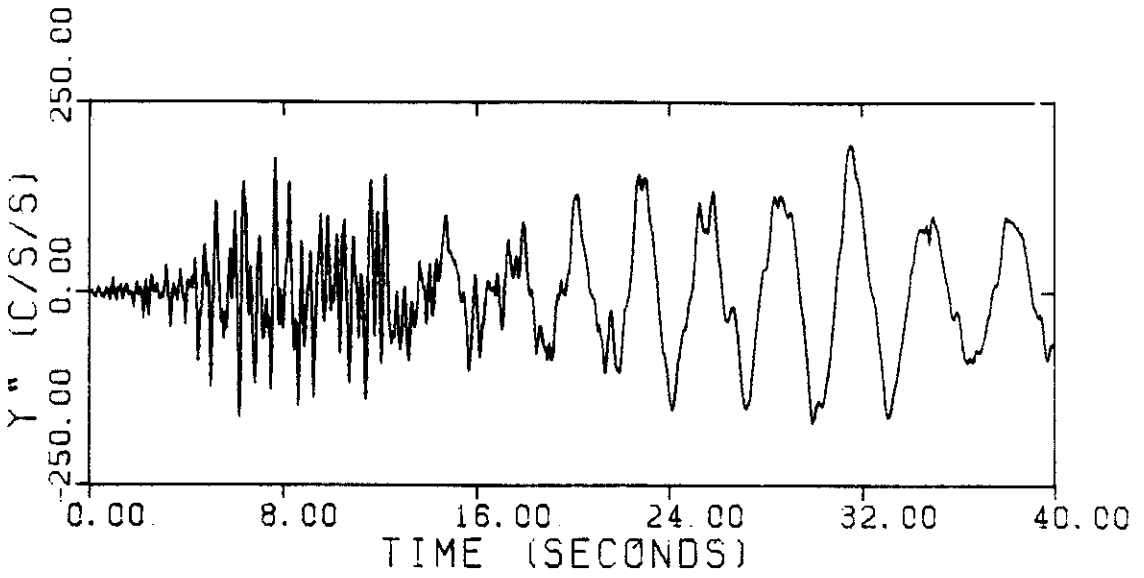

(a)

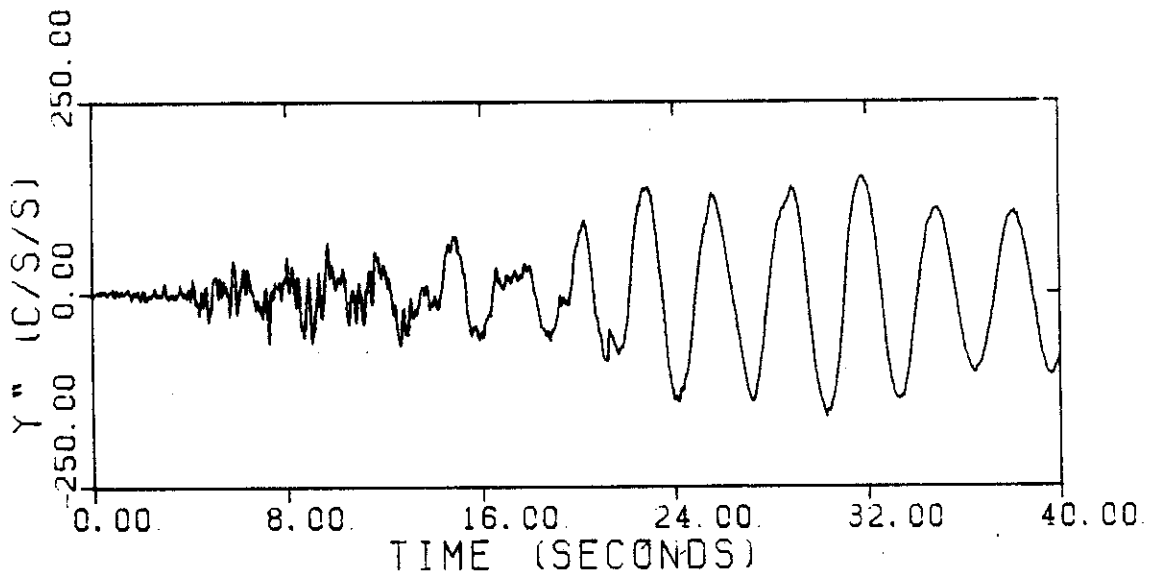

(b)

Figure 5.8 Bank of California building, N79W component. Time history of the absolute acceleration of the roof (a) actual time history (b) approximation given by the DDE model.

This was done in order to establish a reference for comparison with the approximations given by the DDE model. For the N11E component, the optimum values of the linear SDOF model parameters were $\omega_0^2 = 9.43$ sec^{-2} and $\zeta = 9.9\%$. For the N79W component, the corresponding values were $\omega_0^2 = 6.57$ sec^{-2} and $\zeta = 10.1\%$. The participation factor considered in each case was the same used with the DDE model, i.e., 1.5 and 1.3.

Figures 5.9(a) and 5.9(b) show the time history of the response predicted by the linear models compared to the actual responses. It is quite evident that in neither of the two cases does the linear model provide a good estimate of the response. The approximation obtained is unsatisfactory in terms of both the frequency and amplitude of the oscillations.

The large value of the viscous damping coefficient in both cases (approximately 10%) deserves some comments. The Bank of California building suffered considerable structural damage. Consequently, a great deal of the energy dissipated by the structure was associated with yielding or cracking of some structural members. Since the linear SDOF model does not include any mechanism to account for the energy dissipated in this manner, the only way to keep the amplitude of the oscillations under control is by means of a considerable amount of viscous damping. This leads necessarily to extremely high -- and therefore unrealistic -- values for the fraction of critical damping.

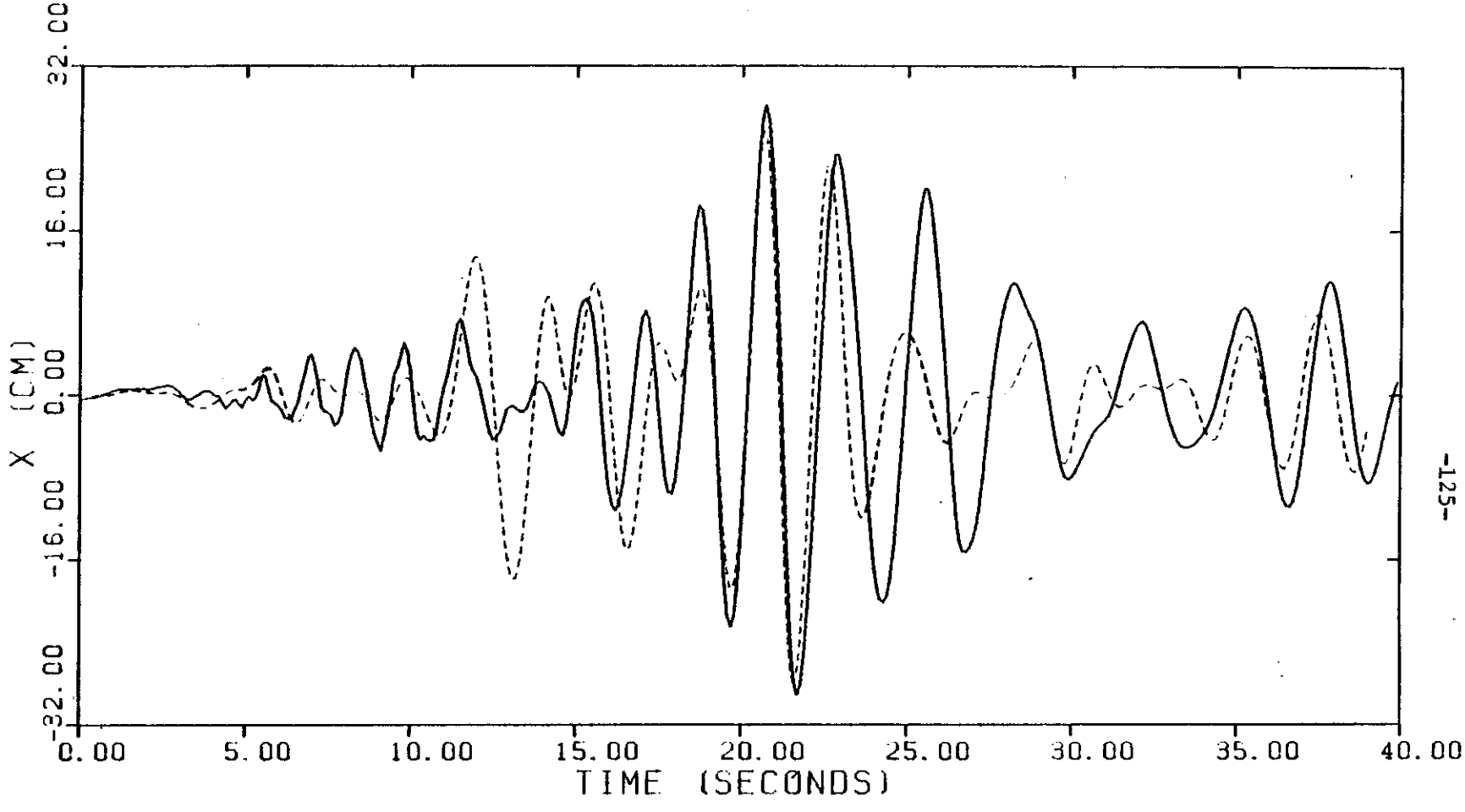

(a)

Figure 5.9 Bank of California building. Comparison between the actual response (solid line) and the response given by an optimal linear model (dashed line). (a) N11E component

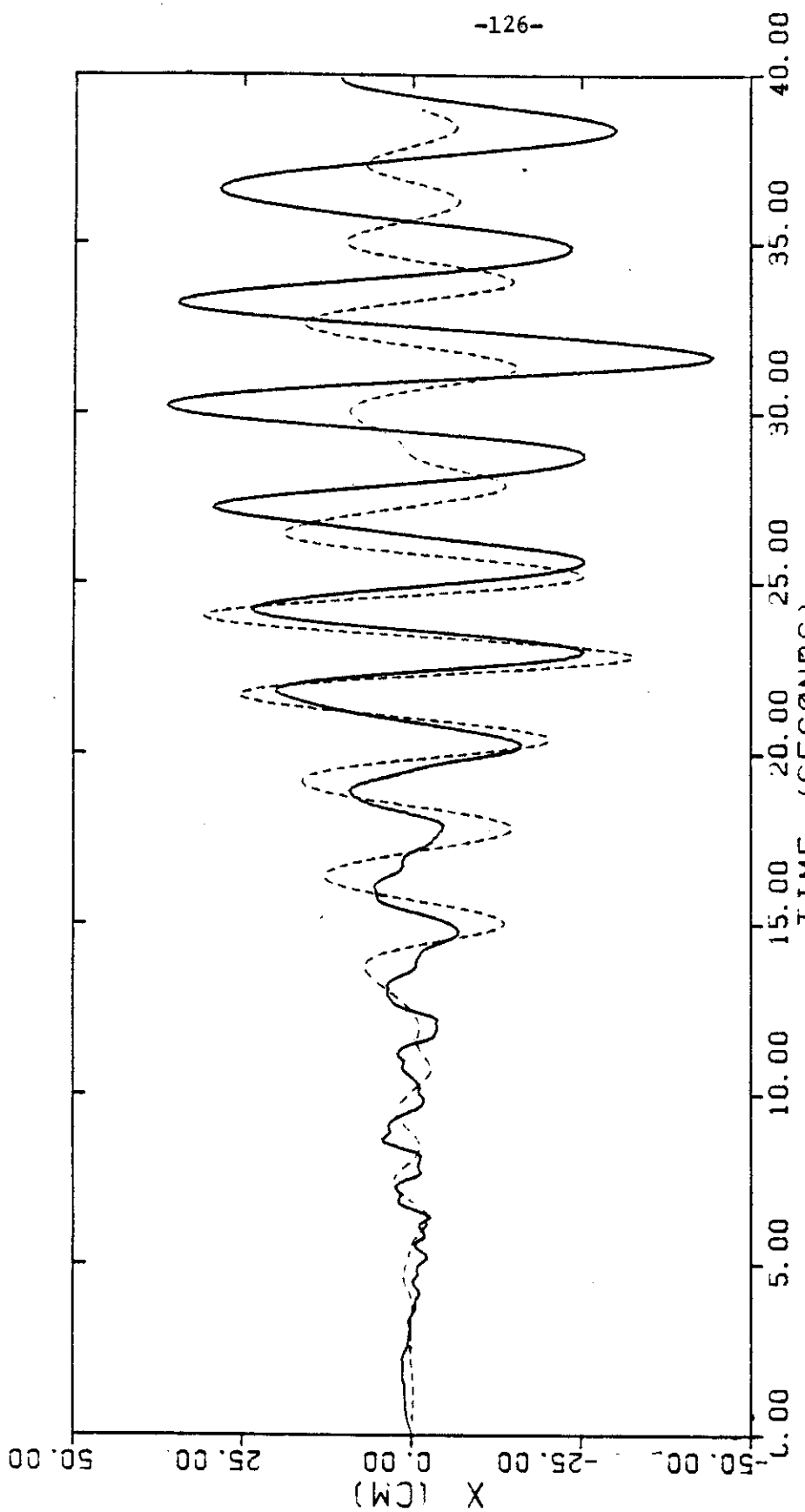

(b)

Figure 5.9 (Continued)
(b) N79W component.

5.3 THE IMPERIAL COUNTY SERVICES BUILDING

The Imperial County Services Building was located at 940 Main Street in El Centro, California. This building was a six-story reinforced concrete frame and shear wall structure. Plan dimensions of a typical floor were 136 ft 10 in by 85 ft 4 in and the total elevation was 81 ft 8 in. The structure of the building resembled a box supported on columns. During the October 15, 1979 earthquake this building suffered important structural damage. The most significant feature was the partial collapse of four reinforced concrete columns located at the east end of the building.

At the time of the earthquake, the building was instrumented with a 13-channel accelerograph system as shown in Figure 5.10. This structure became the first extensively instrumented building to suffer important structural damage. For this study, the records considered were those denoted as number 4 and 13 according to the diagram of Figure 5.10.

Previous analysis of the earthquake records by Rojahn and Mork [5] indicated that the E-W response of the building was markedly nonlinear. By analyzing the frequency content from the earthquake records, they estimated that at $t = 6.8$ seconds damage was initiated and that at $t = 11.0$ seconds the columns collapsed. These findings seem to agree with the features revealed by the restoring force diagram of this structure shown in Figure 5.11. Indeed, $t = 6.8$ seconds corresponds to the beginning of the first "large" hysteresis loop while $t = 11.0$ seconds corresponds to the maximum displacement observed in the hysteresis loop that shows the strongest deteriorating effects. More

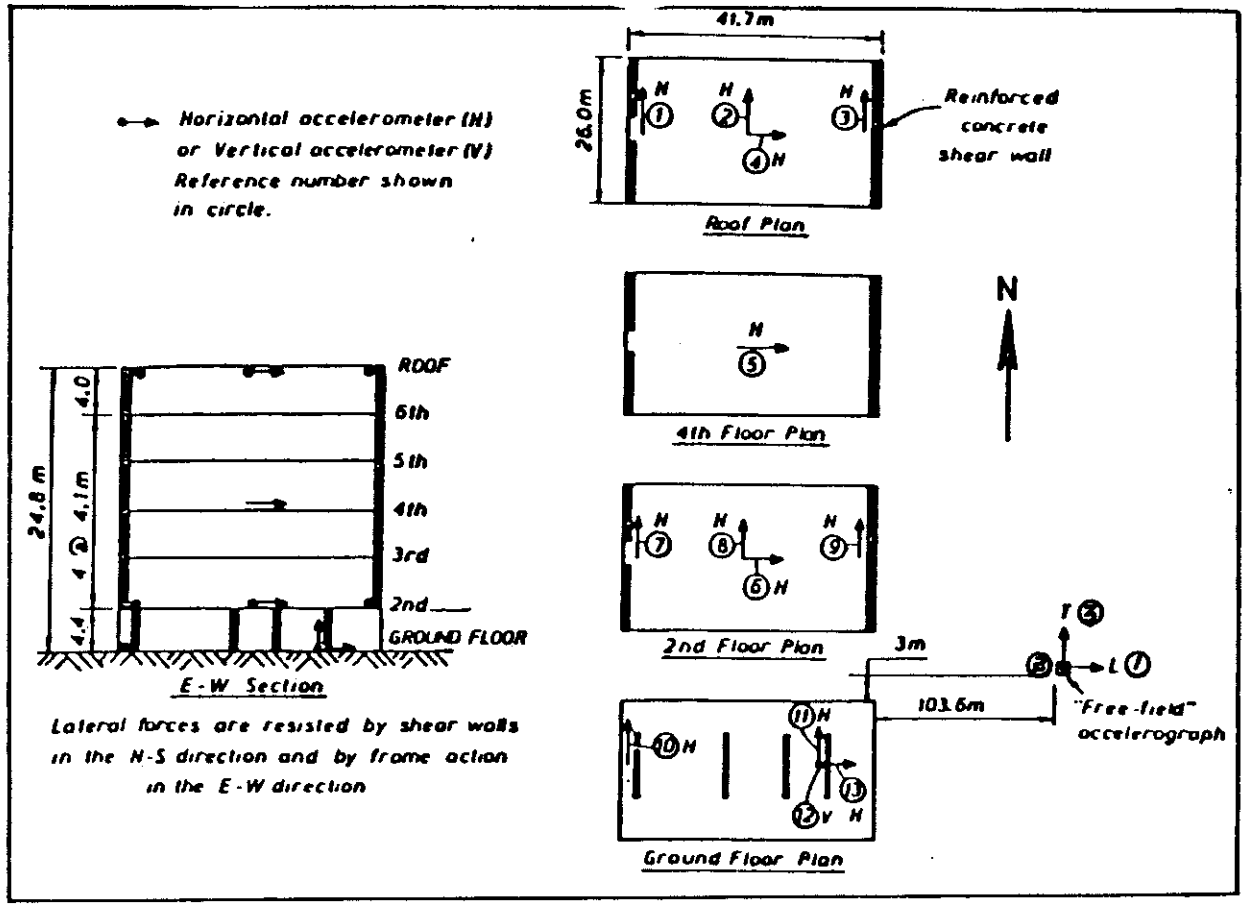

Figure 5.10 Location of strong motion instrumentation in the Imperial County Services Building. From Pauschke et al. [6].

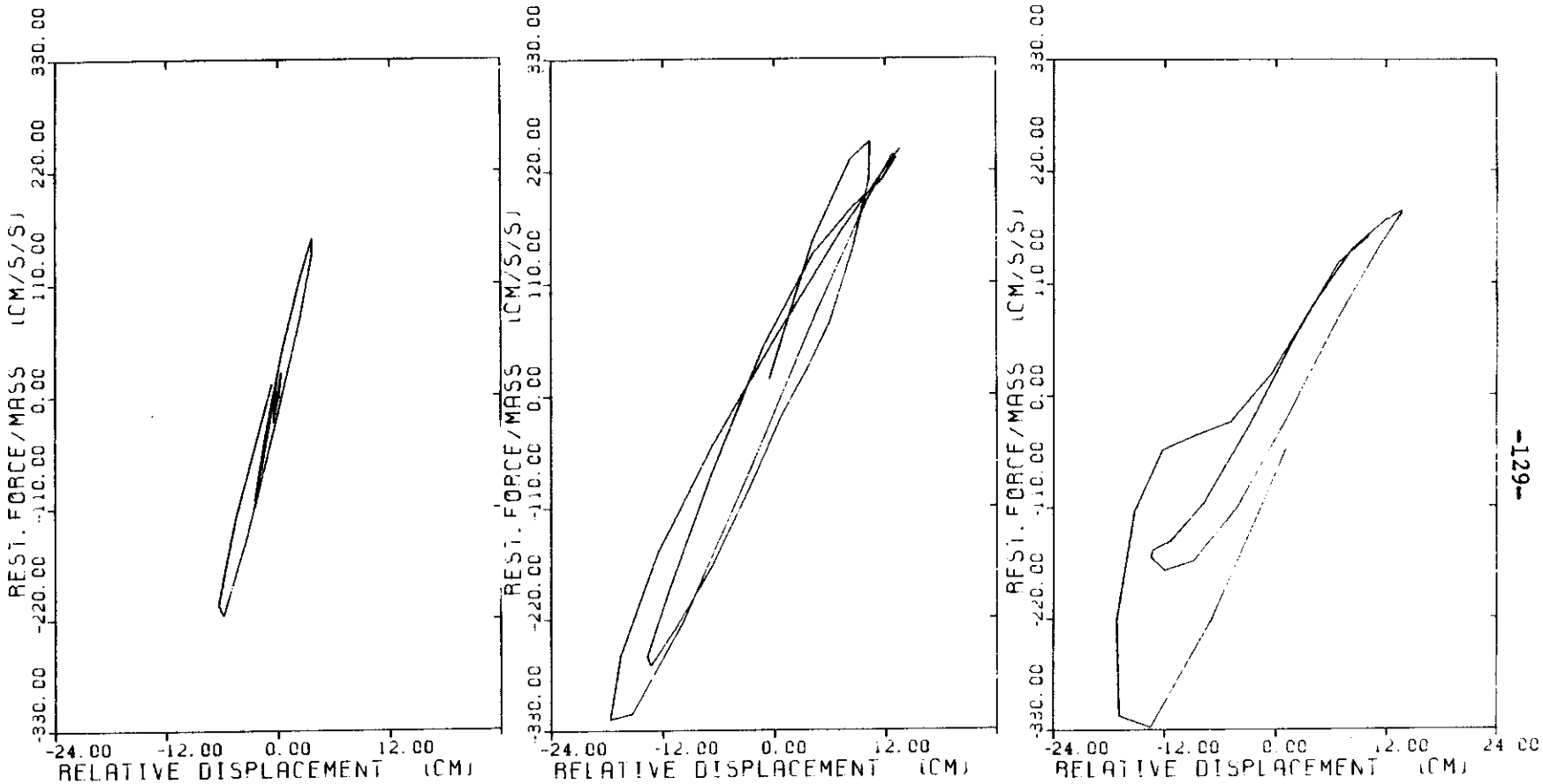

Figure 5.11 Imperial County Services Building, E-W Component. Restoring force diagram for different time intervals (a) 0.0-6.8 seconds, (b) 6.8-10.4 seconds, (c) 10.4-16.0 seconds.

information regarding the performance of this building during the 1979 Imperial Valley earthquake can be found in the reports by Pauschke et al. [6], Kreger and Sozen [7], Kiyomiya and Selna [8] and Jain et al. [9].

5.3.1 Model for the E-W Component

A DDE model with ten (N=10) deteriorating elements is chosen to match the earthquake response of this building. The values assigned to the yielding displacement of each deteriorating element are as follows:

Xy_1 = 2 cm; Xy_2 = 4 cm; Xy_3 = 6 cm; Xy_4 = 8 cm; Xy_5 = 10 cm;
Xy_6 = 12 cm; Xy_7 = 14 cm; Xy_8 = 16 cm; Xy_9 = 18 cm; Xy_{20} = 20 cm.

The system identification is carried out considering the restoring force diagram shown in Figure 2.19(c) and the effective stiffness diagram shown in Figure 2.22(c). Table 5.3 shows the values obtained for the parameters of the model.

TABLE 5.3

Parameters of the DDE Model. Imperial County Services Building, EW Component

K_e $\frac{1}{sec^2}$	K_{ep} $\frac{1}{sec^2}$	Xy_{ep} cm	α	C $\frac{1}{sec}$	A $\frac{cm^2}{sec^2}$
8.75	6.75	11.0	1.2	0.35	97

The participation factor was estimated using expression (4.14) as indicated in Section 4.3.4. The mass matrix $\mathcal{M}$ and the mode shape of the first mode of this structure were obtained from the report by Jain [9]. Hence

$$\mathcal{M} = \begin{pmatrix} 25.2 & & & & & \\ & 33.0 & & & & \\ & & 33.0 & & & \\ & & & 33.1 & & \\ & & & & 32.9 & \end{pmatrix} \qquad (5.10)$$

and

$$\{\phi_1\}^T = (1.00,\ .96,\ .87,\ .74,\ .57,\ .36) \qquad (5.11)$$

which leads to an estimate of α as 1.2. The value of the viscous damping coefficient ($C = .35\ \text{sec}^{-1}$). corresponds to 2.5% of critical damping.

Figure 5.12 depicts the time history of the relative displacement of the roof predicted by the DDE model compared to the actual response. The approximation may be considered satisfactory in spite of some small disagreement in frequency between t = 16.0 seconds and t = 20.0 seconds.

Figures 5.13(a) and 5.13(b) display the absolute acceleration of the roof recorded during the earthquake, and predicted by the model. In this case, the agreement between both time histories of the acceleration is better than in the case of the Bank of California building. This is probably due to the fact that in the present building the earthquake response was dominated by the fundamental mode.

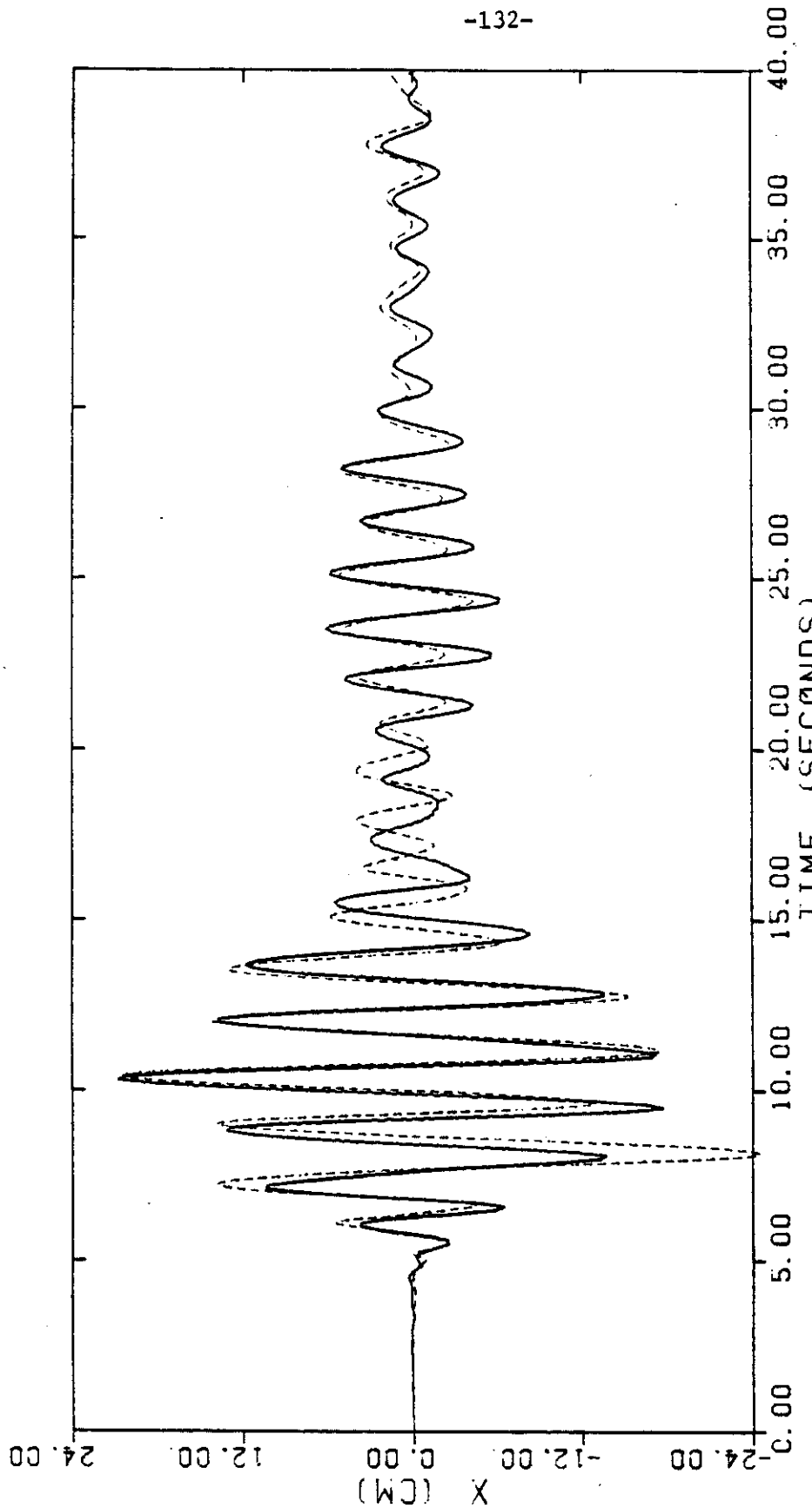

Figure 5.12 Imperial County Services building, E-W component. Comparison between the actual response (solid line) and the response given by the optimal DDE model (dashed line).

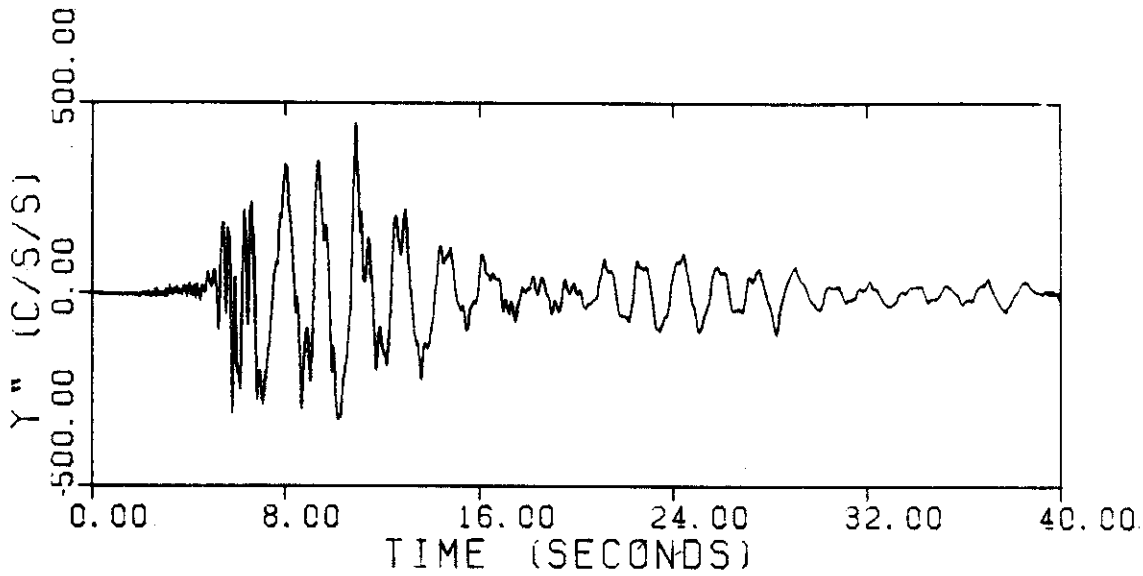

(a)

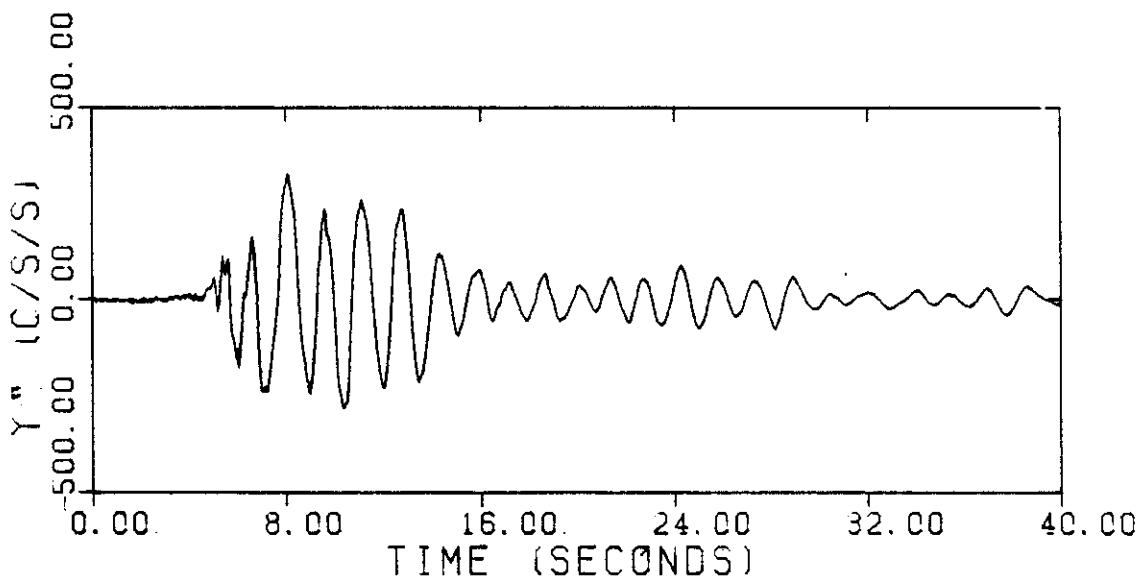

(b)

Figure 5.13 Imperial County Services Building, E-W component. Time history of the absolute acceleration of the roof. (a) actual time history (b) approximation given by the DDE model.

5.3.2 Comparison with Linear Modeling

Figure 5.14 shows the time history of the response predicted by a linear model using the same participation factor used with the DDE model. The estimated values for the parameters of the linear model are $\omega_0^2 = 19.4 \ sec^{-2}$ and $\zeta = 13.6\%$. The approximation given by the linear model shows some disagreement in terms of the frequency compared to the actual response around $t = 14$ seconds. In addition, for the time interval between 22.0 and 30.0 seconds the linear model significantly underestimates the amplitude of the response. This is a direct consequence of a high value of the viscous damping coefficient required to prevent the response from "blowing up" in the time interval between 8 and 13 seconds, corresponding to the strongest ground motion. Consequently, for small amplitude oscillations, the response predicted by the linear model is too small. This is in clear contrast to the case of the DDE model.

5.4 THE HOLIDAY INN ORION BUILDING

The Holiday Inn building is located at 8244 Orion Avenue in Los Angeles. Its distance to the epicenter of the San Fernando earthquake of 1971 is approximately 8 miles. This seven-story reinforced concrete frame structure was the closest instrumented building to the center of the earthquake. The plan is 61 ft by 150 ft and the structure stands 65 ft above the street level.

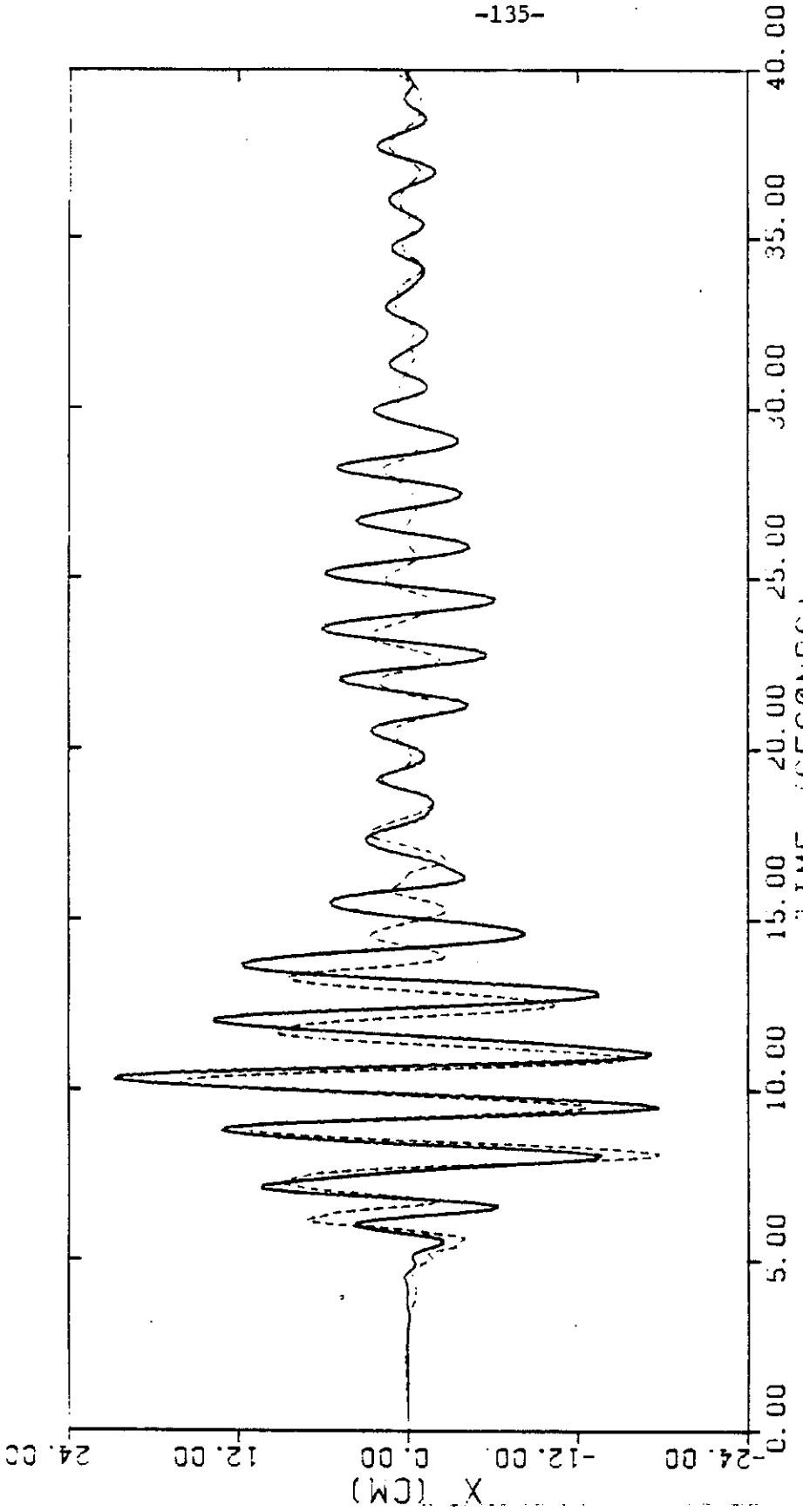

Figure 5.14 Imperial County Services Building, E-W component. Comparison between the actual response (solid line) and the response given by an optimal linear model (dashed line).

This structure suffered both structural and nonstructural damage. Most of the structural damage consisted of cracking of the concrete frame. A more exhaustive description of the structural aspects of the building and the damage that sustained are reported by Blume [1] and Foutch et al. [2].

5.4.1 Model for the N00W Component

A DDE model with ten (N=10) deteriorating elements is used in this case. The assigned values for the yielding displacement of the deteriorating elements are:

Xy_1 = 1 cm; Xy_2 = 2 cm; Xy_3 = 3 cm;
Xy_4 = 4 cm; Xy_5 = 5 cm; Xy_6 = 6 cm;
Xy_7 = 7 cm; Xy_8 = 8 cm; Xy_9 = 9 cm;
Xy_{10} = 10 cm.

The restoring force diagram considered for the system identification process is shown in Figure 2.19(d) and the corresponding effective stiffness diagram is depicted in Figure 2.22(d). The results obtained from the system identification are shown in Table 5.4.

The value assigned to α is 1.2, based on results presented by McVerry [3]. The value C = 0 indicates that the elastoplastic and deteriorating elements are sufficient to represent the energy released during the response of the structure.

TABLE 5.4

Parameters of the DDE Model. Holiday Inn Orion Building, NOOW

K_e $\frac{1}{sec^2}$	K_{ep} $\frac{1}{sec^2}$	Xy_{ep} cm	α $\frac{1}{sec}$	C $\frac{cm^2}{sec^2}$	A
8.3	4.9	2.7	1.2	0.0	30

A comparison between the time history of the response predicted by the model and that recorded during the earthquake is displayed in Figure 5.15. It can be seen that the approximation given by the model is generally acceptable, in spite of some discrepancies with the recorded response around t = 18 seconds. The discrepancy is primarily in terms of the frequency with the overall estimation of the envelope being quite good. Between the origin and t = 15 seconds, and for t larger than 20 seconds, the agreement of the two results is extremely good.

The reason for the discrepancy between t = 16-20 seconds is believed to be the following. In the model, deterioration can take place only up to the moment in which the system experiences its maximum relative displacement. In other words, deterioration depends on the amplitude of the oscillation rather than the number of cycles at a certain displacement. In this particular example, some reduction of stiffness clearly took place after the time at which the maximum displacement was reached. This fact is clearly reflected in the effective stiffness diagram of Figure 2.22(d). This causes the lack of agreement between the fundamental frequency of response which occurs near t = 18 seconds.

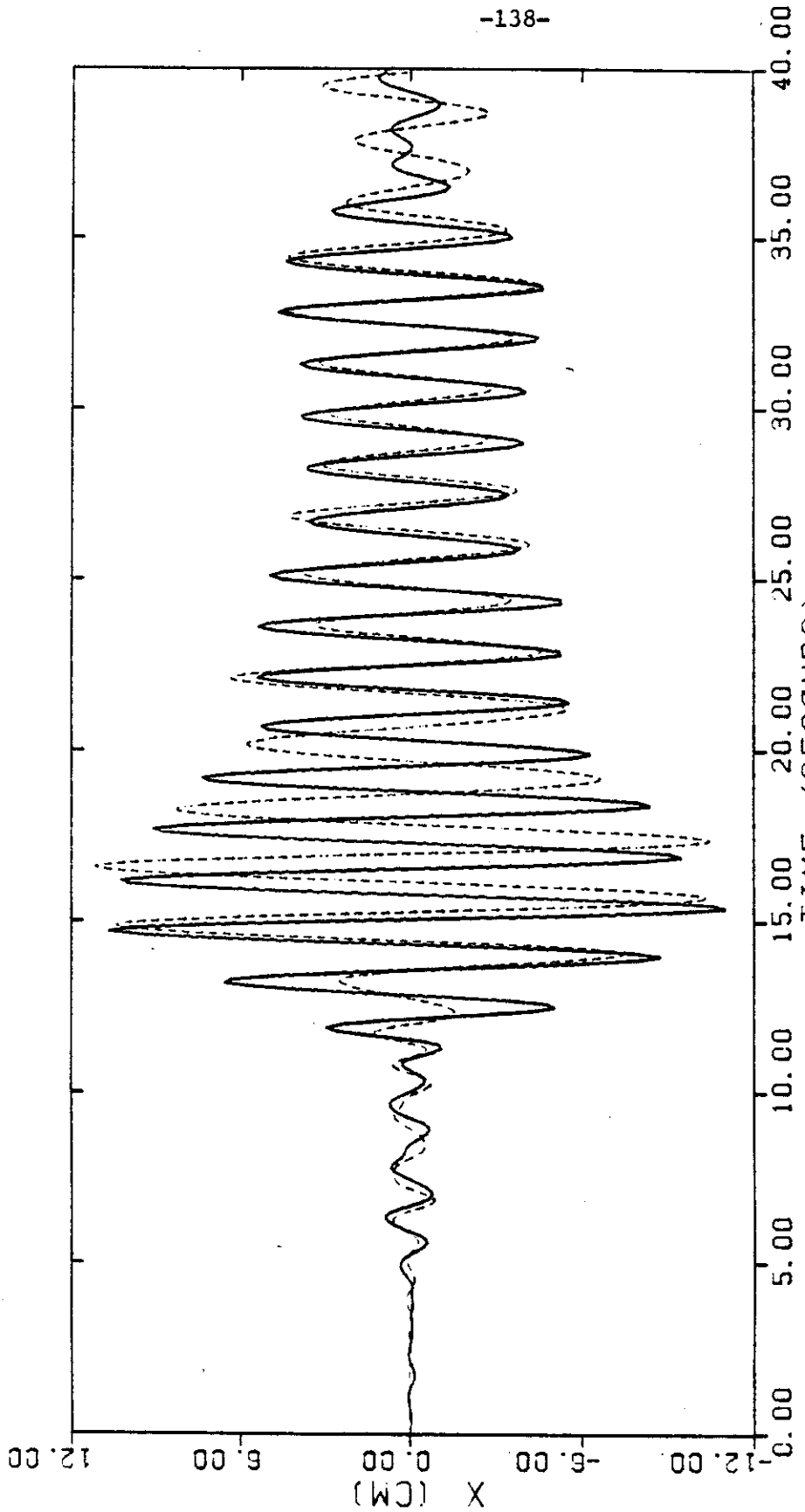

Figure 5.15 Holiday Inn building, NOOW component. Comparison between the actual response (solid line) and the response given by the optimal DDE model (dashed line).

Note that in Figure 5.15 between t = 14.5 seconds and t = 22 seconds, the actual record exhibits 6 peaks while the predicted response shows only 5. This indicates that in this time interval, the period of the actual response was less than the period of the approximated response. Thus, the response predicted by the model was associated with a smaller frequency, and therefore less stiffness. However, after t = 22 seconds, both results again show the same frequency. This indicates that the model concentrated the stiffness degradation into a shorter time interval than the actual response.

5.4.2 Model for the S90W Component

A DDE model with six (N=6) deteriorating elements is employed to predict the response of the Holiday Inn building in the S90W direction. The values of the yielding displacement of the deteriorating elements are:

$$Xy_1 = 1 \text{ cm}; \quad Xy_2 = 2 \text{ cm}; \quad Xy_3 = 3 \text{ cm};$$
$$Xy_4 = 4 \text{ cm}; \quad Xy_5 = 5 \text{ cm}; \quad Xy_6 = 6 \text{ cm}.$$

Figure 2.19(e) shows the restoring force diagram considered for the system identification process and Figure 2.22(e) depicts the corresponding effective stiffness diagram. The participation factor was assigned the value 1.28 according to the results of McVerry [3]. Table 5.5 shows the results obtained from the system identification. The value C = 0.2 sec^{-1} corresponds to 1.5% of critical.

TABLE 5.5

Parameters of the DDE Model. Holiday Inn Orion Building, S90W Component

K_e $\frac{1}{sec^2}$	K_{ep} $\frac{1}{sec^2}$	Xy_{ep} cm	α	C $\frac{1}{sec}$	A_2 $\frac{cm}{sec^2}$
11.9	7.6	2.7	1.25	0.2	30

Figure 5.16 depicts the time history of the relative displacement response predicted by the model compared to the actual response of the building. It may be noticed that the approximation given by the model agrees with the earthquake response of the building in terms of both frequency and amplitude of the oscillation.

5.4.3 Comparison with Linear Modeling

Linear models were determined to approximate the earthquake response of the Holiday Inn building in the N00W and S90W direction.

Figure 5.17 compares the response predicted by the linear model and the actual response, for the N00W component. The characteristic parameters of the linear model were, $\omega_0^2 = 19.55 sec^{-2}$ and $\zeta = 10.7\%$. It is apparent from this figure that the approximation given by the linear model is very poor except for the time interval between 12 and 19 seconds.

Figure 5.18 shows the response predicted by a linear model for the S90W component. In this case, $\omega_0^2 = 27.4\ sec^{-2}$ and $\zeta = 17.2\%$. The approximation given by the linear model is fairly good. However, one may notice a slight tendency to underestimate the peaks in the second

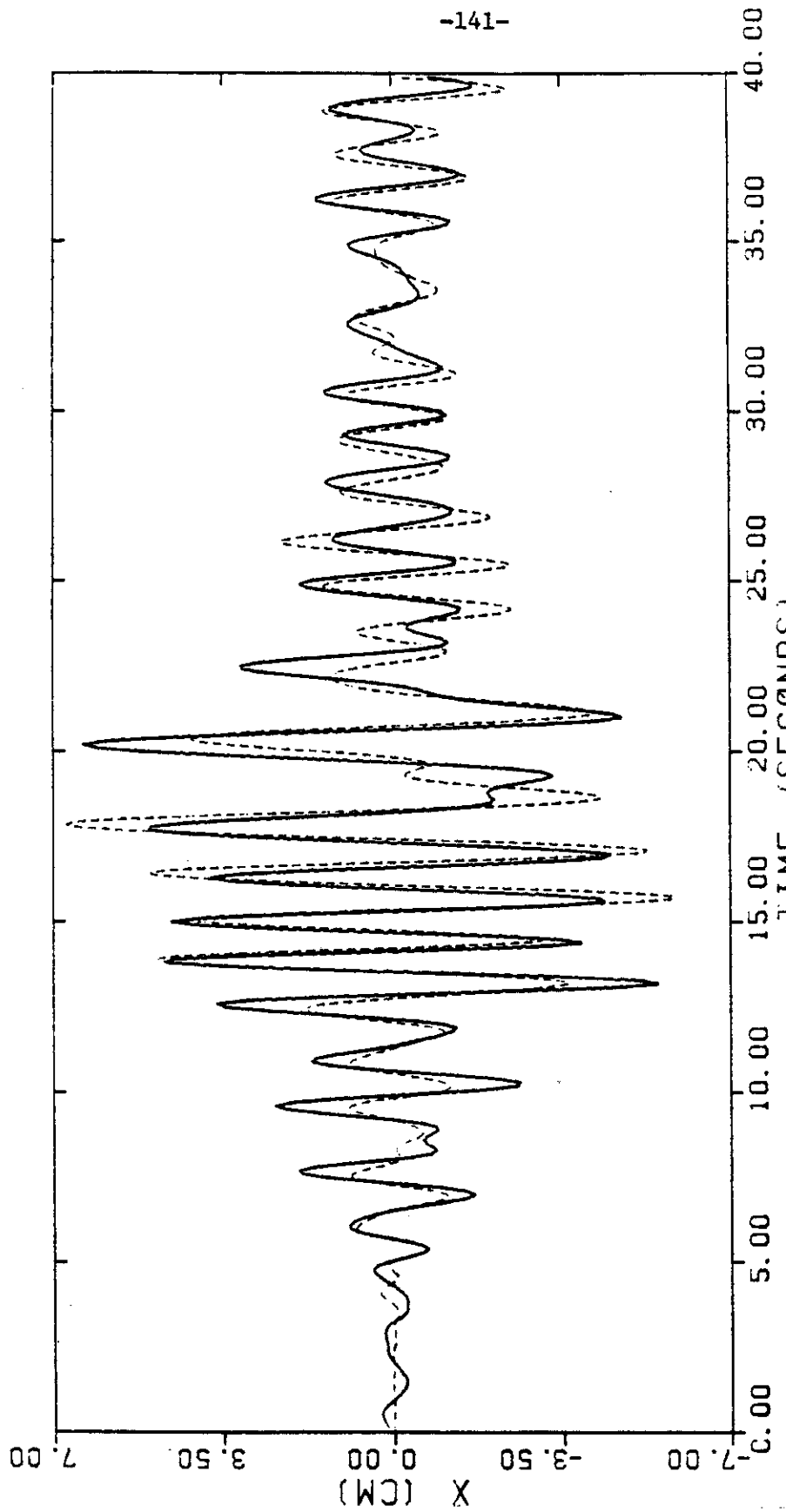

Figure 5.16 Holiday Inn building, S90W component. Comparison between the actual response (solid line) and the response given by the DDE model (dashed line).

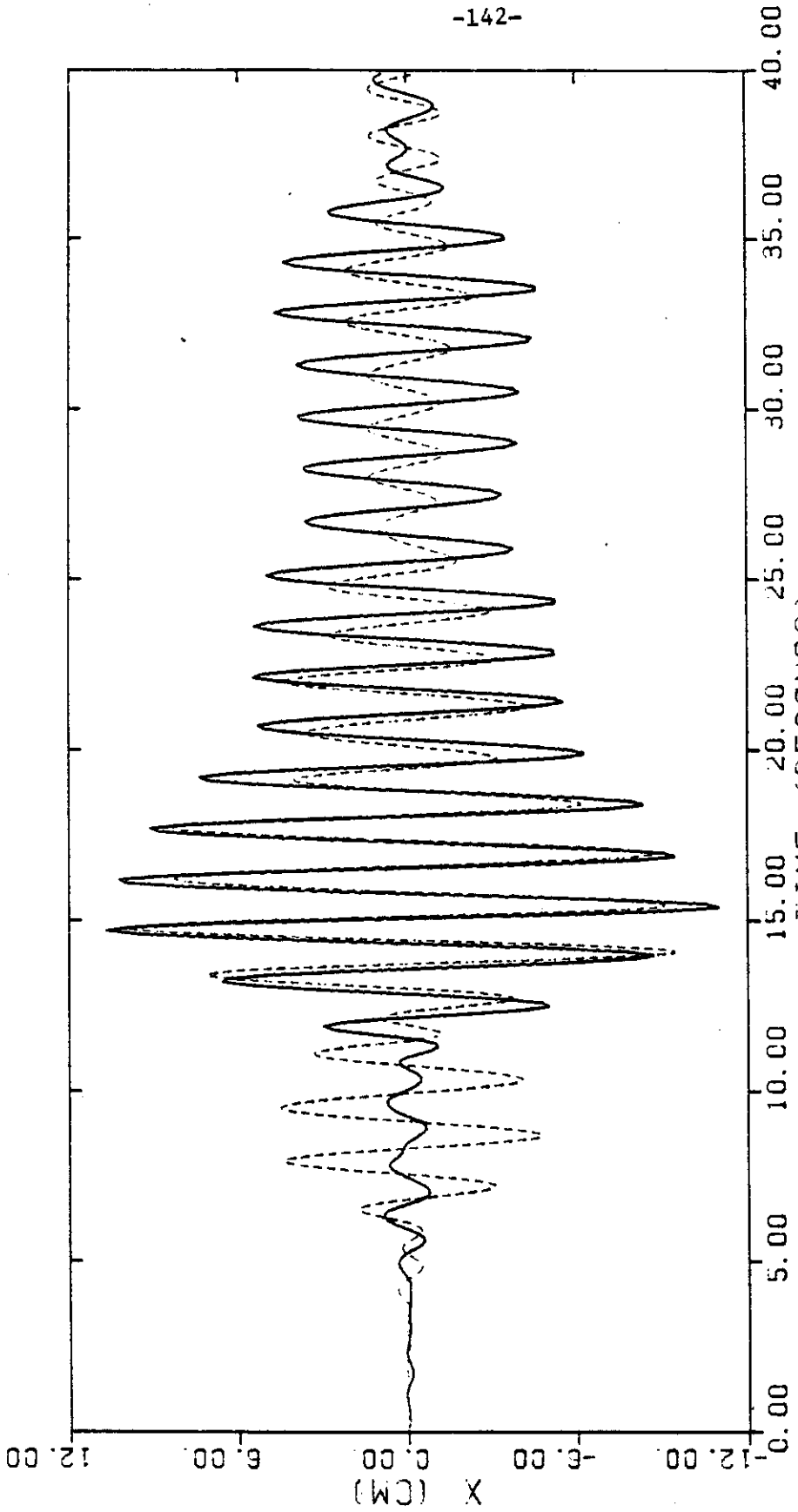

Figure 5.17 Holiday Inn building, N00W component. Comparison between the actual response (solid line) and the response given by an optimal linear model (dashed line).

half of the record. This is in contrast to the approximation given by the DDE model, in which the peaks of the response were approximated well throughout the entire record. The large value of the viscous damping coefficient (17.2%) raises some doubts. It is very likely that other forms of dissipating energy, are somehow hidden behind this large and unrealistic coefficient; namely, energy released as a consequence of hysteretic behavior.

5.5 SOME OBSERVATIONS REGARDING THE BEHAVIOR OF THE ERROR ε

A numerical investigation was performed to detect whether there was any consistent behavior pattern in the error ε. For this purpose, all of the examples previously discussed in this chapter, were considered.

Since the minimization problem introduced in Section 4.3.3 is solved as a sequence of one-dimensional optimization problems, the behavior of the error ε was studied keeping two variables fixed and letting the other varies. Recall that

$$\varepsilon = \varepsilon(K_e, K_{ep}, Xy_{ep}) \tag{5.12}$$

and let $(K_e^*, K_{ep}^*, Xy_{ep}^*)$ be the global optimum of the optimization problem (4.11). First, K_e and K_{ep} are kept fixed at their optimum values, i.e. $K_e = K_e^*$ and $K_{ep} = K_{ep}^*$, and ε is evaluated for several values of Xy_{ep}. Next, ε is evaluated for different values of K_e and K_{ep}, keeping the remaining two variables as constant and equal to their optimum values.

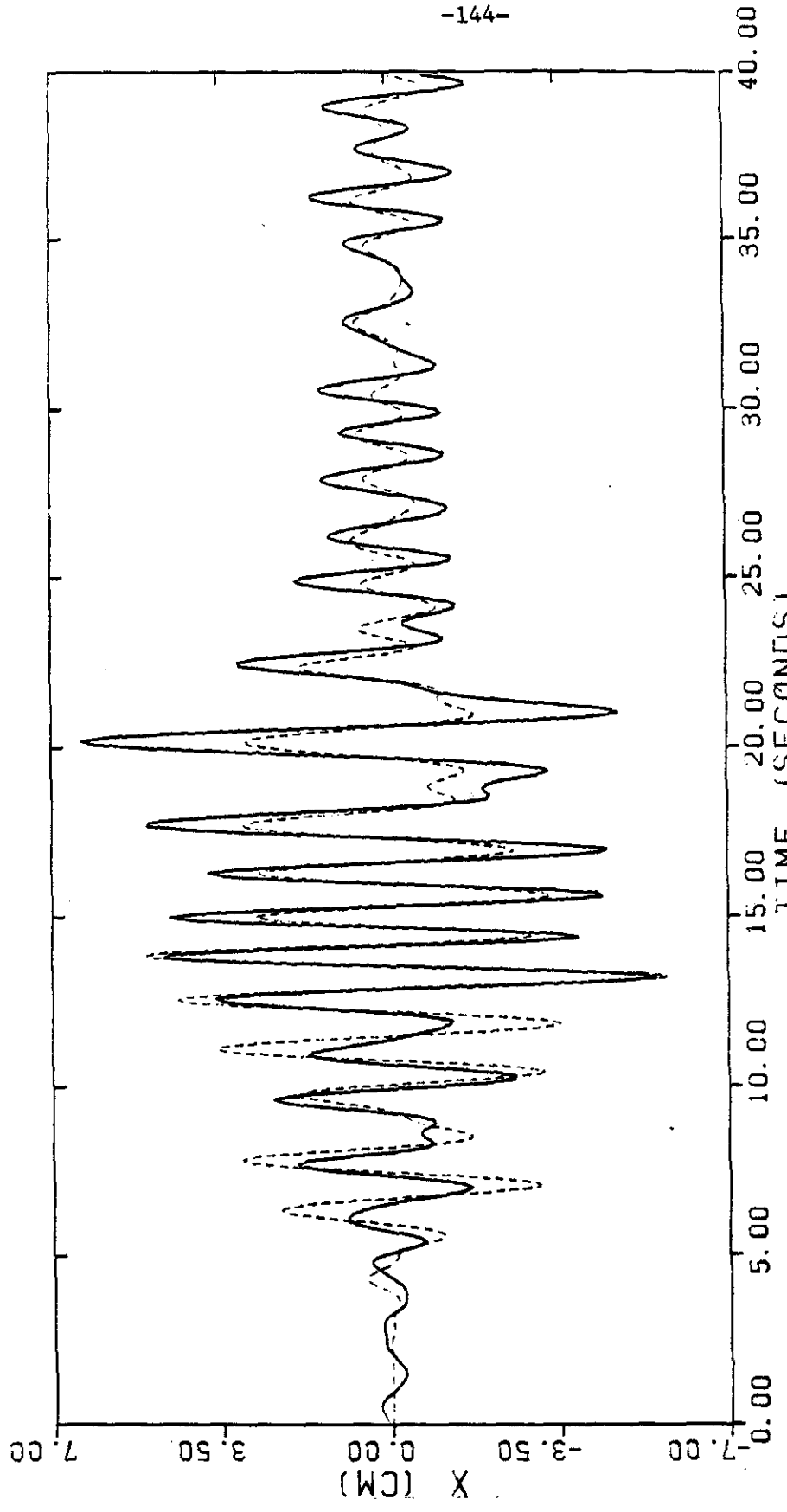

Figure 5.18 Holiday Inn building, S90W component. Comparison between the actual response (solid line) and the response given by an optimal linear model (dashed line).

This analysis reveals that ε considered as a function of K_e only, is a convex function (as indicated in Figure 5.19(a)). A similar situation is observed when K_{ep} is allowed to vary, and K_e and Xy_{ep} are kept as constant (as depicted in Figure 5.19(b)). The situation is slightly different however, when the dependence of ε on Xy_{ep} is studied. It can be noticed that the function ε (as shown in Figure 5.19(c)) is no longer convex and exhibits several local minimums. This situation can produce some problems from the numerical point of view since each local minimum is a stationary point. Therefore the optimization algorithm, at least in principle, can converge to any of these points. This suggests that some judgment must be exercised when solving the optimization problem (4.11) in order to make sure that one has found the global minimum and not just a local minimum.

5.6 SOME SPECULATIONS CONCERNING STRUCTURAL FAILURE

It is interesting to see whether one can derive any conclusion regarding the likelihood of failure of the structures analyzed using the DDE model.

Consider, for this purpose, the SDOF oscillator shown in Figure 5.20. This oscillator consists of a rigid body with a concentrated mass m and a rotational spring K_r in a gravitational field g. It may be assumed that this oscillator is a simplified version of a multistory building which is being excited by a ground acceleration a(t). The spring K_r, is somewhat associated with the stiffness of the building-soil system. The equation of motion for this system can be written as,

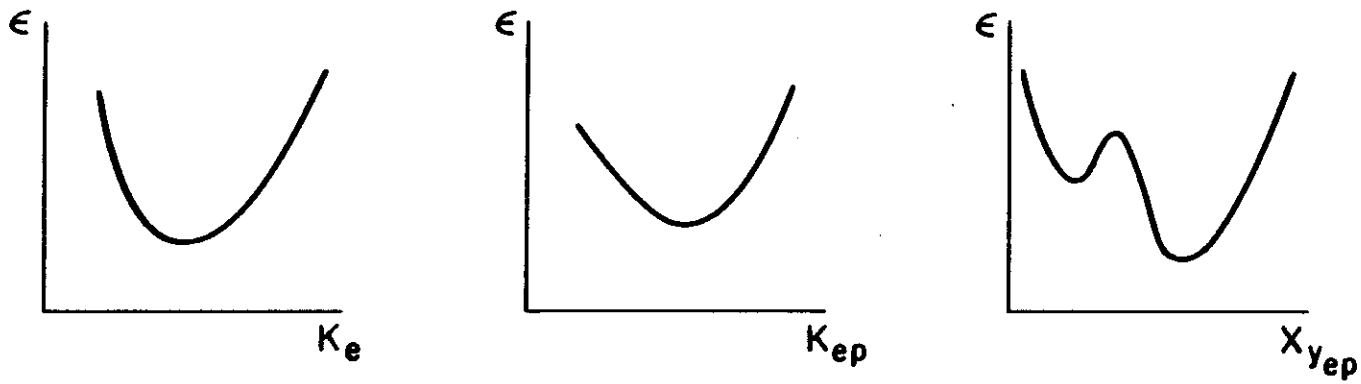

Figure 5.19 Behavior of the error ε

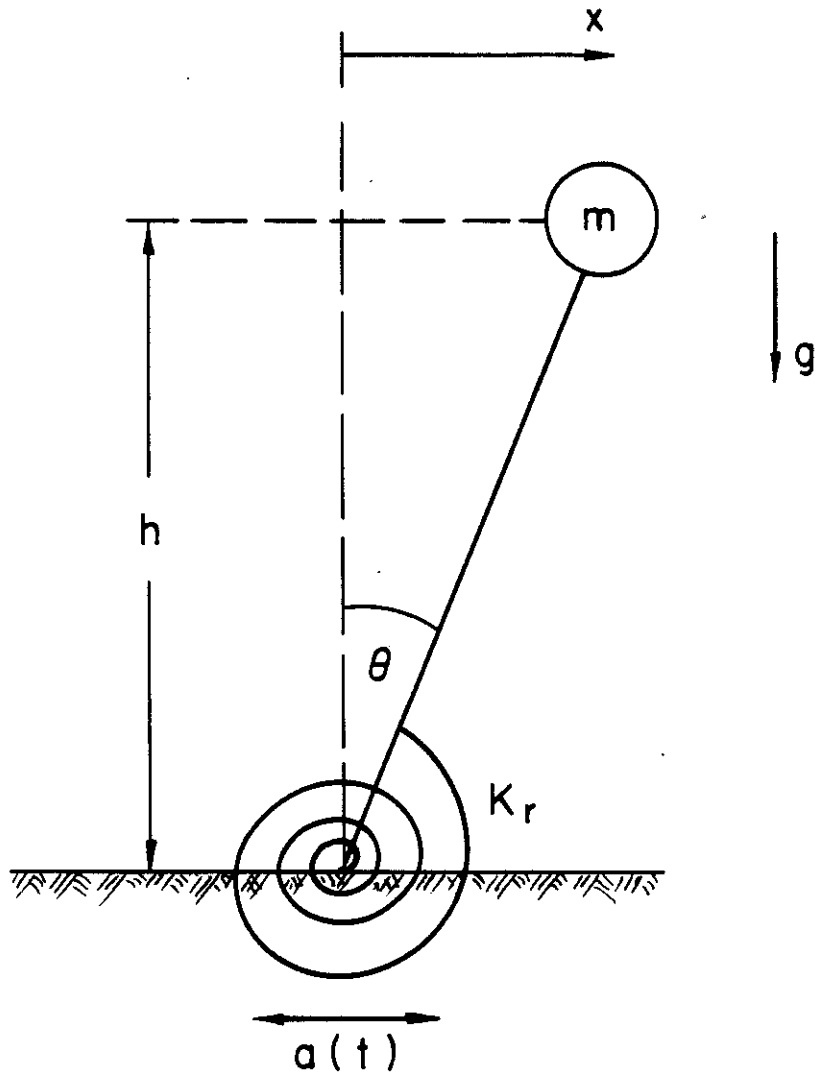

Figure 5.20 Single-degree-of-freedom oscillator with a rotational spring.

$$m(\ddot{x} + a)h + mgx - K_r\theta = 0 \qquad (5.13)$$

Assume that θ can be approximated as x/h. Furthermore, consider that the ground acceleration is equal to

$$a(t) = \alpha\ddot{z}(t) \qquad (5.14)$$

where α is the participation factor of the first mode and $\ddot{z}(t)$ is the ground acceleration recorded at the basement of the building under consideration. Then, equation (5.13) can be rearranged and expressed as

$$K_r = -mh^2\left(\frac{\ddot{x}+\alpha\ddot{z}}{x} + \frac{g}{h}\right) \qquad (5.15)$$

A balance of the horizontal forces in the case of the system shown in Figure 5.20 leads to

$$\ddot{x} + f(x,\dot{x}) = -\alpha\ddot{z} \qquad (5.16)$$

where $f(x,\dot{x})$ is the restoring force per unit of mass. Hence, combining equations (5.15) and (5.16) one obtains

$$K_r = -mh^2\lambda \qquad (5.17a)$$

where

$$\lambda = \frac{g}{h} - \frac{f(x,\dot{x})}{x} \qquad (5.17b)$$

For a stable system the value λ, as given by equation (5.17b), must be negative. If the sign of λ changes from negative to positive, it would indicate that the stability of the system is in jeopardy. Recall that

$f(x,\dot{x})$ can be determined from the earthquake records and the effective height, h, can be estimated from the geometry and stiffness profile of the structure. Therefore λ can easily be evaluated.

Consider, for example, the response of the Bank of California building in the N11E direction. Computing λ throughout the entire duration of the actual response, it is found as anticipated that no sign change occurs ($\lambda < 0$). The response is obviously stable. It is not possible to say with certainty what might have happened if the excitation had been greater, but the DDE model can be used to make some speculations.

Table 5.6 shows predictions made using the DDE model fitted to the N11E component of the Bank of California, using different input accelerations. It is observed that in cases 3, 5 and 6 there was a consistent change in the sign of λ. This suggests that the stability of the structure would have been severely tested if the building had been excited by some other ground acceleration time history. Note that the peak value of the ground acceleration is not in general proportional to the peak value of x predicted by the model. This indicates that estimations of the performance of structures based only on the peak value of the ground acceleration can be misleading.

5.7 CONCLUSIONS

In light of the results presented in this chapter, one may conclude that the DDE model gives a good approximation of the dynamic response of

TABLE 5.6

Predictions Made with the DDE Model Fitted to the N11E Component of the Bank of California Building

	Input Acceleration	Peak Value Input Acceleration	Maximum X Predicted By the DDE Model	Sign λ
1	Bank of California N11E Component	0.22g	30 cm	Negative
2	Bank of California N79W Component	0.15g	13 cm	Negative
3	Input Acceleration Used in Case 1 Multiplied by 2	0.44g	75 cm	It changes from negative to positive
4	Holiday Inn Orion N00W Component	0.25g	35 cm	Negative
5	Holiday Inn Orion S90W Component	0.14g	44 cm	It changes from negative to positive
6	Imperial County Services Building EW Component	0.33g	44 cm	It changes from negative to positive

structures exhibiting hysteretic behavior. The model captures the essential features of the nonlinear behavior of concrete structures and includes the necessary elements to account for the energy dissipated due to hysteresis and deterioration. This results in a small value of the linear viscous damping coefficient which must be incorporated into the structure. Based on computational experience, the number of deteriorating elements which must be included in the model is between five and ten depending on the case considered.

The system identification algorithm proposed in Chapter 4 has proven to be effective for estimating the value of the parameters of the DDE model. The hypothesis that viscous damping could be neglected when

defining the error ε in terms of the restoring force diagram appears to be validated by the results obtained.

Finally, predictions of the time history of the response of the buildings studied made by optimal linear models, compares poorly to those approximations obtained using the DDE model.

REFERENCES

[1] Blume, J.A., "Bank of California, 15250 Ventura Boulevard, Los Angeles," in February 9, 1971', L. M. Murphy (ed.), Vol. I, Part A, 327-357, U.S. Dept. of Commerce, National Oceanic and Atmospheric Administration (NOAA), Washington, D.C. 1973.

[2] Foutch, D.A., Housner, G.W. and Jennings, P.C., "Dynamic Response of Six Multistory Buildings During the San Fernando Earthquake," Earthquake Engineering Research Laboratory Report No. EERL 75-02, California Institute of Technology, Pasadena, California, October 1975.

[3] McVerry, G.H., "Frequency Domain Identification of Structural Models from Earthquake Records," Earthquake Engineering Research Laboratory Report No. EERL 79-02, California Institute of Technology, Pasadena, California, October 1979.

[4] McVerry, G.H. and Beck, J.L., "Structural Identification of JPL Building 180 Using Optimally Synchronized Earthquake Records," Earthquake Engineering Research Laboratory Report No. EERL 83-01, California Institute of Technology, Pasadena, California, August 1983.

[5] Rojahn, C. and Mork, P.N., "An Analysis of Strong-Motion Data from a Severely Damaged Structure -- The Imperial County Services Building, El Centro, California," recorded by the California Division of Mines and Geology Strong-Motion Network, The Imperial Valley, California, Earthquake of October 15, 1979, Geology Survey

Professional Paper 1254, U.S. Dept. of the Interior, 357-375. U.S. Government Printing Office, Washington, D.C., 1982.

[6] Pauschke, J.M., Oliveira, C.S., Shah, H.C. and Zsutty, T.C., "A Preliminary Investigation of the Dynamic Response of the Imperial County Services Building During the October 15, 1979 Imperial Valley Earthquake," The John A. Blume Earthquake Engineering Center, Dept. of Civil Engineering, Stanford University, Report No. 49, January 1981.

[7] Kreger M. and Sozen, M., "A Study of the Causes of Column Failures in the Imperial County Services Building During the 15 October 1979 Imperial Valley Earthquake," Civil Engineering Studies, Structural Research Series No. 509, UILU-ENG-83-2013, University of Illinois at Urbana - Champaign, Urbana, Illinois, August 1983.

[8] Kiyomiya, O. and Selna, L.G., "Nonlinear Analysis of the Damaged RC Structure During an Earthquake," Technical Note of the Port and Harbour Research Institute, Ministry of Transport, Japan, No. 402, December 1981.

[9] Jain, S.K., Hall, J.F., and Housner, G.W., "Features of Structural Response - Simple Analysis (Imperial County Services Building), in "Engineering Features and Studies from the Imperial County Earthquake, October 15, 1979, J.F. Hall (ed.), EERL Report Calif. Inst. of Tech., Pasadena, Calif. (to be published).

CHAPTER VI

SUMMARY AND CONCLUSIONS

The analysis, results and conclusions presented in the previous chapters can be summarized as follows:

1) Earthquake records from the Bank of California, Holiday Inn Orion and Imperial County Services buildings have been examined. These records were selected since previous reports indicated that the dynamic response of these structures had been markedly nonlinear. The restoring force diagram and the effective stiffness diagram determined from the earthquake records for these structures supports this finding. These diagrams indeed show that the response of these buildings was characterized by a significant amount of stiffness reduction. These diagrams allow one not only to obtain valuable physical insight into the stiffness degradation process but also to quantify this phenomenon.

2) A model for the hysteretic behavior of reinforced concrete structures subjected to strong ground motion has been introduced. This model, called the DDE model, has been proposed taking into account the features of the hysteretic behavior of actual structures. It is a physically motivated model having relatively few parameters. It is basically composed of three kind of elements. A first element accounts for those structural members of the building that behave linearly during the shaking. A second element accounts for those members that behave elastoplastically but without reaching a significant level of deterioration. Finally, a third group of elements, called deteriorating ele-

ments, accounts for the behavior of those structural members that suffer deterioration. In the model, energy is dissipated by means of a viscous damper as well as the elastoplastic and deteriorating elements.

3) The validity of the DDE model has been tested against actual earthquake data. Examples using the records from the Bank of California, Holiday Inn Orion and Imperial County Services building have been considered. It is observed that the DDE model appears capable of adequately representing the hysteretic behavior of these reinforced concrete buildings. The model predictions for the time history of displacement match the recorded response very well. The model predictions for the time history of acceleration are satisfactory, even though some of the high frequency content is missing for a single-degree-of-freedom model. The restoring force diagrams generated by the DDE model clearly reflect the stiffness degradation phenomenon that characterizes the behavior of the structures under consideration. The response predictions obtained for the response of these buildings using linear models are very poor. In general they show a significant lack of agreement in terms of both, frequency and amplitude of the oscillation. Furthermore, the values of the viscous damping coefficients associated with the linear models are unrealistic from a physical point of view.

4) A system identification algorithm based upon matching the restoring force behavior of the structure rather than the time history of the response has been presented. This algorithm relies on the information obtained from the restoring force diagram and the effective stiffness diagram of the structure under study. The identification of the

parameters of the model is carried out by minimizing an error which depends on the restoring force diagram. As a consequence of the structure of the DDE model, this error can be very easily evaluated without solving a differential equation each time. This is in contrast to the traditional approach in which an error depending on the time history of the response is defined. This means that the proposed identification algorithm has considerable advantage from a computational point of view.

5) The restoring force diagram obtained directly from the earthquake records has proven to be an important source of information concerning the structural behavior of the building under study. This diagram allows one to visualize and quantify the stiffness degradation process observed in many structures. Moreover, this diagram is a useful tool to detect and correct some digitization errors in the recorded data like lack of synchronization of two records or the presence of long period noise. In fact, by means of this approach it has been possible to discover some errors that may not have been detected in the original version of the digitized records.

In the light of the conclusions presented herein some suggestions for future research can be made. The DDE model presented in this thesis is based on observations made regarding the hysteretic behavior of reinforced concrete buildings. The hysteretic behavior of steel buildings has not been investigated. Therefore, the validity of the DDE model in this context is unknown. Although some similarities can be expected in both cases, the different nature of the two materials does

not allow one to extrapolate the results obtained for concrete to steel. Future research should be devoted to investigate this issue.

Several examples using actual earthquake data have been presented in this thesis. In these examples, the dynamic response of the buildings considered has been approximated by a single-degree-of-freedom DDE model. It might be possible to approximate each mode of response of a building using a different DDE model and combine these approximations to obtain a more complete picture of the actual response of the structure. This approach might give a more accurate representation of the time history of the acceleration. However, the question of how to combine the contribution of each mode to reproduce the overall response of the building needs further examination.

Finally, the problem of the presence of long period errors in digitized earthquake records deserves some further attention. As indicated earlier in Section 2.3.3, several records from the San Fernando earthquake seem to be affected by this problem. This represents a serious obstacle when attempting to obtain reliable information from these records. A more detailed analysis of this problem, using perhaps the approach outlined in this thesis, would be of considerable interest.